DOCTORADO EN
BIOMEDICINA Y FARMACIA

EFFECT OF SGLT-2 INHIBITION IN ABDOMINAL AORTIC ANEURYSM DEVELOPMENT

ROLE OF RORα IN ADIPOSE TISSUE INFLAMMATION ASSOCIATED TO OBESITY

TESIS DOCTORAL

Presentada por:

REBECA ORTEGA HERRAIZ

Dirigida por:

LAURA PIQUERAS RUIZ
MARÍA JESÚS SANZ FERRANDO
JOSÉ TOMÁS REAL COLLADO

VALENCIA, SEPTIEMBRE 2021

VNIVERSITAT DE VALÈNCIA Facultat de Medicina i Odontologia

Doctorado en Biomedicina y Farmacia

Dña. Laura Piqueras Ruiz, Investigadora adscrita al Instituto de Investigación Sanitaria INCLIVA y Profesora Asociada del Departament de Farmacologia de la *Universitat de València*; **Dña. María Jesús Sanz**, Catedrática del Departament de Farmacologia de la *Universitat de València* y **D. José Tomás Real**, Catedrático del Departament de Medicina de la *Universitat de València*

CERTIFICAN:

Que el trabajo presentado por la Graduada **Rebeca Ortega Herraiz**, titulado *"Effect of SGLT-2 inhibition in abdominal aortic aneurysm development. Role of RORα in adipose tissue inflammation associated to obesity"*, para obtener el grado de Doctor, ha sido realizado en la Universitat de València en el Departament de Farmacologia, bajo nuestra dirección y asesoramiento.

Concluido el trabajo experimental y bibliográfico, autorizamos la presentación y defensa de esta Tesis Doctoral para que sea juzgada por el Tribunal correspondiente.

Lo que firmamos en Valencia septiembre de 2021

LAURA|PIQUERAS|RUIZ Firmado digitalmente por LAURA|PIQUERAS|RUIZ Fecha: 2021.09.20 07:58:54 +02'00'

Dra. Laura Piqueras

MARIA JESUS|SANZ|FERRANDO Firmado digitalmente por MARIA JESUS|SANZ|FERRANDO Fecha: 2021.09.20 09:26:32 +02'00'

Dra. Mª Jesús Sanz

JOSE TOMAS|REAL|COLLADO Firmado digitalmente por JOSE TOMAS|REAL|COLLADO Fecha: 2021.09.20 12:06:51 +02'00'

Dr. José Tomás Real

La presente Tesis Doctoral ha sido financiada por las siguientes ayudas económicas:

PROYECTOS:

- Título del proyecto: Estudio de nuevos mecanismos inflamatorios y angiogénicos asociados a la obesidad grave mórbida; Papel del eje CXCR3 y los receptores nucleares ROR.
  Entidad financiadora: Instituto de Salud Carlos III (PI15/00082).
  Duración: De enero 2016 hasta diciembre 2018.
  Investigadores responsables: **Laura Piqueras Ruiz y José Tomas Real**

- Título del proyecto: Identificación de nuevos mecanismos implicados en la angiogénesis e inflamación en pacientes obesos. Modulación por ligandos de receptores nucleares constitutivos de androstano.
  Entidad financiadora: Instituto de Salud Carlos III (PI18/00209).
  Duración: De enero 2019 hasta diciembre 2021.
  Investigadores responsables: **Laura Piqueras Ruiz y José Tomas Real.**

- Título del proyecto: Efecto de la cirugía bariátrica en la inflamación vascular en pacientes con obesidad mórbida y diabéticos.
  Entidad financiadora: Generalitat Valenciana (AICO/2019/250).
  Duración: De enero 2019 hasta diciembre 2020.
  Investigadora responsable: **Laura Piqueras Ruiz**

- Título del proyecto: Estudio de nuevos mecanismos inflamatorios asociados a la obesidad mórbida. Modulación por la cirugía bariátrica.
  Entidad financiadora: Generalitat Valenciana (CDEI-04/20A).
  Duración: De enero 2020 hasta diciembre 2024.
  Investigadora responsable: **Laura Piqueras Ruiz**

- Título del proyecto: Modulación Inmunofarmacológica de la Inflamación Sistémica asociada a Desórdenes Metabólicos. Búsqueda de nuevas dianas terapéuticas y síntesis de fármacos novedosos.
  Entidad financiadora: Ministerio de Economía y Competitividad (SAF2014-57845-R).
  Duración: De enero 2015 hasta junio 2018.
  Investigadores responsables: **María Jesús Sanz Ferrando y Juan Francisco Ascaso Gimilio.**

- Título del proyecto: Modulación farmacológica del sistema inmune como diana clave en la prevención de la enfermedad cardiovascular asociada a desórdenes metabólicos. Síntesis de fármacos novedosos.
  Entidad financiadora: Ministerio de Economía y Competitividad (SAF2017-89714-R).
  Duración: De julio 2018 hasta diciembre 2020.
  Investigadores responsables: **María Jesús Sanz Ferrando y Juan Francisco Ascaso Gimilio.**

BECAS:

- Título de la beca: Beca INCLIVA para estancias formativas en centros de prestigio. Convocatoria 2019.
  Entidad financiadora: Instituto de Investigación Sanitaria – INCLIVA, Valencia, España.
  Datos de la estancia: Duración; desde 2 septiembre 2019 hasta 2 diciembre 2019. Centro de investigación; King´s College London, School of Cardiovascular Medicine & Sciences. Investigador responsable; Albert Ferro.

- Título de la beca: Beca de movilidad internacional para estudiantes de doctorado. Convocatoria 2019.

  Entidad financiadora: Universidad de Valencia. Cofinanciado por el programa Erasmus+ de la Unión Europea.

  Datos de la estancia: Duración; desde 2 septiembre 2019 hasta 2 diciembre 2019. Centro de investigación; King´s College London, School of Cardiovascular Medicine & Sciences. Investigador responsable; Albert Ferro.

A lo largo de esta Tesis Doctoral se han obtenido las siguientes publicaciones:

- Furio E, García-Fuster MJ, Redon J, Marques P, **Ortega R**, Sanz MJ, Piqueras L. (2018). CX3CR1/CX3CL1 Axis Mediates Platelet-Leukocyte Adhesion to Arterial Endothelium in Younger Patients with a History of Idiopathic Deep Vein Thrombosis. *Thromb Haemost* **118**(3):562-571.

- Hueso L†, **Ortega R**†, Selles F, Wu-Xiong NY, Ortega J, Civera M, Ascaso JF, Sanz MJ, Real JT, Piqueras L. (2018). Upregulation of angiostatic chemokines IP-10/CXCL10 and I-TAC/CXCL11 in human obesity and their implication for adipose tissue angiogenesis. *Int J Obes (Lond)* **42**(8):1406-1417.

  † These authors have contributed equally to this work as first authors.

- **Ortega R**†, Collado A†, Selles F, Gonzalez-Navarro H, Sanz MJ, Real JT, Piqueras L. (2019). SGLT-2 (Sodium-Glucose Cotransporter 2) Inhibition Reduces Ang II (Angiotensin II)-Induced Dissecting Abdominal Aortic Aneurysm in ApoE (Apolipoprotein E) Knockout Mice. *Arterioscler Thromb Vasc Biol.* **39**(8):1614-1628.

  † These authors have contributed equally to this work as first authors.

- **Ortega R**†, Hueso L†, Benito E, Ortega J, Civera M, Sanz MJ, Real JT, Piqueras L. (2021). The nuclear retinoid-related orphan receptor RORα controls adipose tissue inflammation in patients with morbid obesity and diabetes. *Int J Obes (Lond).* **45**:1369-1381.

  † These authors have contributed equally to this work as first authors.

- López-Riera M†; **Ortega R**†; Hueso L; Montesinos MC; Gomez-Cabrera MC; Sanz MJ; Real JT; Piqueras L. (2021). Activation of the Constitutive Androstane Receptor inhibits leukocyte adhesiveness to dysfunctional endothelium. Int. J. Mol. Sci. **22**(17):9267.

  † These authors have contributed equally to this work as first authors.

A mi abuela Herminia,

Quien me enseñó que con trabajo y esfuerzo hasta el terreno más pedregoso se puede labrar; que con cariño y amor se siembran los mejores campos; y que con esmero y perseverancia se cosecha el buen grano.

Gracias

Agradecimientos

En primer lugar me gustaría agradecer a las Dras. Laura Piqueras y María Jesús Sanz y al Dr. José Tomás Real, directores de mi Tesis Doctoral, el haberme brindado la oportunidad de iniciar mi carrera científica dejándome formar parte de su grupo de investigación. Darles las gracias también por su confianza en mí y por su interés, esfuerzo y dedicación en todo este tiempo, pues ello me ha permitido crecer profesionalmente cada día más.

Gran agradecimiento a mis compañeros de laboratorio. Elena, Aida, Patrice, Luisa, gracias por estar ahí siempre que os necesito. A Paqui, mi maestra y compañera de bancada, con cuyas enseñanzas y apoyo he podido llegar hasta aquí. Y a Mireia, porque trabajar contigo siempre es fácil. Gracias a todos por vuestro compañerismo y amistad.

También quisiera agradecer a Albert Ferro y a mis compañeros de laboratorio de Londres la cálida acogida que me dieron. Gracias a Vasco, Giulia, Emily, Gabi, Matt, Carlo y Joao porque me hicisteis sentir como en casa.

A Clara, Sara, Lucía y Mireia, porque tan larga senda no habría podido recorrerla sin vosotras a mi lado. Porque tras haber atravesado senderos llanos, montañas con abruptas subidas y valles con resbaladizas bajadas, no hay cima que no hayamos alcanzado. Porque aunque en la vida hay que escalar, subir peldaños y alcanzar nuevas metas, lo importante es disfrutar del camino. Por ello, muchas gracias por los buenos momentos compartidos, por vuestros consejos y vuestro cariño.

A María Isabel, claro ejemplo de que la verdadera amistad dura para siempre, de que no importa la distancia ni el tiempo que pasemos sin vernos, pues sé que puedo contar contigo para lo que necesite. Gracias de corazón. Y gracias también a ti, Amparo, porque desde la carrera has estado apoyándome en todo y ayudándome a seguir adelante.

Gracias a mi hermana Laura, porque con su talento literario siempre encuentra las palabras idóneas para subirme el ánimo. Porque ha sido la mejor compañera de piso que he podido tener en todos estos años. Agradecer tu paciencia y comprensión.

Y por último pero no menos importantes, mis padres, Marcelo y Encarni. Porque desde pequeña me han apoyado en mis estudios y me han acompañado tanto en los buenos como en los malos momentos, porque me han ayudado y aconsejado a la hora de tomar decisiones difíciles y porque sin vuestra confianza y muestras de cariño esta Tesis Doctoral no hubiera sido posible. Mil gracias.

TABLE OF CONTENTS

LIST OF ABBREVIATIONS

AAA – Abdominal aortic aneurysm

Ang II – Angiotensin II

ACE – Angiotensin-converting enzyme

ANOVA – Analysis of variance

ApoB – Apolipoprotein B

ApoE – Apolipoprotein E

ARBs – Angiotensin receptor blockers

AT – Adipose tissue

AT_1R – Angiotensin II type 1 receptor

BAT – Brown adipose tissue

BMI – Body Mass Index

BSA – Bovine serum albumin

CAMs – Cell adhesion molecules

CCL – C-C motif ligand

CD – Cluster of differentiation

cDNA – Complementary DNA

CXCL – C-X-C motif ligand

CX_3CL – C-X_3-C motif ligand

DAB – 3,3'-diaminobenzidine

DBP – Diastolic blood pressure

DMSO – Dimethyl sulfoxide

DBD – DNA-binding domain

DPBS – Dulbecco's phosphate buffered saline

EBM-2 – Endothelial cell basal medium-2

ECM – Extracellular matrix

EDTA – Ethylenediaminetetraacetic acid

EGM-2 – Endothelial growth medium-2

ELISA – Enzyme-linked immunosorbent assay

ESL-1 – E-selectin ligand-1

FBS – Fetal Bovine Serum

FDA – Food and Drug Administration

FFA – Free fatty acids

GAPDH – Glyceraldehyde 3-phosphate dehydrogenase

GLUT4 – Glucose transporter type 4

GlyCAM-1 – Glycosylation-dependent cell adhesion molecule-1

GPCR – G protein-coupled receptors

Groα – Growth-regulated oncogen-α

HAEC – Human aortic endothelial cells

HBSS – Hank's Balanced Salt Solution

HDL-C – High density lipoprotein – cholesterol

H&E – Hematoxylin and eosin

HOMA-IR – Homeostasis model assessment insulin resistance

HUVEC – Human umbilical vein endothelial cells

ICAM-1/2 – Intercellular adhesion molecule-1/2

IL – Interleukin

IR – Insulin receptor

IRS – Insulin receptor substrate

JAMs – Junctional adhesion molecules

LBD – Ligand-binding domain

LDL – Low density lipoprotein

LFA-1 – Lymphocyte function-associated antigen-1

LPAM-1 – Lymphocyte Peyer's patch adhesion molecule-1

Mac-1 – Macrophage-1 antigen

MAdCAM-1 – Mucosal vascular addressin cell adhesion molecule-1

MAPK – Mitogen-activated protein kinases

MCP-1 – Monocyte chemoattractant protein-1

MMP – Matrix metalloproteinase

NF-κB – Nuclear factor kappa-light-chain-enhancer of activated B cells

NRs – Nuclear receptors

PBS – Phosphate-buffered saline

PECAM-1 – Platelet endothelial cell adhesion molecule-1

PFA – Paraformaldehyde

PKB – Protein Kinase B

PMA – Phorbol 12-myristate-13-acetate

PSGL-1 – P-selectin glycoprotein ligand-1

qPCR – Quantitative polymerase chain reaction (also known as Real-time PCR)

RANTES – Regulated upon activation, normal T cell expressed and secreted

RAR – Retinoic acid receptor

RAS – Renin-angiotensin system

RORα – Retinoic acid receptor-related orphan receptor alpha

ROREs – ROR response elements

ROS – Reactive oxygen species

RT-PCR – Reverse transcription polymerase chain reaction

SAT – Subcutaneous adipose tissue

SBP – Systolic blood pressure

SDS-PAGE – Sodium dodecyl sulfate polyacrylamide gel electrophoresis

SEM – Standard error of the mean

SGLT-2 – Sodium glucose cotransporter type 2

SMCs – Smooth muscle cells

T2DM – Type 2 diabetes mellitus

TBS – Tris-buffered saline

TC – Total cholesterol

TEM – Transendothelial migration

TG – Triglycerides

Th1 – T helper 1

TIMP-1 – Tissue inhibitor of metalloproteinases-1

TNFα – Tumor necrosis factor alpha

VAT – Visceral adipose tissue

VCAM-1 – Vascular cell adhesion molecule-1

VEGF – Vascular endothelial growth factor

VSMCs – Vascular smooth muscle cells

VLA-4 – Very late antigen-4

WAT – White adipose tissue

LIST OF FIGURES

LIST OF TABLES

ABSTRACT RESUMEN

ABSTRACT

Abdominal aortic aneurysm (AAA) is a localised dilatation of the abdominal aorta that predisposes to the potentially fatal consequence of aortic rupture. The clinical approach to AAA is currently limited to surgical repair and is not indicated in patients with small AAA or who are asymptomatic. Pathological features of AAA include chronic vascular inflammation of the aortic wall, progressive extracellular matrix degradation and increased neovascularization. Because of the high mortality rate associated with AAA, new effective therapeutic strategies are needed to prevent its progression.

Beyond their glucose-lowering effects, recent studies have shown that sodium-glucose cotransporter type 2 (SGLT-2) inhibitors reduce cardiovascular events and have beneficial effects on several vascular diseases such as atherosclerosis; however, the potential effects of SGLT-2 inhibition on AAA remain unknown. Therefore, the aim of the first study of the present Thesis was to evaluate the effect of the oral treatment with a SGLT-2 inhibitor, empagliflozin, on the progression of the AAA induced by angiotensin II (Ang II) in mice deficient in apolipoprotein E (apoE$^{-/-}$) and its possible anti-inflammatory effects on human aortic endothelial cells and macrophages.

Empagliflozin treatment significantly reduced the Ang II-induced increase in maximal suprarenal aortic diameter independently of blood pressure effects. Immunohistochemistry analysis revealed that empagliflozin diminished Ang II-induced elastin degradation, neovessel formation, and macrophage infiltration at the AAA lesion. Furthermore, Ang II infusion resulted in a marked increase in the expression of chemokines CCL-2/MCP-1 and CCL-5/RANTES, vascular endothelial growth factor (VEGF) and matrix metalloproteinase (MMP)-2 and MMP-9 in suprarenal aortic walls of apoE$^{-/-}$ mice, and all were reduced by empagliflozin cotreatment. Western blot analysis revealed that p38 mitogen-activated protein kinase (p38 MAPK) and nuclear factor-κB (NF-κB) activation was also reduced in the suprarenal aortas of apoE$^{-/-}$ mice cotreated with empagliflozin. *In vitro* studies in human aortic endothelial cells and macrophages showed that empagliflozin inhibited leukocyte-endothelial cell interactions and release of pro-inflammatory chemokines induced by TNFα. In conclusion, the pleiotropic beneficial effects that

empagliflozin exerts to reduce AAA pathology suggest that therapeutic inhibition of SGLT-2 could be a viable strategy to limit AAA growth.

Morbid obesity is a chronic metabolic disease characterised by an excess of body mass due to an imbalance between food intake and energy expenditure. Nowadays, the incidence and prevalence of this pathology is increasing worldwide, specially in developed countries. Some of the main concerns are linked to the wide spectrum of comorbidities related to this disorder such as type 2 diabetes mellitus (T2DM).

Inflammation governs adipose tissue (AT) dysfunction in obesity. In the last years, retinoic acid receptor-related orphan receptor alpha (RORα) has been reported to be associated with inflammation and insulin resistance in animal studies, but its role in human obesity remains elusive. Therefore, the next objective of this Thesis was to investigate the expression and function of RORα in AT from obese diabetic and non-diabetic patients. For this purpose, RORα expression was assessed in paired biopsies of subcutaneous and omental AT from obese patients during Roux-en-Y-gastric surgery and the functional consequences of pharmacological RORα blockade were explored in AT *ex vivo*.

RORα expression was significantly higher in omental AT than in subcutaneous AT and was positively associated with body mass index (BMI) and homeostasis model assessment of insulin resistance. Furthermore, RORα expression was increased in omental AT from diabetic patients in comparation with non-diabetic AT samples and immunofluorescence assays corroborated the colocalization of RORα in endothelial cells (CD31+ cells) and lymphocytes (CD3+ cells). In *ex vivo* assays, CXCL-8/IL-8 and CCL-2/MCP-1 chemokine release was significantly higher in omental fat explants from diabetic patients than from non-diabetics, and this increase was significantly diminished by RORα blockade. Furthermore, inhibition of RORα improved protein kinase B signalling, which was diminished in omental AT from diabetic patients. In addition, under dynamic flow conditions, RORα inhibition prevented mononuclear cell attachment to human dysfunctional endothelial cells induced by TNFα. Therefore, RORα blockade could represent a potential therapy to prevent AT dysfunction and inflammation associated with insulin resistance in human obesity.

RESUMEN

El aneurisma aórtico abdominal (AAA) se define como una dilatación local de la arteria aorta a nivel abdominal cuya consecuencia más grave es su ruptura si no se detiene su crecimiento y progresión. Los rasgos patológicos del AAA incluyen un estado inflamatorio crónico que afecta a la pared vascular de la aorta, una degradación progresiva de la matriz extracelular y un aumento en la neovascularización. Esta enfermedad presenta una elevada tasa de mortalidad y en la actualidad el único tratamiento efectivo que se conoce es la intervención quirúrgica, pero no está indicada en pacientes asintomáticos o que presentan un aneurisma de reducido tamaño. Por ello, es fundamental encontrar nuevas estrategias terapéuticas que resulten eficaces para prevenir y detener el desarrollo del AAA.

Recientemente, se ha visto que los inhibidores del cotransportador sodio-glucosa tipo 2 (SGLT-2) no sólo disminuyen los niveles plasmáticos de glucosa sino que además desempeñan un importante papel cardioprotector. Se sabe que estos inhibidores de SGLT-2 tienen efectos beneficiosos en enfermedades vasculares como la aterosclerosis, sin embargo, se desconoce el efecto que podría tener la inhibición de este cotransportador en el desarrollo y progresión del AAA. Por ello, el objetivo del primer estudio de la Tesis fue evaluar el efecto del tratamiento oral con empagliflozina, un inhibidor de SGLT-2, en la progresión del AAA inducido por angiotensina II (Ang II) en ratones deficientes en apolipoproteína E (apoE$^{-/-}$), así como su posible efecto anti-inflamatorio en células endoteliales de aorta humana y en macrófagos.

Tras el tratamiento oral con empagliflozina se observó que el aumento de diámetro del AAA inducido por Ang II se reducía de manera significativa y de forma independiente al efecto causado en la presión arterial de los ratones. Análisis inmunohistoquímicos revelaron que la empagliflozina atenuaba la degradación de elastina inducida por Ang II y disminuía tanto la formación de nuevos vasos sanguíneos como la infiltración de macrófagos en la lesión. Además, la Ang II provocó un aumento en la expresión de las quimiocinas pro-inflamatorias CCL-2 y CCL-5, del factor angiogénico VEGF (factor de crecimiento vascular endotelial) y de las metaloproteasas MMP-2 y MMP-9 en la pared de la aorta suprarrenal de ratones apoE$^{-/-}$. El tratamiento oral con empagliflozina disminuyó estos mediadores

inflamatorios y angiogénicos. Por medio de la técnica de Western Blot se pudo comprobar que la inhibición de SGLT-2 por empagliflozina reducía la activación de las rutas de señalización de p38 MAPK (p38 proteína kinasa activada por mitógenos) y NF-κB (factor nuclear-κB) inducida por Ang II en la aorta suprarrenal de ratones apoE$^{-/-}$. En estudios *in vitro* con células endoteliales de aorta humana y macrófagos se observó que la incubación con emplagliflozina inhibía las interacciones leucocito-endotelio y la liberación de las quimiocinas pro-inflamatorias CCL-2 y CCL-5 inducido todo ello por TNFα. Por tanto, estos resultados indican que la empagliflozina podría representar una nueva herramienta farmacológica en el tratamiento del AAA.

La obesidad grave mórbida es una enfermedad metabólica crónica caracterizada por un exceso de masa corporal debido a un desequilibrio entre el consumo de calorías y el gasto energético. Actualmente la incidencia y prevalencia de esta patología está aumentando considerablemente, sobre todo en países desarrollados y preocupa especialmente el amplio espectro de comorbilidades que lleva asociadas entre las que destaca la diabetes mellitus tipo 2.

Los individuos con obesidad mórbida suelen presentar un tejido adiposo (TA) disfuncional como consecuencia de un estado inflamatorio crónico. En los últimos años se ha visto en modelos animales que el receptor huérfano relacionado con el ácido retinoico α (RORα) está implicado en el proceso inflamatorio y en la resistencia a insulina, sin embargo, se desconoce el papel que desempeña en la obesidad en humanos. Por ello, el siguiente objetivo de esta Tesis fue investigar la expresión y función de RORα en el proceso inflamatorio asociado a esta enfermedad en el TA de pacientes diabéticos y no diabéticos. Para ello se analizó la expresión de RORα en biopsias pareadas de TA subcutáneo y visceral de pacientes obesos sometidos a cirugía bariátrica y *ex vivo* se evaluaron los efectos funcionales derivados del bloqueo farmacológico de este receptor en el TA.

Se observó que la expresión de RORα está aumentada en el TA visceral de estos pacientes en comparación con el TA subcutáneo, y ello estaba positivamente relacionado con el índice de masa corporal (IMC) y el índice de resistencia a insulina. Además, la expresión de RORα era mayor en el TA visceral de los pacientes diabéticos que de los no diabéticos y por inmunofluorescencia se comprobó la colocalización de RORα en células endoteliales (CD31+) y linfocitos

(CD3+). A continuación, en ensayos *ex vivo* se vio que la liberación de IL-8/CXCL-8 y MCP-1/CCL-2 aumentaba significativamente en el TA visceral de pacientes diabéticos en comparación con el de los no diabéticos y dicho incremento se reducía considerablemente cuando en dichos explantes se bloqueaba la actividad del receptor RORα. También se observó que la inhibición de RORα aumentaba la activación de la vía de señalización de proteína kinasa B en el TA visceral de los pacientes diabéticos. Además, estudios *in vitro* revelaron que bajo condiciones de flujo dinámico, el bloqueo farmacológico de RORα disminuye la adhesión de células mononucleares al endotelio arterial disfuncional. Por todo ello, la inhibición de RORα podría suponer una prometedora diana terapéutica para prevenir la disfunción del TA y la inflamación que subyace a la resistencia a insulina asociada a la obesidad grave mórbida en humanos.

1. INTRODUCTION

1.1 Inflammatory process

1.1.1 General overview

The immune system is the responsible of protecting the organism against infections and tissue injury. Depending on their specificity, immune responses can be divided into innate or adaptive immune responses. The innate immunity is known as the first line of defense against pathogens. It is a non-specific response in which macrophages, dendritic cells, natural killer cells, neutrophils, basophils and eosinophils are involved. On the other side, adaptive immunity generates a specific cellular response to recognise a particular pathogen and it includes T and B lymphocytes [1].

Inflammation is defined as a non-specific defense and healing mechanism exerted by the immune system in the presence of tissue damage or infection in order to restore and maintain corporal homeostasis. Acute inflammation, which is a short-term response, constitutes the main defensive barrier activated by the innate immune system. It promotes vasodilatation and leukocyte-endothelial cell adhesion and it also increases vascular permeability, resulting in an accumulation of fluid and acute-phase proteins from the blood vessels to the damaged tissue leading to edema [2]. This event can be accompanied by other signs of acute inflammation such as redness, heat, pain and loss of function [3]. In response to an inflammatory stimulus, tissue-resident macrophages, mast cells and dendritic cells release pro-inflammatory mediators to attract more innate immune cells from the blood vessels to the injury [4] (**Figure 1**). The primary leukocytes recruited to the infected or damaged area are neutrophils, followed by monocytes, which later on differenciate into macrophages to continue secreting pro-inflammatory mediators. Recurrent acute inflammation can lead to chronic inflammation, which is a persistent condition characterised by mononuclear cell infiltration and fibrosis [5]. Chronic inflammation is considered a dysregulated and maladaptive immune response that can lead to tissue destruction and organ dysfunction and it is responsible of a wide range of disorders that include cancer, rheumatoid arthritis, diabetes, obesity, asthma and neurological, autoimmune and cardiovascular diseases [3] (**Figure 1**).

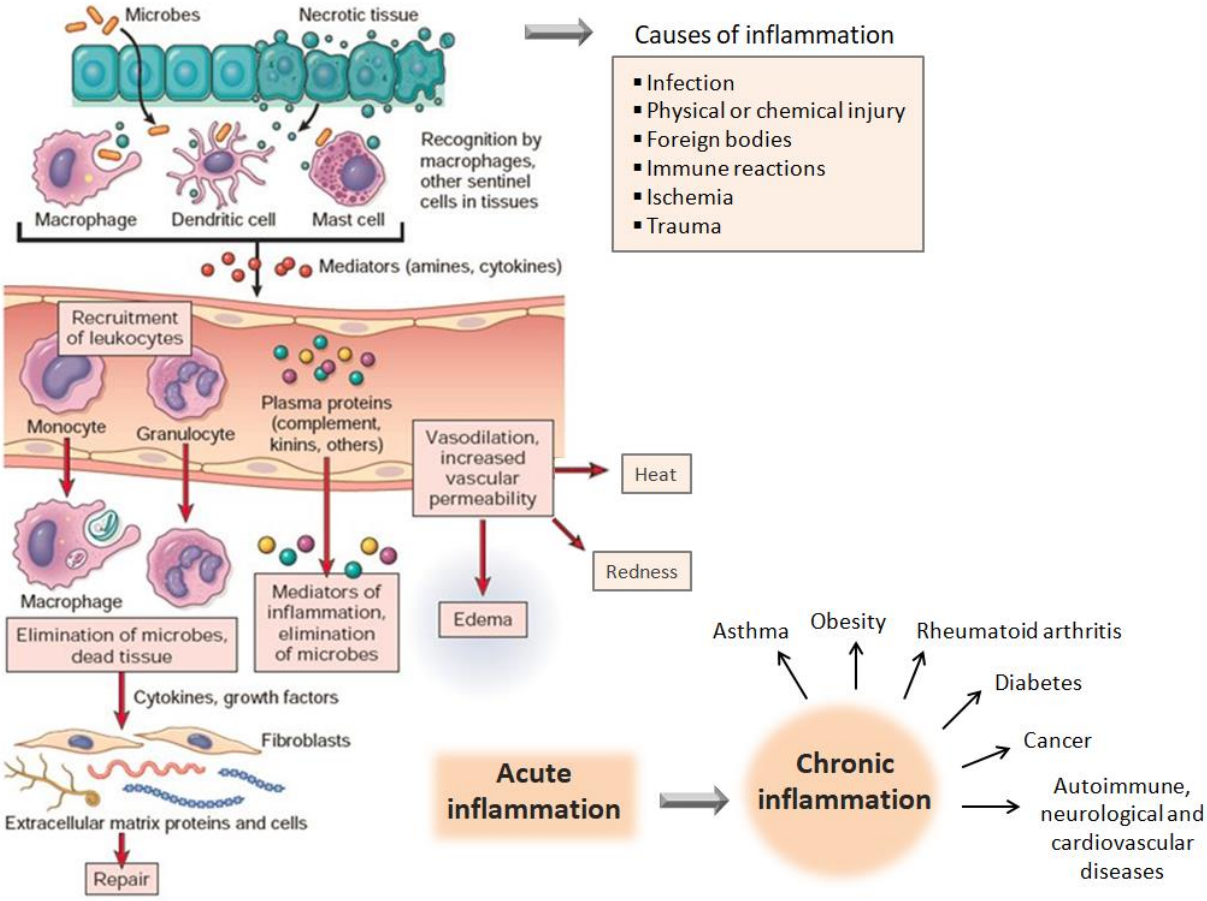

Figure 1. Sequence of events in an inflammatory reaction. In the presence of an inflammatory stimulus, tissue-resident macrophages, mast cells and dendritic cells release pro-inflammatory mediators that promote vasodilatation, vascular permeability and leukocyte recruitment from the blood vessels to the injury. These events produce edema, redness and heat, characteristic signs of acute inflammation. Then, the recruited innate immune cells remove the inciting agent, or repair the damaged tissue by activating fibroblast activity. This immunological response usually lasts a short period of time. However, if acute inflammation prorogues, it derives in chronic inflammation which can lead to the development of different metabolic, neurological, cardiovascular and autoimmune diseases. Adapted from Hoda *et al*. 2015[4].

1.1.2 Leukocyte recruitment cascade

Leukocyte recruitment is a complex process that has been thoroughly studied for the last decades. Several studies carried out with genetically modified mice have been crucial to identify the molecules and proteins implicated in this event and to elucidate the role of the inflammatory mediators in leukocyte extravasation. In addition, research techniques such as the flow chamber or the intravital microscopy of the microcirculation have enabled the visualization of the leukocyte-endothelium interactions which has led to a better understanding of the leukocyte infiltration process [6, 7].

Endothelial dysfunction is characterised by an increase of the vascular permeability and an activation of the immune system, two processes that drive the endothelium to a pro-inflammatory and pro-thrombotic state [8]. This vascular remodelling promotes leukocyte infiltration across the vessel wall to the inflamed tissue to repair and clear the injury or infection. This is a highly regulated event that constitutes one of the earliest stages of the inflammatory response and it is mediated by leukocyte-endothelial cell interactions which are crucial to guarantee the recruitment of immune cells to the arterial surface [9, 10]. Diverse agents that are considered risk factors for cardiovascular diseases such as the tumor necrosis factor α (TNFα), angiotensin II (Ang II), interleukin (IL)-1β, and cigarette smoke are potent inducers of this process as they promote the expression of cell adhesion molecules (CAMs) on the cell surface, increase the secretion of diverse chemoattactant molecules and enhance reactive oxygen species (ROS) production. These events contribute to a firm leukocyte adhesion to the endothelium and their subsequent transmigration to the subendothelial space [11, 12].

Leukocyte recruitment cascade is performed by diverse types of immune cells and inflammatory mediators and it can be divided into four different stages: rolling, activation, firm adhesion and leukocyte transmigration (**Figure 2**) [13].

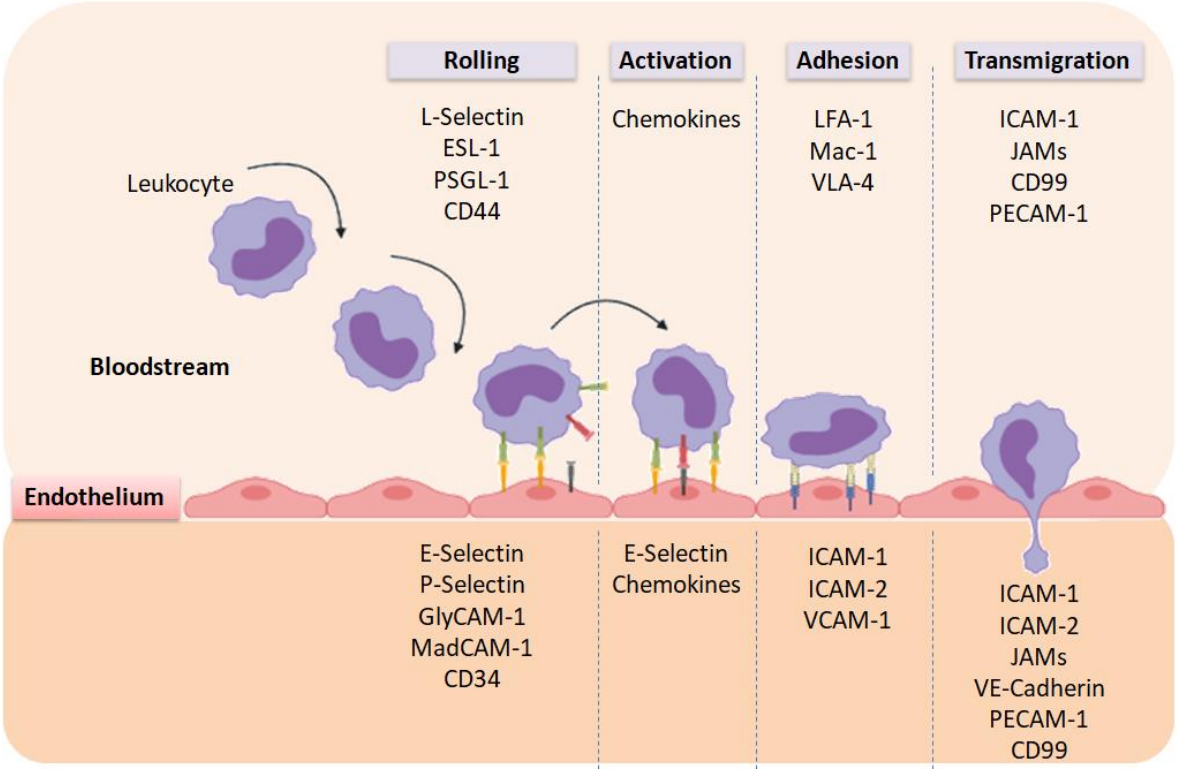

Figure 2. Stages of leukocyte recruitment and extravasation. Under pro-inflammatory conditions, endothelial cells and leukocytes express diverse CAMs that contribute to leukocyte rolling, which is the first step in the leukocyte infiltration process. Then, leukocytes become activated and they firmly attach to the endothelium. After the adhesion stage, leukocytes migrate to the inflammatory focus. Only the most remarkable cell adhesion molecules are shown. Abbreviations: ESL-1, E-Selectin Ligand-1; PSGL-1, P-Selectin glycoprotein ligand-1; CD, cluster of differentiation; VLA-4, very late antigen-4; LFA-1, lymphocyte function-associated antigen-1; Mac-1, macrophage antigen-1; ICAM-1, intercellular adhesion molecule-1; ICAM-2, intercellular adhesion molecule-2; VCAM-1, vascular cell adhesion molecule-1; PECAM-1, platelet endothelial cell adhesion molecule-1; JAMs, junctional adhesion molecules; VE-Cadherin, vascular endothelial cadherin. Created with BioRender.com.

1.1.2.1 Leukocyte rolling

Leukocyte recruitment is a process that requires adhesive and signalling interactions between the leukocytes and the endothelium. This process is mainly mediated by selectins. Under pathological conditions, the activated endothelium promotes the expression of P-selectin and E-selectin on the vascular wall (**Table 1**). In turn, leukocytes express on their surface L-selectin [10]. These three selectins interact with a common ligand, the P-selectin glycoprotein ligand-1 (PSGL-1). PSGL-1 is expressed by leukocytes and endothelial cells and its interaction with

selectins induces a conformational change on leukocyte integrins leading to their activation. Activated integrins show a high affinity and avidity for their specific endothelial ligands favouring thus the slow rolling of leukocytes and their transitory interaction with the endothelium [14, 15]. As shown in **Table 1**, E-Selectin also interacts with E-selectin ligand-1 (ESL-1) and glycosylated CD44, both expressed on leukocytes. The glycosylation-dependent cell adhesion molecule-1 (GlyCAM-1), the mucosal vascular addressin cell adhesion molecule-1 (MadCAM-1) and the mucin-like protein CD34, expressed on endothelial cells are L-selectin ligans [16].

Furthermore, during the acute inflammatory response there is an increase of the vascular permeability that is accompanied by a significant plasma loss and a local hemoconcentration which leads to a lower rate blood flow. This slowing down of the blood flow also facilitates the interaction between the leukocytes and the CAMs expressed by endothelial cells allowing leukocytes to roll along the endothelial surface [17]. Then, depending on the intensity of the inflammatory response, leukocyte can firmly attach to the endothelium and extravasate or conversely, return to the bloodstream. Thus, the rolling stage is critical for the leukocyte infiltration cascade to be continued [15].

1.1.2.2 Leukocyte activation

Reversible leukocyte-endothelium interactions mediated by selectins and the generation of a chemoattractant gradient lead to leukocyte activation [18]. The production and subsequent release of different chemoattractant molecules such as chemokines induces leukocyte activation and polarization and coordinates their locomotion along the endothelial surface.

1.1.2.2.1 Chemokines

Chemokines are small secreted cytokines (approximately 70-80 amino acids residues) with selective chemoattractant properties that orchestrate leukocyte trafficking across the vessel wall and modulate the migration of immune cells to the damaged or inflamed tissue. Chemokines are involved in different human pathologies including cancer, autoimmune and chronic inflammatory diseases [19].

Table 1. Cell adhesion molecules (CAMs) involved in leukocyte infiltration. Adapted from Gerhard *et al*. 2015 [20].

Family	Common name	Immunological name	Main ligands	Cellular expression	Function
Immunoglobulins	ICAM-1	CD54	LFA-1, Mac-1	EC, VSMC, macrophages	Adhesion, transmigration
	ICAM-2	CD102	LFA-1	EC	Adhesion, transmigration
	VCAM-1	CD106	VLA-4, LPAM-1	EC, VSMC	Leukocyte arrest
	PECAM-1	CD31	PECAM-1	EC, platelets, leukocytes	Transmigration
	MAdCAM-1	Addressin	LPAM-1, L-Selectin, VLA-4	Mucosal EC	Leukocyte arrest
Integrins	LFA-1 ($\alpha_L\beta_2$)	CD11a/CD18	ICAM-1,-2	Leukocytes	Arrest, locomotion
	Mac-1 ($\alpha_M\beta_2$)	CD11b/CD18	ICAM-1	Monocytes, granulocytes	Activation Arrest Locomotion Transmigration
	P150/95 ($\alpha_x\beta_2$)	CD11c/CD18	iC3b	Granulocytes, monocytes	Leukocyte adhesion
	VLA-4 ($\alpha_4\beta_1$)	CD49d/CD29	VCAM-1, MAdCAM-1	Monocytes, eosinophils, lymphocytes, basophils	Adhesion, transmigration
	LPAM-1 ($\alpha_4\beta_7$)	CD49d/CD-	VCAM-1, MAdCAM-1	Lymphocytes	Transmigration
	$\alpha_D\beta_2$	CD11d/CD18	ICAM-3, VCAM-1	Macrophages, dendritic cells	Leukocyte arrest
Selectins	E-Selectin	CD62E	ESL-1, PSGL-1, CD44	EC	Slow rolling
	P-Selectin	CD62P	PSGL-1	EC and platelets	Leukocyte rolling and arrest
	L-Selectin	CD62L	PSGL-1, CD34, MAdCAM-1, GlyCAM-1	Granulocytes,monocytes, lymphocytes	Leukocyte rolling and signalling
Cadherins	VE-Cadherin	CD144	α-,β-catenins	EC	Transmigration
	E-Cadherin	CD324	Integrin αEβ7	Epithelial cells	T cells adhesion to epithelial cells

Abbreviations: CD, cluster of differentiation; VSMC, vascular smooth muscle cells; ESL-1, E-Selectin ligand-1; PSGL-1, P-Selectin glycoprotein ligand-1; ICAM, intercellular adhesion molecule; VCAM-1, vascular cell adhesion molecule-1; PECAM-1, platelet endothelial cell adhesion molecule-1; VLA-4, very late antigen-4; LFA-1, lymphocyte function-associated antigen-1; Mac-1, macrophage antigen-1; MAdCAM-1, mucosal vascular addressin cell adhesion molecule-1; GlyCAM-1, glycosylation-dependent cell adhesion molecule-1; LPAM-1, lymphocyte Peyer's patch adhesion molecule-1; iC3b, inactivated complement component 3b; EC, endothelial cells.

To date more than 50 chemokines and 20 chemokine receptors have been described in humans with homologues and orthologs proteins in mice and other vertebrate species. The expression of these soluble small protein ligands (8-12 KDa) generates a chemotactic gradient that induces leukocyte extravasation from the bloodstream to the site of injury or infection. Leukocyte arrest to the endothelium is mediated by the interaction between chemokines and their receptors, G protein-coupled receptors (GPCRs), which are imbedded in the cell membranes of leukocytes [19]. Chemokine receptors, like all members of the GPCR superfamily, consist of seven transmembrane α helices (TM1-TM7) connected by six loops (three extracellular and three intracellular), an extracellular N-terminus and an intracellular C-terminus. External regions are implicated in the ligand binding and internal regions are associated to G proteins and participate in the intracellular signalling [21]. Chemoattractants and GPCRs are tipically highly promiscuous, which means that a single ligand can bind to different receptors but also a single receptor can bind multiple chemokines with variable affinities. This property occasionally allows chemokines to exhibit diverse effects or responses depending on the local environment and the circumstances in which they exert their action [22]. Furthermore, because chemokine receptors are expressed on several cell types, chemokines are involved in multiple biological functions, including angiogenesis; tissue and vascular remodelling; pathogen removal; antigen presentation; leukocyte activation, migration and survival; chronic inflammation; tissue repair or healing; fibrosis; embryogenesis and tumorigenesis [23, 24].

According to the conserved N-terminal cysteine-containing motif and disulfide bridges, chemokines can be classified into four families or groups: C, C-C, C-X-C and C-X_3-C (**Figure 3**). All of them present two N-terminal cysteine residues and two disulfide bridges except the C chemokine group, which only have one N-terminal cysteine amino acid and one disulfide bridge. C-C chemokines are characterised by the fact that they have the first two cysteines adjacent, however, C-X-C and C-X_3-C families have one or three amino acid residues between the two N-terminal cysteines respectively [25]. The majority of the chemokines belong to the C-C chemokine family as it is the case of the monocyte chemoattractant protein-1 (MCP-1/CCL-2) and the regulated upon activation, normal T cell expressed and secreted (RANTES/CCL-5), which are potent chemotactic factors implicated in leukocyte recruitment [26, 27]. The chemokines growth-regulated oncogene alpha (GROα/CXCL-1) and fractalkine (CX_3CL-1), belonging to the C-X-C and C-X_3-C

families respectively, also regulate inflammatory cell infiltration. Unlike the rest of chemokines, fractalkine can exist in a membrane-bound or soluble form. Attached to the membrane, fractalkine promotes leukocyte adhesion whereas the soluble form has a potent chemoattractant activity. Due to the fact that these chemokines have a strong implication in vascular remodelling, several studies have shown their critical role in the development of cardiovascular diseases such as atherosclerosis and abdominal aortic aneurysm [27, 28].

Apart from their structural classification, chemokines can also be grouped attending to their expression patterns and functions into inflammatory or homeostatic. Inflammatory chemokines are also known as inducible chemokines as their expression is induced by pro-inflammmatory mediators. The interaction between the chemokines and their receptors, expressed by activated leukocytes, epithelial and endothelial cells and fibroblasts under inflammatory conditions, promotes leukocyte recruitment and migration to the injured or infected tissue [22]. By contrast, homeostatic chemokines and their receptors are constitutively expressed in certain tissues and cell types and they are involved in homeostatic functions including T cell development, stem cell migration and lymphoid organogenesis. It has also been reported that some chemokines can have both inflammatory and homeostatic functions [19].

In conclusion, the extense and diverse number of chemokines together with their high degree of promiscuity when binding to their receptor and their tightly-regulated transcriptional expression make chemokines a sophisticated and complex communication system used by different types of immune cells to regulate leukocyte transmigration to the inflammatory focus [19, 22].

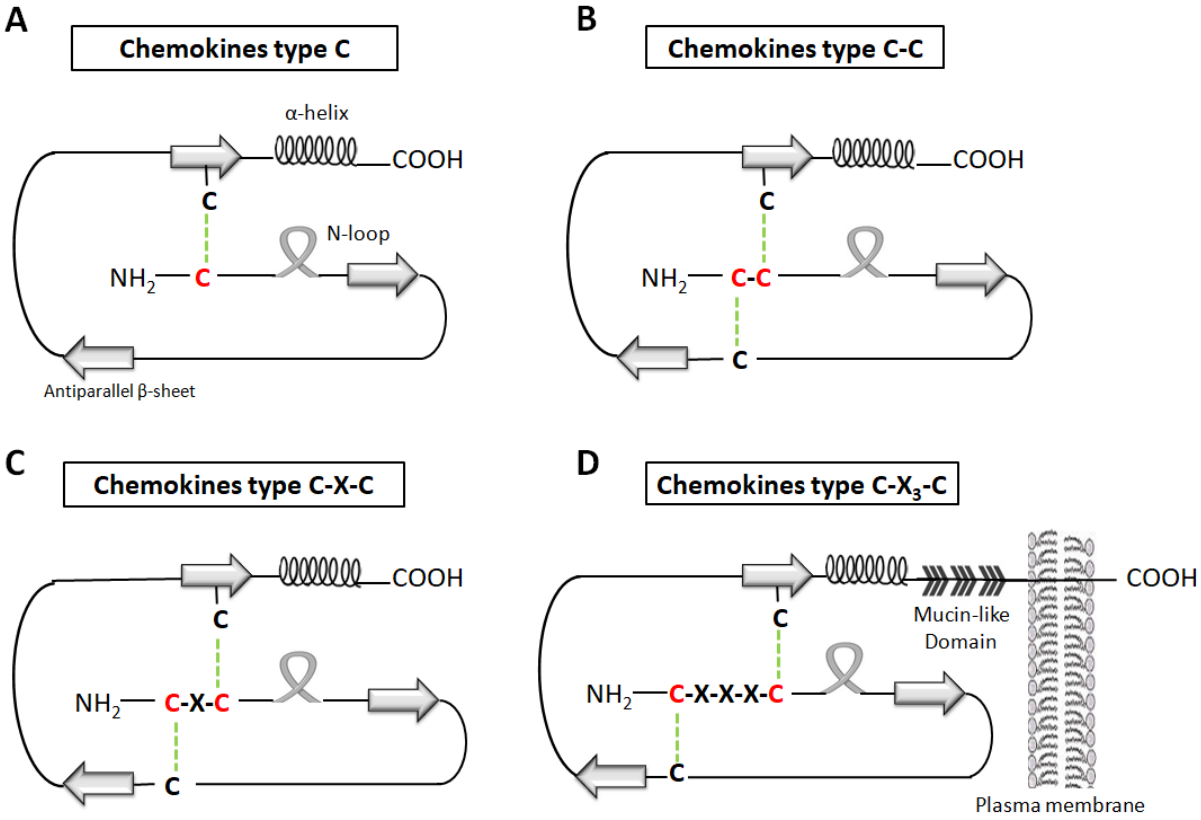

Figure 3. Structure of the different chemokine families. According to the conserved N-terminal cysteine-containing motif, chemokines can be divided into four families: chemokines type C (**A**), chemokines type C-C (**B**), chemokines type C-X-C (**C**) and chemokines type C-X_3-C (**D**). Letter C, in red, refers to a cysteine amino acid and letter X refers to any amino acid different from cysteine. Discontinuous lines in green represent disulfide bridges between cysteine amino acids. Transmembrane region of CX_3CL-1 can be visualised going through the lipid bilayer of the plasma membrane. Adapted from Balakin *et al*. 2008 [25].

1.1.2.2.2 Tumor necrosis factor-α

Tumor necrosis factor alpha (TNFα) is a key pro-inflammatory cytokine involved in endothelial and leukocyte activation. This small molecule (17 KDa) is mainly secreted by monocytes and activated macrophages but also endothelial cells, T-lymphocytes, B-lymphocytes, mast cells, glial cells, natural killer cells and tumor cells are additional sources of TNFα [29-31]. The release of this cytokine can be induced by diverse stimuli such as interleukins, interferon-γ, tumor cells, viruses, endotoxins or antigens derived from funghi or parasites [31]. In the presence of these stimuli, TNFα is considered a primary mediator of the inflammatory acute phase

response and promotes the production and secretion of secondary mediators including interleukins, prostaglandins, growth factors, leukotrienes, bradykinin, cytokines and chemokines [31].

Increased levels of TNFα are involved in the pathogenesis of several metabolic and vascular diseases including atherosclerosis [32], rheumatoid arthritis [33], heart failure [34] and myocardial infarction [35], obesity [36] and metabolic syndrome [37] in which chronic inflammation plays a key role [38].

TNFα acts through the activation of the transcription factor known as nuclear factor kappa-light-chain-enhancer of activated B-cells (NF-κB) [39] and the signalling pathways mediated by p38 proteins, which are a class of mitogen-activated protein kinases (MAPKs) [40]. In the endothelium, the activation of NF-κB and p38 MAPK leads to a greater expression of adhesion molecules implicated in leukocyte recruitment and promotes the synthesis of pro-inflammatory chemokines and cytokines that often induce a positive feedback in these routes enhancing the inflammatory process [40, 41].

1.1.2.3 Leukocyte adhesion

Leukocyte rolling triggers multiple intracellular signalling cascades in order to activate leukocyte integrins, which are essential to get a firm leukocyte adhesion. This signalling process is controlled by several chemokines which via GPCR activate integrins expressed on the surface of leukocytes [42].

Integrins are heterodimeric transmembrane receptors that consist of two different subunits: α (alpha) and β (beta). Both subunits are type I transmembrane glycoproteins and are bound by non-covalent interactions. To date, 18 α-subunits and 8 β-subunits have been described in mammals and different combinations between them allow to conform until 24 integrin αβ dimers [43]. The most remarkable integrins involved in leukocyte adhesion are: the very late antigen-4 (VLA-4 or $\alpha_4\beta_1$ or CD49d/CD29), which is expressed on all leukocytes except neutrophils [44]; the lymphocyte function-associated antigen-1 (LFA-1 or $\alpha_L\beta_2$ or CD11a/CD18), that is expressed on all effector leukocytes [45]; the macrophage antigen-1 (Mac-1 or $\alpha_M\beta_2$ or CD11b/CD18), which can be found in granulocytes and monocytes; P150/P95 ($\alpha_x\beta_2$ or CD11c/CD18), which is expressed on granulocytes and monocytes; the Lymphocyte Peyer's patch adhesion molecule-1 (LPAM-1 or $\alpha_4\beta_7$ or CD49d/CD-), which is found in lymphocytes and the integrin $\alpha_D\beta_2$ (CD11d/CD18), which is

expressed on dendritic cells and macrophages [46] (**Table 1**). These integrins, with the exception of Mac-1, are not constitutively activated on leukocytes, however, their activation is required to ensure a firm adhesion between leukocytes and endothelial cells. This activation process may occur though the interaction of integrins with their ligands, which are CAMs from the immunoglobulin superfamily [46].

CAMs from the immunoglobulin superfamily (IgCAMs) are transmembrane proteins that have one to seven extracellular immunoglobulin domains anchored to the plasma membrane by a single transmembrane helix. IgCAMs include a wide number of adhesion proteins that bind ligands on the surfaces of other cells. These interactions can be classified as homophilic (identical IgCAMs expressed on different cells interact between them) or heterophilic (an IgCAM interacts with a different IgCAM or an integrin) [47]. The most studied IgCAMs are: the intercellular adhesion molecule (ICAM)-1 and ICAM-2, the vascular cell adhesion molecule (VCAM)-1, the mucosal vascular addressin cell adhesion molecule-1 (MAdCAM-1), the platelet and endothelial cell adhesion molecule-1 (PECAM-1) and the junctional adhesion molecules (JAMs), which are mainly expressed on endothelial cells, although some can be found on leukocytes, platelets and other cells (**Table 1**) [48-50]. Frequently, these IgCAMs bind to integrins expressed on the surface of leukocytes. For instance, the integrin VLA-4 interacts with VCAM-1 and LFA-1 and Mac-1 bind to ICAM-1. This attachment secures a proper leukocyte arrest as VCAM-1 and ICAM-1 are anchored to the cytoskeleton of endothelial cells by diverse actin adapter proteins [10, 51]. Once leukocytes are firmly adhered to the endothelium, they reorganise their actin cytoskeleton and extend highly dynamic membrane protusions to generate a contractile uropod with the aim of starting to crawl along the endothelium following a chemoattractant gradient to the inflammatory focus. Leukocyte crawling allows these cells to explore and scan the endothelial surface in order to find a permissive site for transendothelial migration [52].

1.1.2.4 Leukocyte transmigration

To complete the extravasation process, leukocytes must cross the endothelium and migrate to the inflammatory focus. This event is denominated transendothelial migration (TEM) or diapedesis and it is considered the last stage of the leukocyte infiltration cascade. Leukocyte TEM can be transcellular, if it takes place through the endothelial cell body, or paracellular, if it occurs through junctions

between adjacent endothelial cells. In any case, both types of TEM require molecular changes in the endothelium to enable the arrival of leukocytes to the inflamed tissue [53].

Concerning transcellular diapedesis, it occurs via a pore formation through the endothelial layer. This process is mediated by membrane fusion and fission events regulated by fusogenic proteins [54].

Regarding paracellular diapedesis, which is the most common type of TEM, a junctional remodelling and an endothelial cell surface redistribution are required. PECAM-1 and CD99, a highly glycosylated transmembrane protein, are involved in the TEM process. PECAM-1, also known as CD31, belongs to the immunoglobulins superfamily and it is expressed on the borders of endothelial cells and on platelets and leukocytes. CD99 is expressed on endothelial cells, monocytes and neutrophils. Homophilic interactions between leukocyte and endothelial PECAM-1 and leukocyte and endothelial CD99 are needed for TEM [13]. Diapedesis is also mediated by the vascular endothelial (VE)-cadherin, which is considered one the most important regulators of the endothelial integrity. For that reason, destabilisation of VE-cadherin is crucial for TEM as its loss of function contributes to increase junctional permeability [55]. Furthermore, JAMs expressed on platelets, leukocytes and endothelial cells also control leukocyte migration by their heterophilic or homophilic interactions between JAMs or integrins expressed by the connected cells [56] (**Table 1**).

1.2 Abdominal aortic aneurysm

1.2.1 General points

Abdominal aortic aneurysm (AAA) is a cardiovascular disease characterised by a permanent, irreversible and local dilatation of the aorta (**Figure 4**), which is the largest artery in the human body and the most important one supplying blood to the lower limbs [57]. The main risk factors for AAA development are age older than 65 years, male gender, smoking, high blood pressure, presence of cardiovascular and metabolic diaseases such as atherosclerosis, obesity and diabetes and a family history of AAA [58].

Currently, the prevalence of AAA is 4–7% in males over the age of 65, and 1–2% in females [59]. Chronic vascular inflammatory conditions contribute to the progression of AAA until occasionally rise the fatal point of its rupture, an event associated with a high mortality rate [60]. Thus, AAA has been reported to be the main cause of death in approximately 1-2% of total death in developed countries [61].

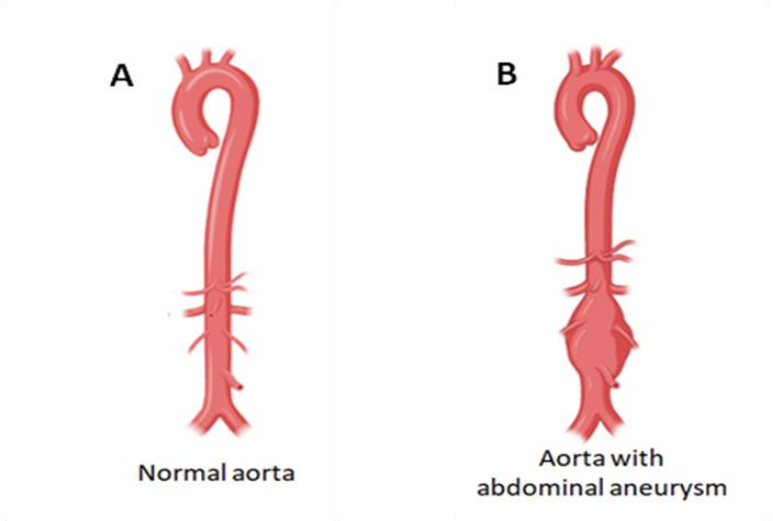

Figure 4. Abdominal aortic aneurysm. (A) Normal aorta under healthy conditions. (B) Aorta with an aneurysm located in the abdominal region. Created with BioRender.com

AAA is diagnosed when the diameter of the abdominal aorta is at least 50% greater than its normal size [62]. However, very often, aneurysm rupture occurs without a previous diagnosis as, surprisingly, most patients that develop this pathology are asymptomatic. For this reason, most cases of AAA are detected incidentally on imaging techniques such as abdominal ultrasonography or computed tomography when they are performed for other purposes [60]. Nowadays, surgery is the only clinical therapy known to be effective to prevent AAA rupture but it is a complex procedure associated with a significant mortality. For this reason, it is only carried out when the risk of spontaneous rupture exceeds the risk of surgical repair [59]. Therefore, because of the high morbidity and mortality rate associated to surgical interventions, new pharmacological treatments are needed to prevent AAA development and rupture.

AAA affects the three layers of the aortic wall. The main aberrant remodelling changes include endothelial damage in the intima, vascular smooth

muscle cell (VSMC) loss in the media and extracellular matrix (ECM) degradation in the media and adventitia [61].

Infiltration of immune cells in the media and adventitia during chronic inflammation promotes oxidative stress and induces the expression of several inflammatory cytokines and proteases that degrade elastin and collagen fibers, the major components of the ECM, contributing to VSMC loss. This event is enhanced by the action of the TNFα secreted by activated macrophages which causes VSMC apoptosis [62]. Apoptotic VSMCs secrete the chemokine CCL-2/MCP-1 that attracts monocytes and other leukocytes to the endothelium. Then, the recruited monocytes differentiate into M1 or M2 macrophages, with inflammatory or anti-inflammatory properties, respectively. This is a key process in AAA development as an overexpression of inflammatory macrophages in the media and adventitia can worsen AAA condition (**Figure 5**) [27, 63].

Degradation of collagen and elastin weakens the integrity of the ECM and reduces its mechanical function. This process is also mediated by metalloproteinases (MMPs). MMPs are a family of zinc-dependent enzymes with proteolytic activity that are mostly secreted in an inactive form, as a zymogen, and their activation requires a proteolytic action [58]. MMPs are responsible of ECM remodelling and degradation and their activity is controlled and regulated by their endogenous inhibitors, the tissue inhibitors of metalloproteinases (TIMPs) [61]. Alterations in the ratio MMPs/TIMPs can promote AAA development. Frequently, imbalances on this ratio are due to an increase of MMPs expression. Under standard conditions, endothelial cells, VSMCs, and adventitial fibroblasts are the only ones that controls MMPs production, however, during AAA progression, inflammatory cells become additional sources of MMPs [64].

Angiogenesis is also implicated in AAA pathogenesis [65]. It is defined as the growth of new capillary branches from existing blood vessels. It is a highly regulated process that includes several events such as degradation of the ECM, migration, differentiation and proliferation of endothelial cells and formation of new capillaries [66]. Under an inflammatory status, the immune cells that have been recruited to the inflamed tissue secrete TNFα and interleukin (IL)-1β, cytokines that induce the expression of the vascular endothelial growth factor (VEGF) [65, 66]. VEGF is considered one of the most important regulators of the vascular homeostasis as it controls vascular permeability and angiogenesis. During angiogenesis, VEGF

induces proliferation and migration of endothelial cells and promotes their survival. Furthermore, VEGF can affect vascular endothelial integrity by altering proteins such as VE-cadherin in the intercellular junctions. This process is also enhanced by the MMP activity that facilitates ECM degradation, being MMP-2 and MMP-9 the most remarkable MMPs during this process. Consequently, vascular permeability is increased and it allows endothelial cells to proliferate and migrate and immune cells to extravasate to the inflamed tissue [67]. Unfortunately, if the endothelium remains dysfunctional and the immune response is not abated, a chronic inflammatory state will govern the vascular system increasing the risk of developing AAA.

For many years, AAA has been deeply studied in order to find effective pharmacological therapies that prevent its development and progression. Several strategies including the use of agents that block MMP activity or the use of angiotensin converting enzyme (ACE) inhibitors or angiotensin type-1 receptor blockers (ARBs) have been considered to minimise its risk of rupture. Furthermore, diverse clinical studies have been carried out to evaluate the effectiveness of these drugs. Nevertheless, clinical data did not reveal very successful results as all therapies failed to inhibit AAA growth or rupture [68]. Consequently, surgical repair is nowadays the only effective treatment for AAA. However, surgery is associated with a high mortality rate. For that reason, further research is needed to discover new pharmacological targets involved in AAA progression with the aim of improving its pathological condition.

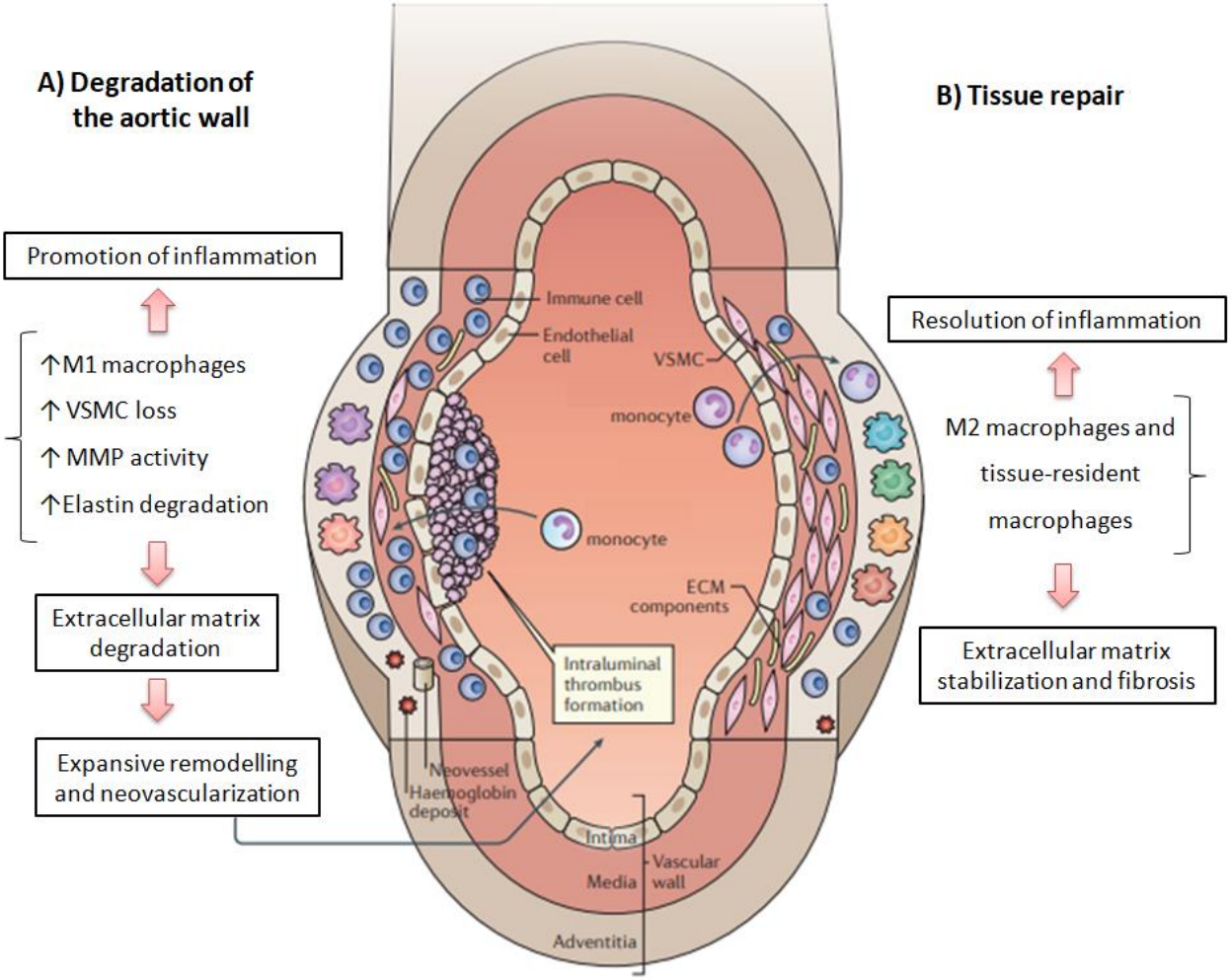

Figure 5. Pathophysiology of the abdominal aortic aneurysm (AAA). (**A**) Degradation of the aortic wall. AAA is characterised by a vascular remodelling that affects the three layers of the aortic wall. Leukocyte infiltration and M1 macropage differentiation, elastin degradation, VSMC loss and excessive MMP activity lead the aorta to a chronic inflammatory state that weakens the vascular wall (**B**) Tissue repair. The inflammatory process associated to AAA progression can be delayed through compensatory mechanisms that contribute to maintain the integrity of the aorta. An increased expression of M2 macrophages in the lesion counteracts ECM deterioration and promotes its stabilization. Additionally, the anti-inflammatory mediators and pro-fibrotic factors released by M2 macrophages contribute to the resolution of inflammation and to the repair of the injured aortic tissue. Abbreviations: VSMC, vascular smooth muscle cell; MMP, extracellular matrix metalloproteinase; ECM, extracellular matrix. *Adapted from Raffort et al. 2017* [63].

1.2.2 The renin-angiotensin system and its implication in AAA

Angiotensin II (Ang II) is a peptide hormone produced by the renin-angiotensin system that controls the blood pressure and the hydroelectrolytic balance [69]. At the vascular level Ang II acts as a potent vasoconstrictor agent increasing blood pressure and, in the kidney, Ang II promotes the secretion of aldosterone from the adrenal glands favouring the retention of sodium and water in the renal tubules [70]. Furthermore, Ang II has been reported to have important proliferative, pro-inflammatory and pro-fibrotic effects in the body playing a key role in autoimmune, inflammatory, metabolic and cardiovascular diseases [71-75].

The renin-angiotensin system (RAS) comprises a number of enzymatic cascades involving serial proteolytic digestions mediated by different enzymes to produce Ang II (**Figure 6**) [76].

Ang II is obtained from the circulating substrate angiotensinogen, which is constitutively released from the liver. This substrate is cleavaged by renin, an enzyme synthesised in the kidney and released into the circulation to generate Ang I. To date, renin is the only known enzyme capable of digesting angiotensinogen, that is why renin is considered a rate-limiting enzyme of the RAS as angiotensinogen is usually present in excess [75, 77]. Just in certain circumstances such as low systemic blood pressure, sodium deprivation, hypovolemia or sympathetic stimulation, the synthesis of renin can be increased [78].

The next step in RAS cascade (**Figure 6**) is the conversion of the inactive decapeptide Ang I into the octapeptide Ang II, the main effector product of the RAS, by the circulating angiotensin converting enzyme (ACE) [79]. ACE is a type I integral membrane protein mainly expressed on the vascular endothelium but also present in the adventitial layer of the aorta and pulmonary artery and in different organs such as lung, intestine, kidney and heart [80-82]. In addition, ACE can be found as a soluble form circulating in plasma or cerebrospinal fluids as the result of an enzymatic cleavage at the transmembrane domain of the membrane-attached ACE [81]. Unlike renin, ACE is not a substrate-specific enzyme as it can cleavage not only Ang I but also substrates such as the vasodilator bradykinin. This aspect coupled with the fact that ACE expression is not affected by Ang II concentration changes, suggests that renin is the main limiting factor in the Ang II production and its

vascular concentration only depends on the expression levels of the circulating renin [75].

Finally, another alternative pathway to generate Ang II in cardiac, vascular and renal tissue is that one mediated by the enzyme chymase, a serine protease that generates Ang II from Ang I in an ACE-independent manner. Chymase is expressed in the heart by mast cells, cardiac fibroblasts, vascular endothelial cells and mesenchimal interstitial cells and in the kidney by SMCs during acute and chronic tissue injury and remodelling [70, 78].

The biological actions of Ang II are mediated through the interaction of this peptide with the angiotensin receptor type 1 (AT_1R) or type 2 (AT_2R). These receptors are located on the cell surface and belong to the GPCR family [81, 83].

The AT_1R is mainly expressed on diverse cells and organs including VSMCs, endothelium, kidney, adrenal glands, brain and adipose tissue [84]. Whereas human cells only express a single AT_1R, rodents such as rats and mice present two subtypes namely AT_1AR and AT_1BR, displaying the first one a major homology to the human AT_1R and a similar expression profile [71].

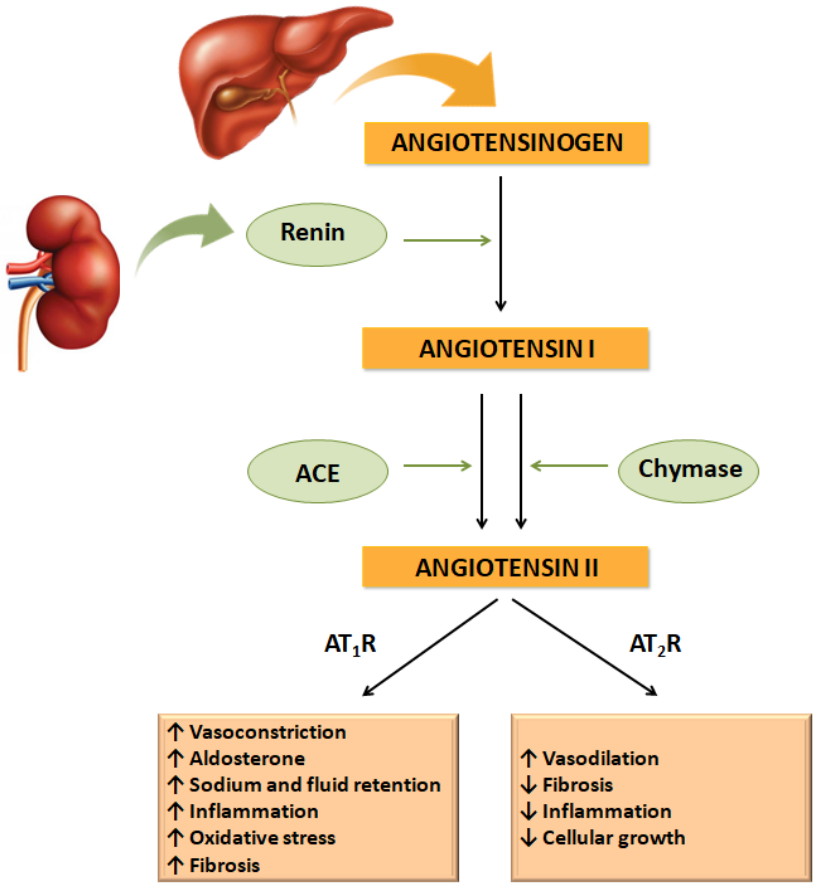

Figure 6. The renin-angiotensin system (RAS). Renin is an enzyme synthesised in the kidney that cleavages the circulating angiotensinogen released from the liver to generate Ang I. Then, Ang I is converted into Ang II by the ACE or alternatively by the chymase. Ang II effects differ depending on the receptor it binds, AT_1R or AT_2R. Abbreviations: ACE, angiotensin converting enzyme; AT_1R, angiotensin type 1 receptor; AT_2R, angiotensin type 2 receptor. Adapted from Benigni *et al.* 2010 [70].

Ang II signalling via AT_1R has been reported to modulate inflammatory and immune responses. It is known that the stimulation of AT_1R promotes the synthesis of prostaglandins and VEGF resulting in an increase of the vascular permeability, which is the first event in the onset of the inflammatory process. AT_1R also mediates the activation of p38 MAPK and NF-κB, whose signalling pathways lead to an increase in the secretion of pro-inflammatory mediators such as TNFα and CCL-2/MCP-1 by resident cells, and to a greater expression of different MACs such as P-selectin, ICAM-1 and VCAM-1 on vascular endothelial cells and SMCs. Consequently, immune cells migrate to the inflamed tissue to solve the injury or infection [71, 85, 86].

Furthermore, it is known that AT_1R signalling plays a crucial role in the regulation of arterial blood pressure and renal function [87]. In the kidney and VSMCs, Ang II via AT_1R stimulates proximal tubular sodium reabsorption and promotes vasoconstriction, respectively. In adrenal glands, Ang II-AT_1R interaction stimulates aldosterone production, which also contributes to renal sodium reabsorption. Consequently, a hyperactivation of RAS can provoke hypertension [88]. Besides, an excessive AT_1R stimulation may induce renal tissue injury because of the vasoconstrictor and inflammatory properties of the Ang II via NF-κB activation. The main features of renal damage are known to be a high level of glomerular protein filtration, ECM deposition and glomerular fibrosis and inflammation [89].

In addition, dysregulation of the RAS not only can induce hypertension and inflammatory, renal and cardiovascular diseases but also it can promote metabolic disorders such as obesity and insulin resistance. Several studies carried out in mice and humans show that the overexpression of AT_1R on adipocytes and the local increase of the Ang II production in these cells and at systemic level, induce adipose dysfunction and promote the development and progression of visceral obesity [90-92].

In the last years, several RAS inhibitors have been used for the clinical treatment of these pathologies. For instance, ACE inhibitors have been reported to be effective for treating hypertension, heart failure, myocardial infarction and diabetic nephropathy as they inhibit Ang II production [93]. Additionally, AT_1R blockers have also shown beneficial effects in the treatment of these disorders reducing the morbidity and mortality of these patients [94].

As previously mentioned, RAS is implicated in several inflammatory diseases whose most important pathological features are mediated by the stimulation and activation of the Ang II/AT_1R axis. Ang II, the main effector of RAS, through AT_1R, regulates several processes such as endothelial dysfunction, vascular remodelling and inflammation and plays a critical role in the development of AAA [95-97].

Previous studies have showed that Ang II/AT_1R interaction induces the release of IL-6 and IL-4 and markedly increases TNFα expression, whose signalling through p38 MAPK phosphorylation and NFκB activation further enhances the expression of CAMs including P-selectin, E-selectin, ICAM-1 and

VCAM-1 and the production of pro-inflammatory cytokines and chemokines such as CXCL-8/IL-8, CCL-2/MCP-1, CCL-5/RANTES and CX_3CL-1/fractalkine. The expression of these pro-inflammatory mediators promotes monocyte infiltration and macrophage accumulation in the vascular wall. Furthermore, oxidative stress caused by an increase of reactive oxygen species (ROS) in vascular cells activates MMPs like MMP-2 and MMP-9. This process is induced by Ang II via AT_1R and provokes ECM degradation, which is one of the main mechanisms involved in AAA initiation and progression. Ang II-induced ROS production also promotes VSMCs apoptosis. The loss of VSMCs together with elastin disruption seriously affects the integrity of the arterial wall contributing to AAA growth (**Figure 7**) [86, 98].

During the last years, several animal models have been used with the aim of finding new therapeutic strategies to treat AAA. In 2000, an experimental model was established by Daugherty et al. [99] to assess the development and treatment of AAA. In this preclinical model, AAA is induced by a continuous subcutaneous Ang II infusion in apolipoprotein E deficient ($apoE^{-/-}$) mice. As a result, the aortic wall of Ang II-infused mice undergoes a vascular remodelling that is characterised by macrophage infiltration, MMPs release and ECM degradation, angiogenesis, loss of VSMCs and deterioration of the elastic layer; pathological features that promote AAA development and progression or even its rupture. Simultaneously, it was demonstrated that Ang II can be also infused in low density lipoprotein (LDL) receptor knockout mice fed with a fat diet, obtaining a similar pattern of AAA development [100, 101].

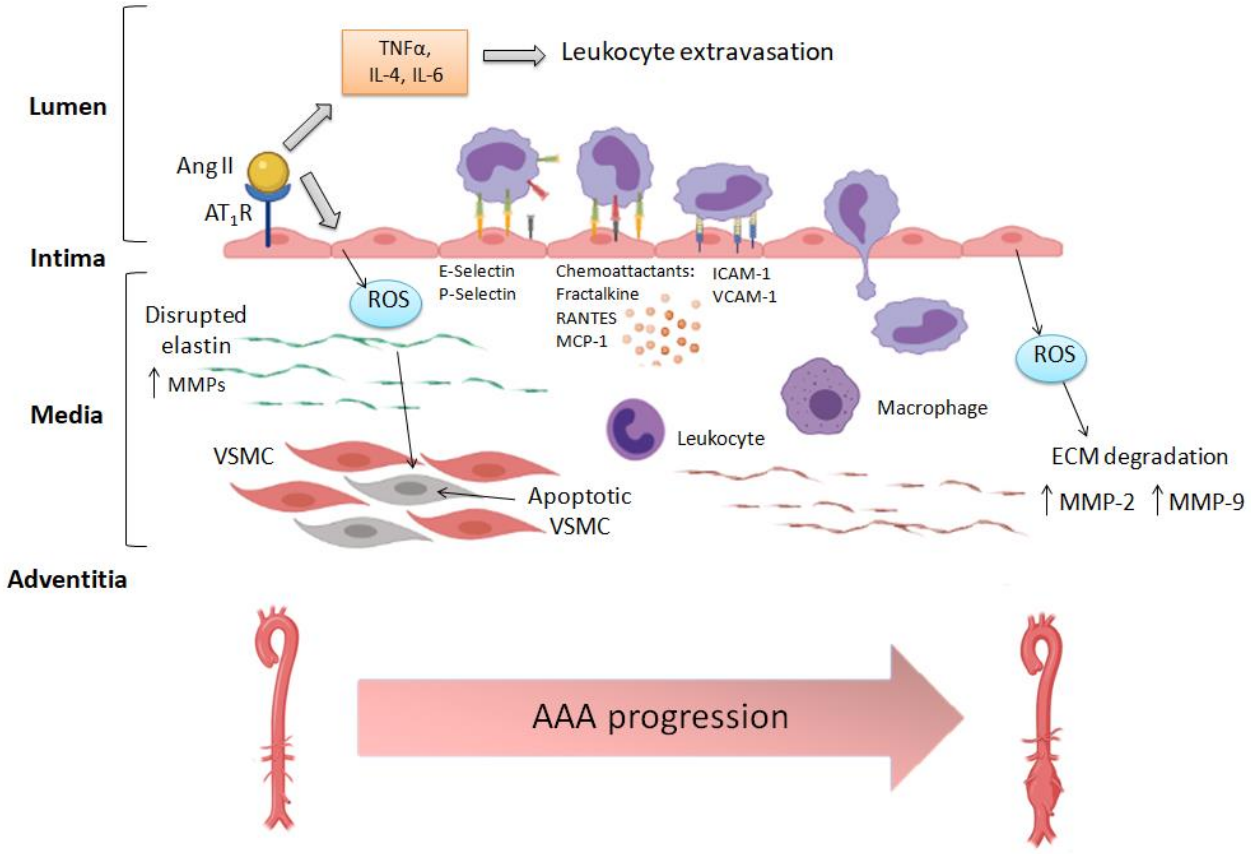

Figure 7. Effect of AT_1R activation on leukocyte infiltration and vascular remodelling. The interaction Ang II/AT_1R triggers an inflammatory response that promotes AAA development. Ang II-induced TNFα, IL-4 and IL-6 release leads to endothelial activation and leukocyte recruitment, which are processes mediated by E-Selectin and P-Selectin increased expression. Then, a chemotactic gradient established along the endothelium regulates leukocyte adhesion and ICAM-1 and VCAM-1 expression allows immune cells extravasation. Ang II signalling also increases ROS production in the vascular endothelium. ROS production increase MMP activity, which promotes ECM remodellig and VSMCs apoptosis. The loss of VSMCs and elastin degradation associated with macrophage accumulation in the media contributes to the weakening of the vessel wall and AAA growth. Abbreviations: Ang II, angiotensin II; AT_1R, angiotensin receptor type 1; TNFα, Tumor Necrosis Factor alpha; IL, interleukin; VSMCs, vascular smooth muscle cells; ROS, reactive oxygen species; ECM, extracellular matrix; MMP, metalloproteinase; RANTES, regulated upon activation normal T cell expressed and presumably secreted; MCP-1, monocyte chemoattactrant protein-1, AAA, abdominal aortic aneurysm. Adapted from Zhao *et al.* 2021 [98] with BioRender.com.

1.2.3 Sodium glucose cotransporter type 2 inhibitors

In the last years, numerous studies have reported the beneficial effects of gliflozins (canagliflozin, dapagliflozin, empagliflozin and ipragliflozin) on body weight, lipid profile, blood pressure, endothelial function and, interestingly, most of them are known to exert cardioprotective [102-104] and renoprotective [105] effects as well. Recently, preclinical and clinical studies have demonstrated the effectiveness of these antihyperglycaemic agents on the treatment of cardiovascular and metabolic diseases such as atherosclerosis [106], heart failure [107], non-alcoholic steatohepatitis [108, 109] and obesity [110-112].

The sodium-glucose cotransporter type 2 (SGLT-2) is codified by the *SLC5A2* gene [113] and it is expressed on the luminal surface of the epithelial cells located along the S1 and S2 segments of the proximal tubule of the nephron, where the majority of the glucose reabsorption takes place (**Figure 8**). SGLT-2 allows the transport of the glucose from the apical to the basolateral membrane of the renal proximal tubular cells. This action is mediated by the sodium-potassium pump, which generates a sodium gradient that allows SGLT-2 to introduce a molecule of glucose and a sodium ion into the epithelial cell (**Figure 9**) [114]. Thus, this cotransporter is involved in the regulation of blood pressure [115] and glucose metabolism [113].

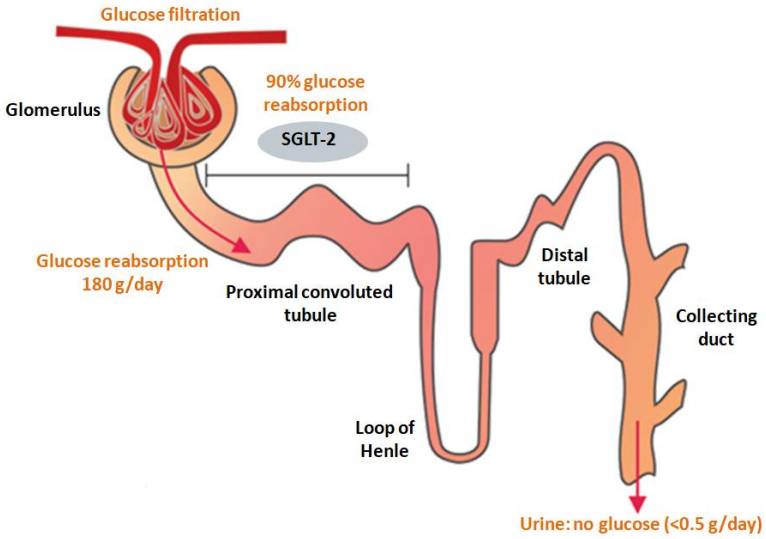

Figure 8. Nephron structure and SGLT-2 localization. The majority of the filtered glucose in the glomerulus is then reabsorbed in the proximal convoluted tubule of the nephron, where SGLT-2 is mainly expressed. Adapted from Kalra *et al*. 2016 [116].

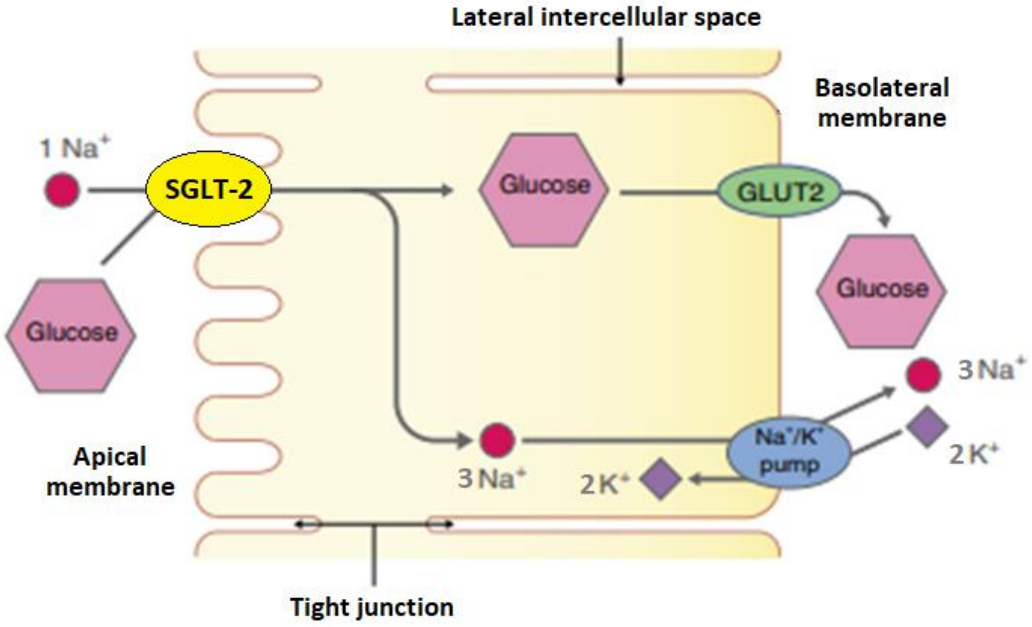

Figure 9. Glucose reabsorption from the apical to the basolateral membrane of the renal proximal tubular cells. The Na^+/K^+ pump releases three sodium ions (Na^+) for every two potassium ions (K^+) entering into the epithelial cell, creating inside a negative electrical potential, which is used by the SGLT-2 to introduce a molecule of glucose together with a Na^+ ion in the epithelium. Finally, the accumulated glucose is released through the basolateral membrane by the glucose transporter-2 (GLUT-2). Adapted from Ghezzi *et al*. 2018 [114].

Empagliflozin is a potent selective SGLT-2 inhibitor whose molecular formula is $C_{23}H_{27}ClO_7$ and its IUPAC name is (2S,3R,4R,5S,6R)-2-[4-chloro-3- [[4-[(3S)-oxolan-3-yl]oxyphenyl]methyl]phenyl]-6-(hydroxymethyl)oxane-3,4,5-triol [117]. The chemical structure of empagliflozin is shown in **Figure 10**.

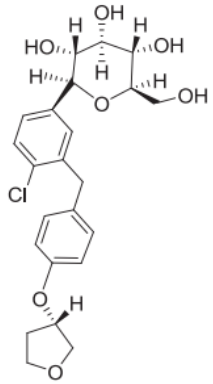

Figure 10. Chemical structure of empagliflozin. Adapted from Chawla *et al.* 2019 [117].

The clinical use of empagliflozin was approved by the Food and Drug Adminstration (FDA) in 2014, since then, empagliflozin treatment has been demonstrated to reduce renal reabsorption of glucose from the glomerular filtrate and increase its urinary excretion. This event can cause natriuresis and glycosuria and it may rise the risk of urinary tracts infections [118]. For that reason, a correct gene regulation of the *SGLT-2* expression is primordial to maintain appropiate plasma glucose levels. In type 2 diabetes mellitus (T2DM), SGLT-2 is overexpressed and renal glucose reabsorption threshold is increased, exceeding the normal rate of 180 g/day of glucose uptake. This fact may exacerbate the hyperglycemic condition that affects most of the diabetic patients [116]. Although further studies are needed to better understand the pathogenesis of diabetic nephropathy, there is evidence that hyperglycemia, albumin and Ang II upregulate the expression of SGLT-2 in T2DM [119].

In the last years, empagliflozin has been shown to inhibit SGLT-2 exerting beneficial effects on the treatment of T2DM. However, the most remarkable fact is that this inhibitor seems to also improve cardiovascular condition in diabetic profiles.

The EMPA-REG OUTCOME trial (BI 10773 [Empagliflozin] Cardiovascular Outcome Event Trial in Type 2 Diabetes Mellitus Patients) designed to determine the long-term safety of the SGLT-2 inhibitor empagliflozin in a cohort of patients with T2DM and high cardiovascular risk, reported a markedly decreased body weight, blood pressure and plasma glucose levels compared with placebo and also a reduced risk of heart failure, myocardial infarction and mortality rate for cardiovascular causes [120, 121].

Additionally, previous studies carried out in animal models of atherosclerosis demonstrated that empagliflozin significantly reduced the atherosclerotic lesion and this effect was accompanied by mitigation of the inflammatory response and improvement of insulin reisistance condition [122-124]. Similar results were obtained in other studies carried out in streptozotocin-diabetic mice. Regression of the atherosclerotic plaque was greater in mice treated with empagliflozin than in vehicle-treated mice and this effect was associated with an attenuation of the endothelial dysfunction and a lower content of infiltrated immune cells in the lesion [125, 126]. In agreement with these findings, a recent study in an experimental model of metabolic syndrome has also reported the efficacy of empagliflozin in reducing systolic blood pressure and improving endothelial dysfunction and cardiac remodelling in obese ZSF_1 rat [127].

However, in spite of the cardioprotective function of empagliflozin previously described, the impact of this SGLT-2 inhibitor in the development of AAA has not been explored. In line with these promising cardiovascular benefits obtained under empagliflozin treatment, the present Thesis is focused on studying the effect of the SGLT-2 inhibitor empagliflozin on the progression of AAA in Ang II-infused $apoE^{-/-}$ mice.

1.3 Obesity and adipose tissue dysfunction

Obesity is defined as an excess of body weight due to fat accumulation [128]. In the clinical practice, a gradual scale has been established to classify each individual in a body weight status according to the body mass index (BMI). BMI is calculated as the body weight expressed in kilograms divided by height in squared meters [129]. Depending on the value of the BMI, subjects can be considered to be underweight, normal, overweight or obese. The ranking of BMI and the body weight status associated to it are shown in **Table 2** [130].

Obesity is a chronic multifactorial metabolic disease whose prevalence is reaching pandemic proportions and nowadays is a major and worldwide health problem [131, 132]. Some of the main concerns are linked to the wide spectrum of comorbidities related to this disorder. These include T2DM, hypercholesterolemia, hypertension, metabolic syndrome, fatty liver disease, adipose tissue fibrosis, obstructive sleep apnoea and cardiovascular diseases [128, 133].

In most cases, the onset of obesity lies in an imbalance between food intake and energy expenditure. A high caloric consumption and poor physical activity can contribute to the development of this metabolic disease. However, diet is not the only one factor implicated in the etiology of obesity. Genetic, psychological, physiologic, social, environmental, economic, and even political factors can also influence the progression of this pathology [134].

Although a healthy lifestyle based on a balanced diet and daily exercise is beneficial to fight obesity [135, 136], frequently, its effect on the body weight is not high enough to allow individuals to achieve normal values of BMI. For that reason, most of the obese patients require pharmacological treatments that help them to decrease their corporal weight [137, 138].

Table 2. Weight status classification according to Body Mass Index (BMI). Adapted from Abdelaal *et al*. 2017 [130].

BMI (Kg/m^2)	Classification	Obesity Class
< 18.5	Underweight	
18.5 – 24.9	Normal	
25 – 29.9	Overweight	
30 – 34.9	Obesity	I
35 – 39.9	Severe obesity	II
40 – 49.9	Morbid obesity	III
≥ 50	Severe morbid obesity	IV

Abbreviations: BMI, Body Mass Index

Adipose tissue (AT) is considered an immune and endocrine organ which is implicated in energy storage and also responsible for keeping metabolic homeostasis [139]. Several roles have been attributed to this active tissue including synthesis and production of diverse cytokines, extracellular matrix compounds,

hormones and different vasoactive and growth factors whose release to the systemic circulation exerts pleiotropic effects in the organism [140]. It is known that a dysregulation or dysfunction of the AT can impair the correct function of the energy metabolism. A dysfunctional AT is characterised by a chronic inflammatory state which is accompanied by ECM remodelling and angiogenic events. These processes can lead to a situation of metabolic stress, fat accumulation and alterations in the energy consumption resulting in the development of metabolic disorders such as obesity, which may appear associated to other comorbidities including insulin resistance and T2DM [141].

AT is composed by adipocytes and adipocyte progenitors but also contains other types of cells such as fibroblasts, immune cells and endothelial cells [142]. AT can be differentiated into white AT (WAT) or brown AT (BAT) depending on its metabolic function. The first one is implicated in fat storage and the second one is involved in thermogenesis [143]. In turn, WAT can be divided in subcutaneous AT (SAT) and visceral AT (VAT). These two types of WAT differ in their corporal localization and in their immunological and metabolic properties and actions. SAT can be found under the skin whereas VAT is present in the internal organs of the abdominal cavity [144] and it shows a higher metabolic activity. Under healthy and pathological conditions, VAT is more vascularised and owns widespread blood irrigations, it contains more immune and inflammatory cells and harbours a bigger number of large adipocytes in comparation with SAT. VAT plays a key role in free fatty acids synthesis and glucose uptake, by contrast, SAT tends to absorb circulating free fatty acids and triglycerides. All these features make VAT more sensitive to lipolysis and more insulin-resistance than SAT [143, 145]. Attending to these features and regarding previous studies, there is a wide evidence that supports the fact that VAT is a more pathogenic depot than SAT and its dysfunction or metabolic alteration increases the risk to develop AT-associated inflammation and insulin resistance [129].

1.3.1 Unresolved inflammation in adipose tissue

Excessive caloric intake can trigger morphological modifications in WAT, specially in visceral depots. Some alterations include adipocyte hypertrophy (cell size increase) and hyperplasia (cell number increase) [140]. In hypertrophic adipocytes, the metabolic and inflammatory profile changes leading to a

dysfunctional VAT. Basal lipolysis and free fatty acid degradation rate increase substantially and pro-inflammatory cytokines and chemokines such as TNFα, IL-6, IL-1β, IL-8, M-CSF-1, CCL-5/RANTES and CCL-2/MCP-1 are thoroughly secreted by AT-resident macrophages, generating an inflammatory environment that promotes leukocyte recruitment and infiltration [143, 144, 146]. Macrophages are known to be the main immune cells found in VAT. There, they control ECM remodelling, angiogenesis, adipocyte differentiation and they remove the dead cells present in the tissue [141]. Under an inflammatory stimulus, innate and adaptive immune systems are activated and T helper 1 (Th1) cells accumulate in AT inducing a new wave of monocyte recruitment promoting a phenotypic change of resident macrophages from an anti-inflammatory to a pro-inflammatory state [139, 140] increasing, thus, adipokine secretion (**Figure 11**). Under these pathological conditions, some serine kinases including the inhibitor of nuclear factor-κB (IκB) kinase (IKK) are activated [147]. In particular, the isoform IKKβ has been reported to activate NF-κB, a nuclear transcription factor that plays a pivotal role in the inflammatory response. In a healthy environment, NF-κB remains in the cytoplasm of the cells bound to IκB proteins. In the presence of an inflammatory stimulus, IKKβ phosphorilates IκB proteins which are subsequently degraded in the proteasome. Once NF-κB is released from these proteins, it starts its traslocation to the nucleus to activate pro-inflammatory genes that promote the expression of adhesion molecules and pro-inflammatory cytokines and chemokines [148, 149]. In addition, IKKβ in adipocytes and hepatic cells inhibits the phosphorylation of insulin receptor substrate (IRS)-1 and IRS-2 resulting in the blockage of insulin signalling. This effect together with AT dysfunction and inflammation impairs glucose and lipid metabolism contributing to the development of T2DM [147, 150]. Fortunately, exercise has been proven to ameliorate the inflammatory condition underlying in most of the obese patients as it increases fat burning. In vascular cells, adipocytes and macrophages, the saturated free fatty acids (FFA) activate the IKK/NF-κB pathway. However, when physical activity is performed, plasma FFA concentration is lessened, resulting in a lower activation of NF-κB target genes [151].

1.3.2 Type 2 diabetes mellitus development in obesity

Under healthy conditions, insulin binds to its receptor, the insulin receptor (IR), located in the plasma membrane of cells from different tissues and organs including adipose tissue, liver, skeletal muscle and heart [152]. Insulin signalling starts

when this hormone binds to the IR. This interaction induces a phosphorylation cascade that leads to the activation of the serine/threonine protein Kinase B (PKB), also known as AKT [153]. This signalling pathway is involved in different metabolic processes including glucose uptake. Activated AKT promotes the translocation of the glucose transporter type 4 (GLUT4) to the plasma membrane of adipocytes and skeletal muscle cells favouring glucose entrance. Furthermore, once AKT is activated, the glycogen synthase activity is promoted favouring glycogen synthesis and storage in hepatocytes and muscle cells (**Figure 12**) [154, 155]. However, low insulin response results in poor AKT signalling that impairs glucose and lipid metabolism, causing dyslipidemia and hyperglycemia, two metabolic features frequently detected in T2DM patients that present insuline resistance [156].

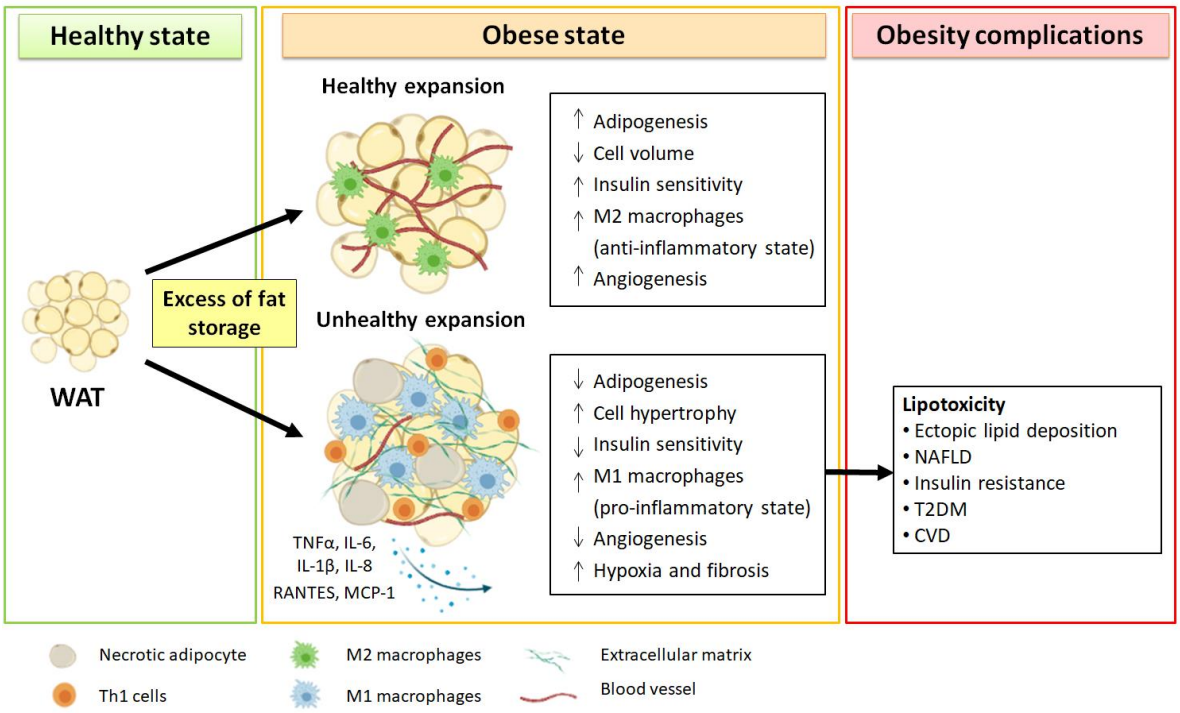

Figure 11. Differences between healthy and unhealthy WAT expansion in obesity. In response to an excess of fat storage, WAT tends to expand. A healthy WAT expansion is characterised by a low-grade inflammation and wide blood irrigation. By contrast, unhealthy WAT expansion presents a high amount of inflammatory immune cells, low blood irrigation and increased extracellular matrix deposition. All these factors promote the development of metabolic and cardiovascular diseases. Abbreviations: WAT, white adipose tissue; TNFα (Tumor Necrosis Factor α); IL, (interleukin); RANTES, (Regulated upon Activation, Normal T Cell Expressed and Presumably Secreted); MCP-1 (monocyte chemoattactant protein-1); NAFLD (non-alcoholic fatty liver disease); T2DM (type 2 Diabetes Mellitus); CVD (cardiovascular disease). Adapted from Longo *et al*. 2019 [144] with BioRender.com.

Insuline resistance is defined as the loss of the capacity of this hormone to exert its biological functions due to a poor signalling on its target organs and tissues [157]. The lack of insulin sensitivity in the liver impairs glucose metabolism increasing endogenous glucose production and promoting gluconeogenesis. In AT, insulin resistance promotes triglyceride lipolysis that leads to increased concentration of plasma FFA [158]. The high levels of plasma FFA exert lipotoxicity in hepatic and muscle cells and prevent the glucose transport and its subsequent uptake, increasing markedly the plasma concentrations [159, 160]. All of this contributes to the development of T2DM, a pathological condition that leads to the development of hyperglycemia and other comorbidities such as nephropathy, retinopathy, neuropathy, adipose tissue dysfunction, hypertension and cardiovascular diseases [153, 161].

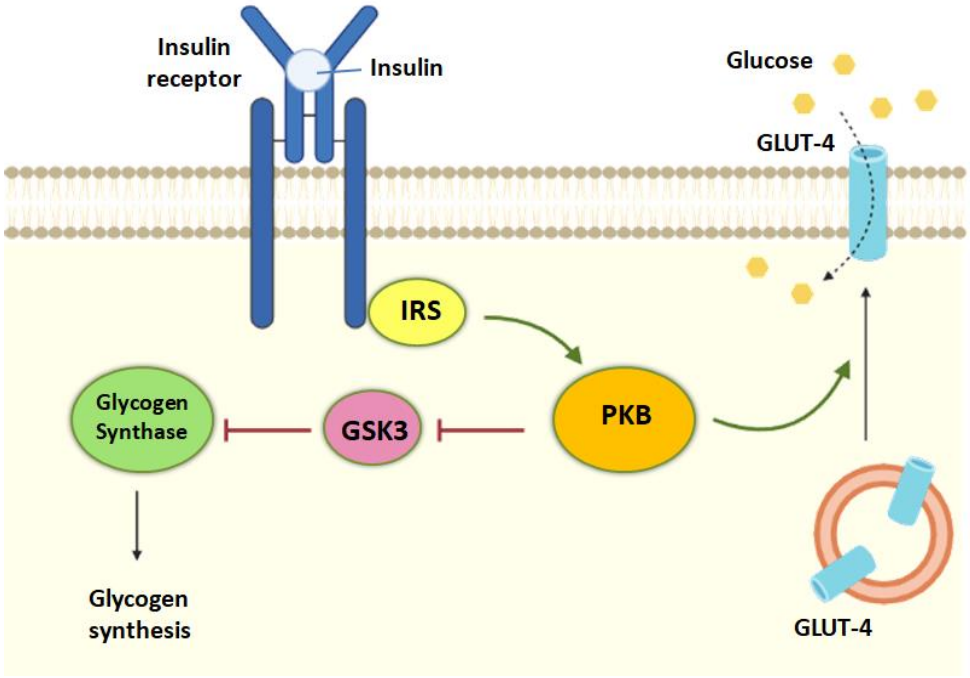

Figure 12. Insulin signalling pathway. The interaction between insulin and its receptor triggers a signalling cascade that leads to the phosphorylation and activation of PKB. This kinase promotes the translocation of GLUT-4 to the plasma membrane. This mechanism allows the entrance of glucose into the cell. Simultaneously, the phosphorylated form of the PKB activates glycogen synthase and glycogen synthesis is promoted. Abbreviations. IRS, insulin receptor substrate; PKB, protein kinase B; GSK3, glycogen synthase Kinase 3; GLUT-4, glucose transporter type 4. Adapted from Arneth *et al*. 2019 [154] with BioRender.com.

1.3.3 Retinoic acid receptor-related orphan receptors (RORs)

Nuclear receptors (NRs) belong to a family of ligand-regulated transcriptional factors which are crucial in the regulation of the gen expression [162]. NRs control diverse biological processes including cell proliferation and differentiation, development, metabolism and homeostasis [163]. To date, 48 members of NRs have been identified in humans [164]. All of them share a similar structure which allows the interaction with their respective ligands to subsequently bind to specific regions of the genome and modulate the transcription of their target genes.

Retinoic acid receptor-related orphan receptors (RORs) belong to the superfamily of NRs. Their denomination is due to their similarity with the sequence of the retinoic acid receptor (RAR) and they are considered orphan receptors as their natural ligands do not exist or have not been discovered yet [165]. RORs act as ligand-dependent transcriptional factors that are involved in diverse physiological, metabolic, immunological and inflammatory processes [166]. Three different isoforms of RORs have been described: RORα, RORβ and RORγ; and all of them have four common regions [167]. These regions include an N-terminal domain, a highly conserved DNA-binding domain (DBD) that contains two zinc fingers, a ligand-binding domain (LBD) and a hinge domain located between the DBD and the LBD [167, 168]. RORs regulate the transcription of their target genes by binding to their ROR-response elements (ROREs) (**Figure 13**). The assembly of the ligand to the LBD can activate or inhibit the transcriptional activity of these NRs. Thus, ROR agonists induce conformational changes in the LBD resulting in the release of a co-repressor complex, a key process that allows the binding of a co-activator complex and the subsequent activation of ROR [166].

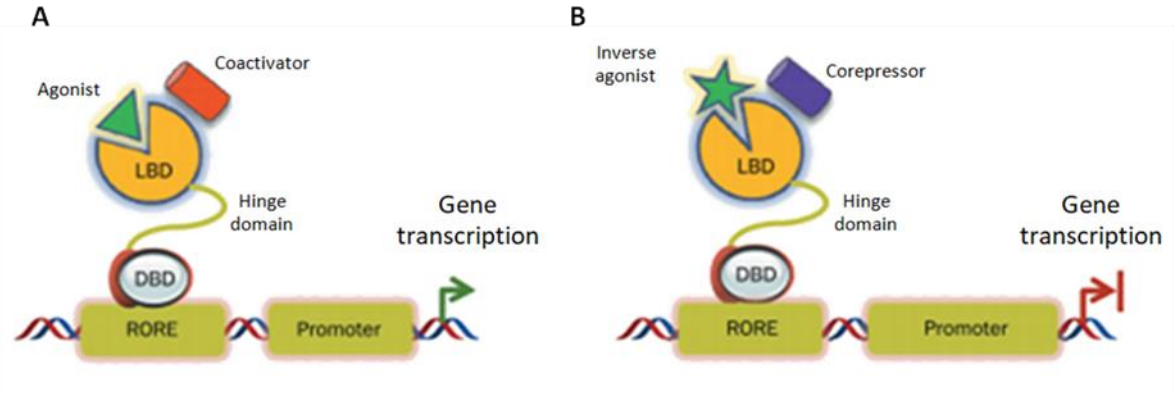

Figure 13. Modulation of the transcriptional activity of RORα. (**A**) Transcriptional activation of RORα target genes. The interaction between an agonist and the LDB of the transcription factor RORα promotes the recruitment of a coactivator. The complex formed binds to the DNA and activates gene transcription. (**B**) Transcriptional repression of RORα target genes. In the presence of an inverse agonist, RORα interacts with a corepressor which inhibits the transcriptional activity of RORα. Abbreviations: LBD, ligand binding domain; DBD, DNA binding domain; RORE, ROR-response element. Adapted from Zhang *et al*. 2015 [163].

In the early 1990s, RORα was identified and it was the first ROR isoform in being characterised [167]. RORα was found to be expressed in several tissues with high metabolic activity such as adipose tissue, liver, skeletal muscle [163, 168, 169] and vascular endothelial cells [170]. Although RORs are orphan receptors, melatonin, cholesterol and cholesterol sulfate have been identified by crystallographic techniques as RORα natural ligands and they act as agonists after their assembly to the ligand binding pocket of the receptor [171]. Accumulating evidence supports that RORα is involved in the development of obesity-related insulin resistance and inflammation associated to atherosclerosis [172-174]. In fact, several preclinical studies have demonstrated the implication of RORα in these metabolic and cardiovascular diseases. For instance, RORα-deficient staggerer mice fed with a high fat diet ameliorated their metabolic profile in terms of adiposity, insulin resistance and AT dysfunction compared with the wild-type peers [175, 176]. Another study revealed that pharmacological inhibition of RORα in a mouse model of atherosclerosis exerted benefficial effects in the treatment of this patology [177]. According to these observations RORα seems to be critical in the development of specific alterations of the metabolic syndrome. However, although RORα has been explored in the area of metabolism and vascular biology, most of the studies have been carried out

in murine models whereas the implication of this receptor in human obesity has not been elucidated.

2. OBJECTIVES

1. Abdominal aortic aneurysm (AAA) is a pathological condition of permanent vessel dilatation that predisposes to the potentially fatal consequence of aortic rupture [57]. Sodium-glucose cotransporter type 2 (SGLT-2) inhibitors have emerged as powerful pharmacological tools for type 2 diabetes mellitus treatment. Beyond their glucose-lowering effects, recent studies have shown that SGLT-2 inhibitors reduce cardiovascular events and have beneficial effects in several vascular diseases such as atherosclerosis [120, 121]; however, the potential effects of SGLT-2 inhibition on AAA remain unknown. Therefore, **the first objective** of this Thesis was to evaluate the effect of oral chronic treatment with empagliflozin, an SGLT-2 inhibitor, on dissecting AAA induced by angiotensin II (Ang II) infusion in apolipoprotein E knockout ($apoE^{-/-}$) mice.

2. Given that endothelial dysfunction is one of the early steps in AAA development, **the second objective** of this Thesis was to evaluate the possible consequences of SGLT-2 inhibition in the dysfunctional endothelium induced by Ang-II. More precisely, we have studied in human aortic endothelial cells the impact of SGLT-2 inhibition with empagliflozin on mononuclear cell adhesion, chemokine release and the underlying mechanism involved in this response.

3. Obesity is a metabolic disease characterised by a chronic low-grade inflammation associated to adipose tissue (AT) dysfunction [178]. Retinoic acid-receptor-related orphan receptor alpha (RORα) is a transcriptional factor belonging to the superfamily of nuclear receptors, which have been demonstrated to regulate the expression of genes implicated in diverse metabolic, immunologic and inflammatory processes [171]. However, less is known about the role of RORα in human obesity. Thus, **the third objective** of this Thesis was to evaluate the expression and function of RORα in the AT of patients with morbid obesity and its association with metabolic parameters linked to AT dysfunction and insulin resistance. Furthermore, the *ex vivo* effects of functional RORα blockade on AT were also investigated.

4. Endothelial dysfunction is a pathogenic feature of obesity, which might explain the high incidence of cardiovascular disease in these patients [178, 179]. TNFα is a key adipokine in the endothelial dysfunction associated with obesity

and is a potential risk factor in the early progression of atherosclerotic lesion by the stimulation of different leukocyte-recruiting chemokines and cellular adhesion molecule expression in the endothelium[180-183]. Because RORα activity has been reported to be involved in atherosclerosis development in animal models[177], **the fourth objective** of this Thesis was to evaluate the consequences of pharmacological RORα blockade in human endothelial cells stimulated with TNFα and the underlying mechanisms.

3. MATERIAL AND METHODS

3.1 Study of the effects of SGLT-2 inhibition in abdominal aortic aneurysm development and endothelial dysfunction

3.1.1 Animal studies

Protocols followed the European Union guidelines for animal care and protection were approved by the Ethics Review Board of the Faculty of Medicine, University of Valencia (Spain). All efforts were made to minimize the number of animals used and their suffering.

Homozygous apoE$^{-/-}$ C57BL/6 male mice were provided by Charles River Laboratories (Chatillon-sur-Chalaronne, France) and they were housed in a specific pathogen-free environment under constant conditions (22±2°C temperature, 60-65% humidity and 12 h dark/light cycles) with *ad libitum* access to a normal chow diet and water.

3.1.1.1 Experimental protocol

Twelve-week-old male apoE$^{-/-}$ C57BL/6 mice were used. Only male mice were studied because female mice have a low incidence of Ang II-induced AAA [184]. Osmotic minipumps (Alzet, Model 2004; Charles River Laboratories, Inc, Wilmington, MA) were subcutaneously implanted in the dorsum of the neck of the mice under isoflurane anaesthesia to infuse saline (n=10), or Ang II (CAS 4474-91-3; Calbiochem, San Diego, CA) at a rate of 1000 ng/kg per minute (n=48) for 28 days. During this period of time some of the Ang II infused mice were orally cotreated with vehicle (carboxymethyl cellulose; n=16) or empagliflozin (BV-2877-10; Tocris Bioscience, Bristol, UK) at a dose of 1 mg/kg per day (n=16) or 3 mg/kg per day (n=16).

To study the acute phase of dissecting AAA formation apoE$^{-/-}$ mice were infused with Ang II (1000 ng/kg per minute) and treated with empagliflozin (3 mg/kg per day) or vehicle for 5 days (n=5 per group). The doses of empagliflozin used in the present study were based on the published efficacy and pharmacokinetic data from murine models [185-187].

3.1.1.1.1 Measurement of blood pressure

Systolic blood pressure (SBP) was measured in conscious mice using a noninvasive tail-cuff system (CODA-6; Kent Scientific, Torrington, CT) and following the indications previously described [188, 189]. During blood pressure data acquisitions, conscious mice were placed in a retainer tube on a warming platform maintained at 37°C (model LE5510; PANLAB, Barcelona, Spain). Mice were acclimatised to the instrument for at least seven consecutive days before baseline measurements and the implantation of the osmotic minipumps. Data acquisitions were taken every day at the same time, between 8 and 10 a.m, to avoid variations in blood pressure due to the circadian cycle. Animals were subjected to 10 initial pressure readings to acclimatise them to the procedure and then 10 additional cycles were measured to obtain the mean systolic pressure. The criteria for data acceptance were the acquisition of at least 10 of 20 measurements and a standar deviation of <30 mm Hg for each session.

3.1.1.1.2 Determination of biochemical parameters. Quantification of glucose levels and lipid profile

To analyse circulating glucose levels and lipid profile, mice were fasted overnight. Glucose measurements were obtained from blood samples using a Contour Next USB blood glucose meter (Bayer HealthCare, Basel, Switzerland). Lipid profile was determined from plasma samples. To obtain the plasma, blood were collected in a tube containing EDTA (ethylenediaminetetraacetic acid, SIGMA, St. Louis, EEUU) as anticoagulant. To determine triglyceride (TG) and total cholesterol (TC) concentrations, two commercial kits were used, “LabAssay Triglyceride” and “LabAssay Cholesterol” (WAKO Chemicals, Neuss, Germany) respectively, based both on enzymatic procedures which lead to a blue product that can be determined with a spectrophotometric microplate reader (Infinite 200, #30016056, TECAN, Austria) by measuring the absorbance of the blue color at 600nm wavelength. Lipid concentrations were calculated using a standard curve generated from serial dilutions of the appropiate internal standard and following the manufacturer’s instructions. Using the same method previously described for TC measurement, High Density Lipoprotein-Cholesterol (HDL-C) was quantified after having precipitated apolipoprotein B (apo B) with dextran sulfate/$MgCl_2$ (SIGMA, St. Louis, MI, EEUU) [190].

3.1.1.2 Aorta isolation and aneurysm quantification

At the end of the experimental protocols mice were sacrificed by anaesthetic overdose consisting of a mixture of medetomidine hydrochloride (1 mg/mL; Orion Corporation, Espoo, Finland) and ketamine (50 mg/mL, Orion Corporation) that was intraperitoneal injected to the animals before dissection. Then, each mouse was cut and opened ventrally to access to the left cardiac ventricle which was perfused with 10 mL of phosphate-buffered saline (PBS) with an exit through the severed right atrium to prevent blood clots in the vessels. Once the aorta was isolated it was exposed under a dissecting microscope to remove the periadventitial tissue and to be photographed (Leica DMD108 Digital; Leica Microsystems, Wetzlar, Germany). Suprarenal regions of the abdominal aorta were identified between the last pair of intercostal arteries and the right renal branch. Maximal external diameter of the suprarenal aorta was measured ex vivo using ImageJ (National Institutes of Health). To evaluate aneurysm severity, four different stages were established according to previous studies [191]. The most remarkable features of each stage are the following ones: stage I, dilated lumen in the suprarenal region of the aorta without thrombus or with a small thrombus; stage II, dilated lumen and remodeled tissue in the suprarenal region of the aorta with a pronounced bulbous form that contains thrombus; stage III, dilated lumen in the suprarenal region of the aorta with the presence of multiple aneurysms; stage IV, corresponding to the rupture of the aneurysm. Necropsies were performed in all mice that died during the experimental treatment. Aortic rupture was defined as the observation of blood clots in the retroperitoneal cavity (abdominal aortic rupture) or in the thoracic cavity (thoracic aortic rupture). Animals presenting tissue degradation were excluded from the analysis but they were used for mortality and rupture-rate data. The ex vivo diameters of the ascending, thoracic and suprarenal regions of the aorta were measured as described [192]. The studied regions of the aorta are shown in **Figure 14**. After diameter quantification and aneurysm classification, a second researcher matched the scored aneurysms to the different treatments of the mice.

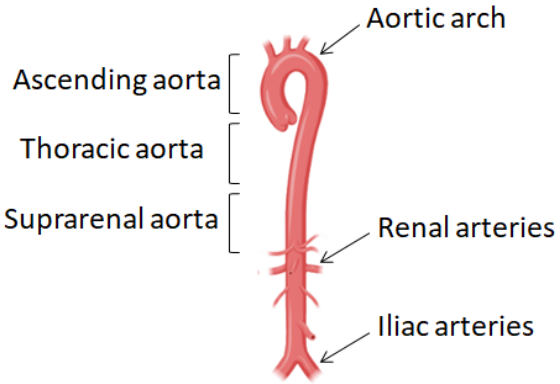

Figure 14. Anatomy and regions of the aorta. The aorta originates from the left ventricle of the heart and descends until the abdomen, where it bifurcates into two smaller arteries called iliac arteries. Aorta is divided in three different regions: ascending aorta which arises from the aortic oriffice from the left ventricle and ascends to become the aortic arch; thoracic aorta, which extends along the thorax and suprarenal aorta, which is located between the last pair of intercostal arteries and the right renal branch. Created with BioRender.com

3.1.1.3 Histological analysis

Once the aortas were removed from mice and cleaned from the remaining tissues, the suprarenal region of the aorta was divided into two sequential regions (A and B) cutting at the level of maximal dilatation and using a Leica DMD108 Digital Microscope (Leica Microsystems). Region A was kept at -80°C for molecular analysis. Region B was fixed in 4% paraformaldehyde (PFA; PanReac AppliChem) for 6 h and then it was manteined in phosphate buffer saline (PBS) overnight. As paraffin is hydrophobic, a dehydration process of the aortas is needed. To dehydrate the aortas, they were immersed in serial ethanol solutions of increasing concentrations until pure for 15 min in each ethanol solution. Then, the aortas were submerged twice in a mixture of pure ethanol/xylene (1:1) for 7 min each time and finally they were twice immersed in pure xylene for 7 min each time. The next step was to embed the aortas in paraffin to proceed to cut them into histological sections (5 µm thick) making use of a microtome (Leica RM2245; Leica Biosystems, Wetzlar, Germany). At least 10 slides containing 4 tissue cross sections from the aorta of each animal were taken on microscope slides Superfrost® plus (Thermo Fisher Scientific) to carry out the subsequent histological analyses.

3.1.1.3.1 Hematoxylin and eosin staining

Histological cross sections were hydrated immersing them in xylene (3 x 5 min) and then in serial ethanol solutions of decreasing concentration from pure to milli-Q water as following indicated: 100% ethanol (2 x 5 min), 95% ethanol (2 x 5 min), 70% ethanol (2 x 2 min), 50% ethanol (2 x 2 min) and Milli-Q water (1 x 2 min). Next, aortic cross sections were washed with PBS 1X for 5 min. To stain the nucleus, they were immersed for 5 min in filtered Harris hematoxylin (Sigma-Aldrich, St. Louis, MO) and then washed in running water for 10 min. Then, samples were twice quickly immersed in differentiation solution (0,25 mL concentrated hydrochloric acid in 100 mL 70% ethanol), washed again in running water for 10 min and immersed in 95% ethanol for 30 seconds. To stain the cytoplasm, aortas were plunged in eosin (Sigma-Aldrich, St. Louis, MO) diluted in 95% ethanol (1:1) for 90 seconds and washed in water to remove the excess of staining. To finish the process, they were dehydrated immersing them in serial ethanol solutions of increasing concentrations (70%, 95% and 100% ethanol) for 2 min in each solution followed by a final 2 minute xylene bath. Finally, slides were mounted with Bio-Mount synthetic mounting medium for histology and cytology (Bio-Optica, Milan, Italy) and aortas were photographed (Axio Observer A1; Carl Zeiss, NY) under x10 and x40 magnification.

3.1.1.3.2 Verhoeff-Van Gieson staining and evaluation of elastin degradation

Verhoeff-Van Gieson staining (HT25A-1KT, Sigma-Aldrich, St. Louis, MO) was used to stain elastic fibers in the aortas with the aim of determining the level of elastin degradation.

First, histological cross sections were hydrated as described in **Section 3.1.1.3.1** and immersed in Working Elastic Stain Solution (**Table 3**, Sigma-Aldrich) for 10 min. Then, samples were washed in running water for 10 min, immersed in Working Ferric Chloride Solution (**Table 3**, Sigma-Aldrich) for 3 min, washed again in running water and cleared in 95% ethanol for 2 min. A third wash in water was done before immersing the aortas in Van Gieson Solution (Sigma-Aldrich) for 2 min and then in 95% ethanol for 2 min. Finally, samples were dehydrated as detailed in **Section 3.1.1.3.1** and slides were mounted with Bio-Mount (Bio-Optica, Milan, Italy).

Table 3. Reagents used to prepare the Working Elastic Stain Solution and the Working Ferric Chloride Solution for Verhoeff-Van Gieson staining.

Solutions	Reagents	Volume (mL)
Working Elastic Stain Solution	Hematoxylin	120
	Ferric Chloride	18
	Weigert's Iodine Solution	48
	Distilled water	30
Working Ferric Chloride Solution	Ferric Chloride	18
	Distilled water	222

To evaluate the level of elastin degradation four different grades were established according to previous studies [193]. The main features of each grade are: grade 1, absence of elastin degradation, well organised elastic fibers; grade 2, elastic laminae with some interruptions and breaks; grade 3, elastic laminae with multiple interruptions and breaks; grade 4, severe elastin fragmentation or loss. To carry out the qualitative analysis of elastin degradation, 5 fields of each suprarenal aorta stained with Verhoeff-van Gieson staining were captured and digitized (Axio Observer A1; Carl Zeiss, NY) under x10 and x40 magnification. Then, the qualitative evaluation of elastin degradation was performed by a blinded observer.

3.1.1.4 Immunohistological analysis

Macrophage infiltration, microvessel formation, extracellular matrix degradation and expression of inflammatory mediators were studied by immunohistochemical techniques.

After having hydrated the aorta samples as mentioned in **Section 3.1.1.3.1**, the antigen of interest was unmasked and exposed to the surface using proteinase K (#55020, Dako, Glostrup, Denmark). Next, endogenous peroxidase was inactivated with the reagent Peroxidase-Blocking Solution (#S2023, Dako, Glostrup, Denmark). Then, samples were blocked for 1 h with goat serum (5% in PBS; Abcam, Cambridge, UK) to avoid non-specific interactions and incubated overnight at 4°C with different primary antibodies (**Table 4**) diluted in antibody diluent (#S2022, Dako, Glostrup, Denmark). For quantification of inflammatory cells, a rat monoclonal anti-mouse Mac3 antibody (1:100, catalog No. SC19991; Santa Cruz Biotechnology, CA) was used. CD31 staining was performed with a

rabbit polyclonal anti-mouse CD31 antibody (1:50, catalog No. ab28364; Abcam, Cambridge, United Kingdom) to detect microvessel formation. A rabbit polyclonal anti-mouse MMP-2 (1:1000, catalog No. ab37150; Abcam) or a rabbit polyclonal anti-mouse MMP-9 (1:200, catalog No. ab38898; Abcam) antibody was used to analyse extracellular matrix degradation, and a rabbit polyclonal anti-mouse TIMP (tissue inhibitor of metalloproteinase)-1 antibody (1:1000, catalog No. ab38978; Abcam) was used for TIMP-1 detection. Inflammatory mediators such as MCP-1 and RANTES were detected with a polyclonal goat anti–mouse MCP-1 antibody (1:100, catalog No. AF479; R&D) and a polyclonal goat anti-mouse RANTES antibody (1:50, catalog No. AF478; R&D). SGLT-2 expression was analysed using a rabbit polyclonal antibody against mouse SGLT-2 (1:50, catalog No. ab37296; Abcam). Specific labelling was detected with biotin-conjugated secondary antibodies (Dako, Glostrup, Denmark). To detect the brown coloured product, a solution containing 3,3'-diaminobenzidine (DAB; Dako, Agilent Technologies) was used as substrate of the enzymatic reaction. Then, aortas were counterstained with Harris hematoxylin and dehydrated and mounted as described in **Section 3.1.1.3.1.**

Table 4. Antibodies for immunohistochemistry.

Name	Vendor or Source	Catalog #	Working concentration
Anti-MMP-2	Abcam	ab37150	1 µg/mL
Anti-MMP-9	Abcam	ab38898	10 µg/mL
Anti-TIMP-1	Abcam	ab38978	1 µg/mL
Anti-SGLT-2	Abcam	ab37296	10 µg/mL
Anti-RANTES	R&D Systems	AF478	4,8 µg/mL
Anti-MCP-1	R&D Systems	AF479	1 µg/mL
Anti-CD31	Abcam	ab28364	18 µg/mL
Anti-Mac-3	Santa Cruz Biotechnology	SC19991	1 µg/mL

To visualise vascular smooth muscle cells in the media of the aorta, an immunofluorescence assay was performed using a specific rabbit monoclonal anti-α smooth muscle actin antibody conjugated to Cy3 (1:100, catalog No. C6198; Sigma-Aldrich) (**Table 5**).

Additionally, double immunofluorescence was carried out to determine SGLT-2 expression in macrophages (Mac3+ cells) and endothelial cells (CD31+ cells) in the suprarenal aortic aneurysm. The assay was performed with a rat

monoclonal anti-mouse Mac3 antibody (1:100, catalog No. SC19991; Santa Cruz Biotechnology, CA); a rat polyclonal anti-mouse CD31 antibody (1:50, catalog No. ab56299; Abcam) and a rabbit polyclonal antibody against mouse SGLT-2 (1:50, ab37296; Abcam). The cellular localization of MMPs and TIMP-1 in the suprarenal aortas was investigated by double immunofluorescences for MMPs/Mac3; TIMP-1/Mac3 and MMPs/CD31; TIMP-1/CD31. A rat polyclonal anti-mouse CD31 antibody (1:50, catalog No. ab56299; Abcam) was used to detect CD31+ cells. The antibodies used for MMPs, TIMP-1 and Mac3 detection are the same described in this section and detailed in **Table 5**. Specific labeling was detected with an Alexa Fluor 633 goat anti-rat secondary antibody (1:500 dilution, catalog No. A21094; Molecular Probes/ Invitrogen, Carlsbad, CA) or an Alexa Fluor 488 goat anti-rabbit secondary antibody (1:500 dilution, catalog No. A11034; Molecular Probes) (**Table 5**). Secondary antibodies were incubated at room temperature in the dark for 2 h. Then, cell nuclei were counterstained with 4′,6-diamidino-2-phenylindole (DAPI, blue) and samples were mounted with Slow Fade® Gold antifade Reagent (Molecular Probes, Thermo Fisher Scientific).

To confirm specificity of antibodies, a rabbit IgG polyclonal isotype control (Abcam) and a rat IgG isotype control (Invitrogen antibodies) were used as negative controls. Fields from each suprarenal aortic section were photographed under x10 and x40 magnification (Axio Observer A1; Carl Zeiss, NY) and then analysed. Scoring was performed blinded on coded slides.

Table 5. Antibodies for immunofluorescence

Name	Vendor or Source	Catalog #	Working concentration
Anti-CD31	Abcam	ab56299	10 µg/mL
Anti-MMP-2	Abcam	ab37150	1 µg/mL
Anti-MMP-9	Abcam	ab38898	10 µg/mL
Anti-TIMP-1	Abcam	ab38978	1 µg/mL
Anti-SGLT-2	Abcam	ab37296	10 µg/mL
Anti-Mac3	Santa Cruz Biotechnology	SC19991	2 µg/mL
Anti-SM-α actin	Sigma-Aldrich	C6198	2 µg/mL
Alexa Fluor 488 goat anti-rabbit	Invitrogen	A11034	4 µg/mL
Alexa Fluor 633 goat anti-rat	Invitrogen	A21094	4 µg/mL

3.1.1.5 Reverse transcription polymerase chain reaction (RT-PCR)

3.1.1.5.1 RNA extraction and quantification

Total RNA was extracted from aortas by homogenization using TRIzol® Reagent (Invitrogen, Thermo Fisher Scientific, Waltham, MA). Then, RNA concentration was determined with a NanoDrop spectrophotometer (ND-100 v3.7.1; Thermo Fisher Scientific) measuring the absorbance at a wavelength of 260 nm. The purity of DNA was estimated by the ratio absorbance at 260/280 nm wavelengths ($A_{260/280}$). This ratio must be higher than 1.8 in the analysed RNA extracts.

3.1.1.5.2 Reverse transcription (RT)

Reverse transcription was performed to obtain complementary DNA (cDNA). High Capacity cDNA Reverse Transcription kit (Applied Biosystems, Thermo Fisher Scientific) was used. 1 µg of RNA was retrotranscribed using the MultiScribe™ Reverse Transcriptase (50 U/µL; Applied Biosystems, Thermo Fisher Scientific) and the Master Mix for the RT. All the reagents for the mix are compiled in **Table 6**.

After RNA quantification, each sample was diluted in nuclease-free water to get RNA in a concentration of 100 µg/mL. Then, 10 µL of diluted RNA were added in a new nuclease-free microtube containing 10 µL of the mix for RT (**Table 6**). Then, samples were placed in a SimpliAmp™ Thermal Cycler (Applied Biosystems, Thermo Fisher Scientific) under the specific conditions detailed in **Table 7**.

At the end of the process the obtained cDNA was stored at -20°C until further use.

Table 6. RT Master Mix reagents.

Reagent	Volume (µL) per sample
10x RT Buffer	2
25x dNTPs Mix (100 mM)	0,8
10x RT Random Primers	2
MultiScribe™ Reverse Transcriptase	1
Applied Biosystems™ RNase Inhibitor (20 U/µL)	1
Nuclease-free water	4,2
RNA sample	1 µg

Table 7. RT Thermal cycling profile.

Step	Temperature (°C)	Time (min)
1	25	10
2	37	120
3	85	5
4	4	∞

3.1.1.5.3 Quantitative polymerase chain reaction (qPCR)

The ABI Cycler 7900 Fast System thermal cycler (Applied Biosystems) was used to carry out the qPCR assay. To determine gene expression, cDNA was amplified with the TaqMan™ Universal PCR Master Mix (Applied Biosystems; Thermo Fisher Scientific, Waltham, MA) and specific murine TaqMan probes (Applied Biosystems) were used (**Table 8)**. Different reagents were added as detailed in **Table 9**.

Table 8. Probes used for qPCR assay.

Gene	TaqMan™ Gene Expression Probe
Mouse *Mcp-1/Ccl-2*	Mm00441242_m1
Mouse *Rantes/Ccl-5*	Mm01302427_m1
Mouse *Vegf*	Mm00437306_m1
Mouse *Mmp-2*	Mm00439498_m1
Mouse *Mmp-9*	Mm00442991_m1
Mouse *Timp-1*	Mm00441818_m1
Mouse *Gapdh*	Mm99999915_g1

Table 9. Reagents used for TaqMan qPCR.

Reagent	Volume(µL) per sample
TaqMan™ Universal PCR Master Mix	6,25
Probe	0,625
Nuclease-free water	4,3
cDNA	2,5

After having mixed all the reagents, qPCR was performed following the cycling protocol shown in **Table 10**.

Table 10. TaqMan qPCR cycling protocol.

Step	Temperature (°C)	Time	Number of cycles
UDG-pretreatment	50	2 min	1
Initial denaturation	95	10 min	1
Denaturation	95	15 s	40
Annealing/Extension	60	60 s	

Sglt-2 expression was determined using primers sequences (**Table 11**) designed in previous studies [194]. qPCR was performed with the Luminaris Color HiGreen HigRox qPCR Master Mix (Thermo Fisher Scientific, Waltham, MA) mixing all the reagents as indicated in **Table 12**. Then, to determine gene expression, the ABI Cycler 7900 Fast System thermal cycler (Applied Biosystems) was used following the protocol specified in **Table 13**.

Table 11. Primers used in the qPCR assay for the analysis of Sglt-2 expression.

Gene	Primer	Sequence 5'→3'
Mouse *Sglt-2*	Forward	AACAGCAGTAGCACGCTCTT
Mouse *Sglt-2*	Reverse	AAAGACCGCAGACACTGGAG
Mouse *Gapdh*	Forward	TGACCACAGTCCATGCCATC
Mouse *Gapdh*	Reverse	GACGGACACATTGGGGGTAG

Table 12. Reagents used for qPCR with Luminaris Color HiGreen.

Reagent	Volume(µL) per sample
Luminaris Color HiGreen	5
Forward primer	0,6
Reverse primer	0,6
Nuclease-free water	4
cDNA	2,5

Table 13. Luminaris Color High Green qPCR Cycling protocol.

Step	Temperature (°C)	Time	Number of cycles
UDG-pretreatment	50	2 min	1
Initial denaturation	95	10 min	1
Denaturation	95	15 s	40
Annealing/Extension	60	60 s	

Quantification of the different transcripts was determined with the $2^{-\Delta\Delta Ct}$ method and mRNA levels were normalised to the levels of glyceraldehyde 3-phosphate dehydrogenase (*Gapdh*) used as endogenous control. Results were analysed using the software provided by the manufacturer (QuantStudio™ Design & Analyses; Applied Biosystems; Thermo Fisher Scientific).

3.1.1.6 Protein expression determination by western blotting (WB)

Aorta segments were homogenized in lysis buffer (Pierce™ Lysis Buffer #87787, ThermoFisher) containing proteases and phosphatases inhibitors (HaltTM Protease & Phosphatase inhibitor Cocktail, #1861281, Thermo Fisher). Then, protein concentrations in samples were determined using the Bradford method [195]. Next, samples diluted in Laemmli buffer 4X (**Table 14**) were denatured and subjected to sodium dodecyl sulfate-polyacrylamide (SDS-PAGE) electrophoresis using a 10% running gel (**Table 15**). Electrophoresis was carried out employing a running buffer 1X (**Table 16**) and applying 50V/gel for 90 min. Then, samples were transferred to nitrocellulose membranes (Catalogue No. 10600021, GE Healthcare Life Sciences, Germany). Transference was performed at 60V for 120 min and 4°C in transfer buffer 1X (**Table 16**). Non-specific binding sites were blocked with 5% Bovine Serum Albumin (BSA, #BP9703-100, Fisher Scientific) diluted in Tris Buffer Saline (TBS) 1X (**Table 16**) for 1 h and membranes were incubated overnight at 4°C with the primary antibodies showed in **Table 17**. After the incubation period,

membranes were washed 3 times with washing buffer (**Table 16**) and incubated at room temperature for 1h with the secondary enzyme horseradish peroxidase–linked anti-rabbit antibody (1:2000 dilution, catalog No. P0448; Dako) or anti-mouse antibody (1:2000 dilution, catalog No. P0447; Dako). Signals were detected using a chemiluminescence procedure (ECL Select™ Western Blotting Detection Reagent, Amersham, UK) and recorded using a luminescent analyzer (ImageQuant LAS 500, GE Healthcare, Sweden). Protein quantification was determined using the ImageJ program.

Table 14. Laemmli Buffer composition 4X

Name	Vendor or source	Catalog #	Final Concentration
Tris-HCl pH 6.8	AppliChem Panreac	77-86-1	0.25 M
Glycerol	Sigma-Aldrich	G8773	40 %
Sodium Dodecyl Sulfate (SDS)	Sigma-Aldrich	151-21-3	0.28 M
2-Mercaptoethanol	Sigma-Aldrich	M7154	20 %
Bromophenol Blue	BioRad	115-39-9	0.005 %

Table 15. SDS-PAGE Electrophoresis

10% Separating gel		6% Stacking gel	
Reagent	**Volume**	**Reagent**	**Volume**
H_2O	4.1 mL	H_2O	2.7 mL
Acrylamide (30%)	3,3 mL	Acrylamide (30%)	0.8 mL
Tris 1.5M (pH 8.8)	2,5 mL	Tris 1M (pH 6.8)	0.5 mL
SDS (20%)	50 µL	SDS (20%)	20 µL
APS (10%)	100 µL	APS (10%)	40 µL
TEMED	10 µL	TEMED	4 µL

Abbreviations. SDS, sodium Dodecyl Sulfate; APS, ammonium persulfate; TEMED, N,N,N′,N′-Tetramethylethylenediamine.

Table 16. Western blotting buffers composition

Buffer	Components	Final Concentration
Running Buffer 10X (pH 8.3)	Tris Base	25 mM
	Glycine	192 mM
	SDS	0.1 %
Transfer Buffer 10X (pH 8.3)	Tris Base	25 mM
	Glycine	192 mM
	Methanol	20%
Tris Buffer Saline 10X (TBS, pH 7.6)	Tris Base	0.2 M
	NaCl	1.5 M
Washing buffer	TBS	1X
	Tween-20	0,05%

Abbreviations. SDS, sodium Dodecyl Sulfate

Table 17. Primary antibodies

Name	Vendor or source	Catalog #	Working concentration
Anti-phospho-p38 MAPK	Cell Signaling Technology, Inc.	9211	0,1 µg/mL
Anti-p38 MAPK	Cell Signaling Technology, Inc.	9212	0,1 µg/mL
Anti-phospho-p65	Cell Signaling Technology, Inc.	3031	0,2 µg/mL
Anti-p65	Cell Signaling Technology, Inc.	8242	0,4 µg/mL
Anti-SGLT-2	Abcam	ab37296	1,7 µg/mL
Anti-β-actin	Cell Signaling Technology, Inc.	3700	0,3 µg/mL

3.1.1.7 MMP activity detection

Total MMP activity was determined in protein extracts from suprarenal aortas using a MMP Assay Kit (catalog No. 112146; Abcam) following manufacturer's instructions. This assay was performed in order to evaluate the MMP proteolytic activity on the basis of substrate degradation. The MMP enzymatic action deteriorates the substrate. As a result, a quantificable color reaction is obtained, which is directly proportional to the MMP activity. First, protein extracts from aorta samples were obtained as described in **Section 3.1.1.6**. Samples were incubated with 4-aminophenylmercuric acetate for 3 h at 37°C to activate MMPs. Next, the MMP Green substrate was added for 1 h. Fluorescence signal was measured in a fluorescent microplate reader (Gemini XPS Spectrofluorometer;

Molecular Devices, Sunnyvale, CA) at Excitation/Emission=490/525 nm. MMP activity was expressed as fluorescence units.

3.1.2 Human Aortic Endothelial Cell (HAEC) studies

3.1.2.1 Cell culture

Human aortic endothelial cells (HAEC) were used in the third passage (Lonza, Verviers, Belgium) and maintained in human endothelial cell–specific medium (EBM-2) supplemented with endothelial growth media (EGM-2) (both from Lonza) and 10% fetal bovine serum (FBS; Biowest, Nuaillé, France). Cells were kept growing at constant conditions of temperature (37°C) and CO_2 concentration (5%).

3.1.2.2 Leukocyte-HAEC interactions under flow conditions

3.1.2.2.1 Treatments

HAEC were grown to confluence on 35 mm diameter plates and they were pre-treated with empagliflozin (0.1–3 μM) for 24 h before stimulation with Ang II. The following day, cells were stimulated with 1 μM Ang II for 24 h. The control group was incubated for 24 h with vehicle (0.1% dimethyl sulfoxide, DMSO). All treatments were added to the medium culture containing 1% FBS.

3.1.2.2.2 Human mononuclear cell isolation

All research with human samples was performed following the principles outlined in the Declaration of Helsinki and all protocols were approved by the Institutional Ethics Committee of the University Clinic Hospital of Valencia (Spain). Written, informed consent was obtained from all volunteers. Human mononuclear cells were obtained from buffy coats of healthy donors using the reagent Lymphoprep™ (#AXS-1114544, Axis-Shield, Norway). First, blood collected in tubes containing heparin as anticoagulant and diluted in 0,9% sodium chloride (NaCl) in equal volumes was carefully added to 50 mL tubes containing Lymphoprep™ reagent. Tubes were then centrifuged at 800 g at room temperature for 30 min. After centrifugation, the mononuclear cells (lymphocytes and monocytes) were localised in the medium interface as shown in **Figure 15**. The mononuclear cells were collected, washed in Hank's Balanced Salt Solution (HBSS; Lonza) and centrifuged at 1300 rpm at room temperature for 10 min.

Supernatants were discarded and the pellet resuspended in 1 mL of HBSS. Cell counting was performed in a Neubauer chamber (Marienfeld, Germany). Finally, mononuclear cells were again resuspended in HBSS to obtain a final concentration of 1×10^6 cells/mL.

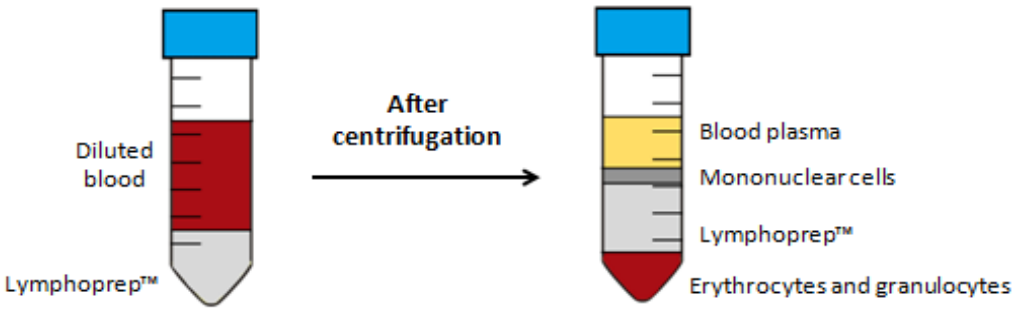

Figure 15. Mononuclear cell isolation using the Lymphoprep™ reagent. Diluted whole blood was layered over Lymphoprep™ reagent. After centrifugation, a density gradient was observed. Erythrocytes and granulocytes sedimented while mononuclear cells were retained at the medium interface.

3.1.2.2.3 Study of leukocyte-HAEC interactions under flow conditions

Parallel-plate flow chamber procedure allows the visualization of cell adhesion under dynamic flow conditions, mimicking the physiological milieu. As shown in **Figure 16**, the parallel flow chamber system consists in a base plate with an entrance and exit port through which cells and media are perfused. Coupled to this base plate are a vacuum pump and a gasket that controls the chamber diameter. Under the base plate there is a 35 mm diameter culture plate, on which the endothelial cell monolayer is grown. As a result, a flow channel is created over the endothelial monolayer, with the infusion rate being regulated by the suction pump, thus emulating the blood flow over the human endothelium.

To measure leukocyte adhesion, HAEC were seeded on 35 mm diameter culture plates pre-coated with 5.5 µg/mL fibronectin. Once confluence was reached and after having treated the cells as described in **Section 3.1.2.2.1**, the plates were placed in a dynamic flow assay using a parallel flow chamber (GlycoTech flow, Gaithersburg, MD).

The GlycoTech flow chamber was assembled and placed onto an inverted microscope stage, and human mononuclear cells were then perfused through the HAEC monolayers. Leukocyte adhesion was determined after 5 min at 0.5 dyn/cm^2. Cells interacting on the surface of the endothelium were visualised and recorded (x20 objective, x10 eyepiece) using a phase-contrast microscope (Axio Observer A1, Carl Zeiss microscope, Oberkochen, Germany) connected to a video camera (SSC-DC80P, Sony, Tokio, Japan). At least 5 fields were recorded for 10 s each. Those leukocytes that established a stable contact with the endothelial monolayer for at least 10 s were considered adherent. Adherent cells were counted while the perfusion medium remained in continuous infusion.

Finally, images were recorded and saved on a computer for further analysis.

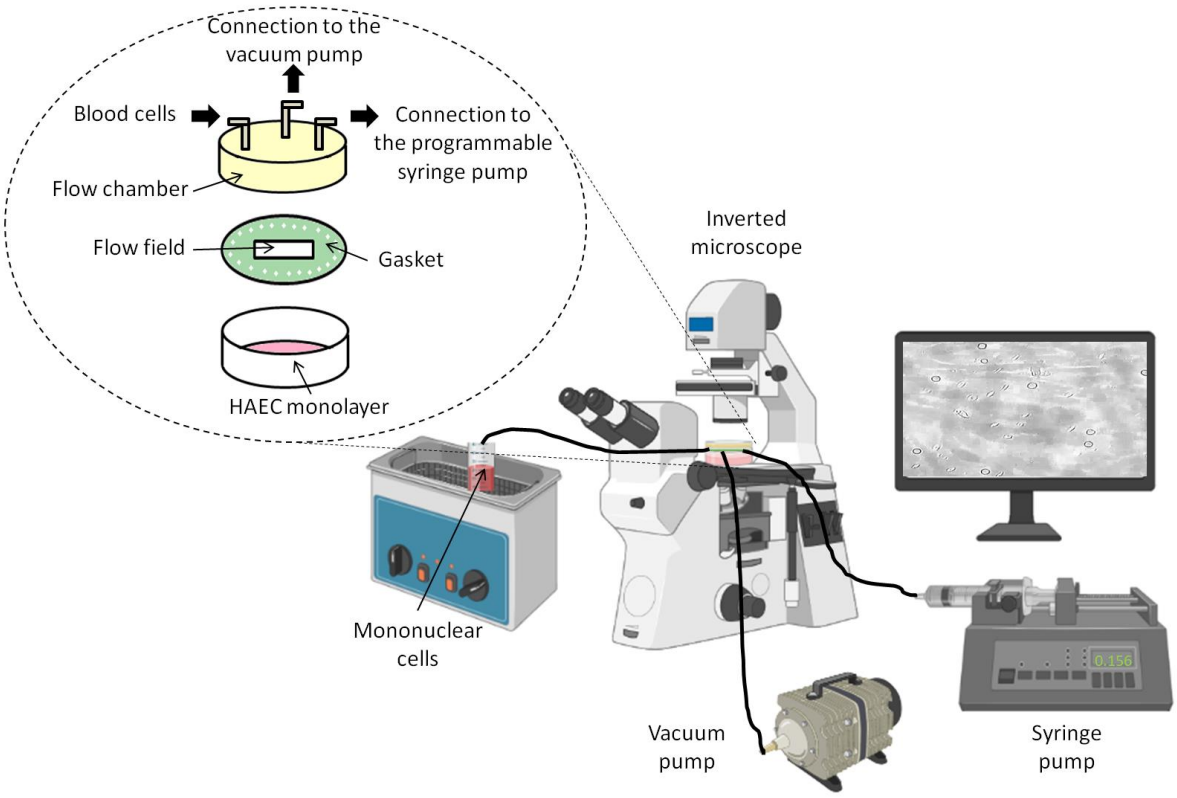

Figure 16. Parallel-plate flow chamber system. The system has a vacuum pump, a syringe pump, the flow chamber and a phase-contrast inverted microscope connected to a computer where cellular adhesion can be visualised and recorded. Created with BioRender.com

3.1.2.3 Immunofluorescence studies

Confluent HAEC were grown on glass coverslips and stimulated with Ang II (1 µM) for 24 h. Some of the stimulated cells were also pre-treated 24 h before the stimulus with empagliflozin (3 µM). After treatments, HAEC were washed twice with PBS 1X and fixed with 4% PFA for 10 min at 4°C. Then, cells were washed with 0,1% BSA diluted in TBS 1X solution (**Table 16**) and non-specific binding sites were blocked with 1% BSA/TBS 1X for 1 h. HAEC were incubated at 4°C overnight with primary rabbit polyclonal antibodies against human VCAM-1 (1:100, catalog No. ab106777; Abcam) and ICAM-1 (1:100, catalog No. ab53013; Abcam) in a 0.1% BSA/PBS 1X solution. Immunofluorescence signals were detected using an Alexa Fluor 488–conjugated goat anti-rabbit secondary antibody (1:1000 dilution, catalog No. 11034; Molecular Probes). Nuclei were counterstained with DAPI. Finally, glass coverslips were mounted on microscope slides using SlowFade® Gold antifade Reagent and images were captured with a fluorescence microscope (Axio Observer A1).

3.1.2.4 Determination of SGLT-2 expression and signalling studies

Western blotting was performed in order to determinate SGLT-2 expression and p38 MAPK and NFκB activation.

HAEC were grown in 6-well plates to confluence and stimulated with Ang II (1 µM) for 24 h. Some cells were pretreated with empagliflozin (3 µM) or vehicle for 24 h before stimulation with Ang II. Next, HAEC were washed with cold PBS (1X) twice, detached from the plate using a scraper and resuspended in 500 µL of PBS 1X to be then centrifuged. After 5 min of centrifugation at 6000 rpm at 4ºC, supernatant was discarded and the pellet was resuspended in 50 µL of RIPA lysis buffer mixed with a cocktail of protease and phosphatase inhibitors (dilution 1:100). Then, samples were centrifuged at 12000 rpm, at 4ºC for 15 min to remove cell debris. The total protein extract was quantified using the Bradford method [195]**.**

Western Blot was performed following the instructions detailed in **Section 3.1.1.6**. A 10% running gel (**Table 15**) and the primary antibodies described in **Table 17** were used. Membranes were subsequently washed, incubated for 1h with the secondary enzyme horseradish peroxidase–linked anti-rabbit antibody (1:2000 dilution, catalog No. P0448; Dako) or anti mouse antibody (1:2000 dilution, catalog No. P0447), and detection was carried out using a chemiluminescence procedure

(ECL Select™ Western Blotting Detection Reagent, Amersham, UK). Signals were recorded using a luminescent analyzer (ImageQuant LAS 500, GE Healthcare, Sweden) and protein was quantified using ImageJ software.

3.1.2.5 Determination of pro-inflammatory chemokines

HAEC were grown in 6-well plates to confluence and stimulated with Ang II (1 µM) for 24 h. Some cells were pretreated with empagliflozin (3 µM) or vehicle 24 h before the stimulus. After treatments, supernatants were collected. CCL-2/MCP-1 and CCL-5/RANTES were determined by enzyme-linked immunosorbent assay (ELISA) using commercial ELISA kits (Human Duoset® kits, R&D Systems, Abingdon, United Kingdom) and following manufacturer´s instructions (**Table 18**). Chemokine values were expressed as pg/ml.

3.1.3 Human macrophage studies

The THP-1 human monocytic cell line (ATCC, Manassas, VA) was grown in RPMI 1640 (Lonza) medium supplemented with 10% fetal bovine serum at 37°C in a humidified atmosphere with 5% CO_2. THP-1 monocytes were differentiated into macrophages using phorbol 12-myristate 13-acetate (PMA; 10 nmol/L) for 72 h and then rested in medium free of the diester for additional 24 h before the treatments. Then, some cells were incubated with empagliflozin (3 µM) 24 h before stimulation with tumor necrosis factor-α (TNFα; 20 ng/mL, 24 h). Human chemokines MCP-1/CCL-2 and RANTES/CCL-5, metalloproteinases MMP-2 and MMP-9 and VEGF were measured in THP-1 supernatants using commercial ELISA kits (**Table 18**) and following manufacturer's instructions.

Table 18. Commercial ELISA kits

Duoset® kit	Vendor or source	Catalog No
Human CCL2/MCP-1	R&D Systems, UK	DY279
Human CCL5/RANTES	R&D Systems, UK	DY278
Human MMP-2	R&D Systems, UK	DY902
Human MMP-9	R&D Systems, UK	DY911
Human VEGF	R&D Systems, UK	DY293B

3.2 Study of the role of RORα in adipose tissue from morbid obese patients with or without diabetes

3.2.1 Subjects and sample collection

The local Ethics Committee of the University Clinic Hospital of Valencia approved the present study and all subjects gave written informed consent. The research was carried out in accordance with the tenets of the Declaration of Helsinki. The study cohort consisted in forty-one patients with morbid obesity selected for Roux-en-Y gastric bypass who were referred to our Endocrinology and Nutrition Unit. The group was composed by 30 women and 11 men, aged 43 ± 2 years, with a mean body mass index (BMI) of 43.3 ± 0.8 kg/m^2. All patients underwent an extensive preoperative evaluation, including a medical history (complete dietetic history, demographics, smoking habits, dietary habits, physical activity, vascular risk factors, personal or family history of diseases) and physical examination. Individuals aged < 18 or > 60 years, pregnancy, and with current history of autoimmune diseases, cancer or thrombotic diseases were excluded. Patients were diagnosed with diabetes if they had fasting plasma glucose ≥126 mg/dl and/or HbA1c ≥6.5%, were taking glucose lowering drugs or had history of diabetes. Paired omental and subcutaneous fat depots were intraoperatively obtained from the greater omentum and the lower abdominal wall, respectively, during the bariatric surgery. Immediately after their removal, AT samples were placed in a sterile tube with cold PBS.

3.2.2 Clinical and biochemical determinations

One month before the scheduled surgery, blood samples and anthropometric determinations from the patients were obtained. Fasted venous blood samples were collected from each participant between 09:00 and 10:00 am. Heparinized whole blood was centrifuged and plasma samples were maintained at -80ºC until analysis. Glucose, insulin, lipid profile and high-sensitivity C-reactive protein (CRP) concentrations were measured according to standard procedures [196]. BMI was determined as the weight (kg)/height (m^2). Insulin resistance was estimated using the validated homeostasis model assessment (HOMA-IR) = insulin (mUI/l) × glucose (mmol/l)/22.5. Systolic and diastolic blood pressures were also measured.

3.2.3 Quantitative real-time RT–PCR analysis

TRIzol® Reagent *was* used for RNA isolation from subcutaneous and visceral AT samples. RNA (1 µg) was reverse transcribed using the TaqMan Reverse Transcription Reagent Kit (Applied Biosystems, Thermo Fisher Scientific, Waltham, MA). The procedures followed for the extraction and the subsequent reverse transcription were previously described in **Section 3.1.1.5.1** and **Section 3.1.1.5.2.** Once the cDNA was obtained, it was amplified with human-specific *RORA* probe from Applied Biosystems (Hs00536545_m1). RT–PCR was carried out using the Universal Master Mix (Applied Biosystems). The reagents and the cycling protocol are specified in **Table 9** and **Table 10** in **Section 3.1.1.5.3**. Finally, the expression of the transcripts was determined using the $2^{-\Delta\Delta Ct}$ method. *18s* rRNA was employed as endogenous control (Applied Biosystems).

3.2.4 Adipose tissue explant cultures and chemokine measurements

AT samples were placed in a 6-well plate with prewarmed (37ºC) Dulbecco's phosphate buffered saline (DPBS). AT was dissected to remove blood vessels and connective tissue before cutting the tissue into small fragments. Samples were washed with DPBS at 37ºC by centrifugation at 400*g* for 1 min to eliminate blood cells and other debris. AT explants were cultured in DPBS containing penicillin (50 U/ml), streptomycin (50 mg/ml), L-glutamine (2 mM), 2% BSA and 10 % FBS. To quantify chemokine release, some AT explants were cultured for 48 h in 12-well plates (100 mg/well) and treated with vehicle (0.1% DMSO) or the RORα inverse agonist SR3335 (10 µM) (Cayman Chemical, Ann Arbor, MI).

CXCL-8/IL-8 and CCL-2/MCP-1 chemokine release from AT explants was determined by ELISA kits (R&D Systems; Abingdon, UK) (**Table 19**). Chemokine values were expressed as pg/ml/mg tissue.

Table 19. Reagents used for chemokine determination.

Duoset® kit	Vendor or source	Catalog No
Human CCL-2/MCP-1	R&D Systems, UK	DY279
Human CXCL-8/IL-8	R&D Systems, UK	DY208

3.2.5 Immunofluorescence analysis in adipose tissue

Subcutaneous and visceral AT samples obtained from patients subjected to bariatric surgery were incubated in PFA 4% for 48h and then washed in PBS1X before starting the dehydration process as described in **Section 3.1.1.3**. Then, samples were embedded in paraffin. Five-micrometer sections of formalin-fixed, paraffin-embedded AT were stained for RORα, CD31 and CD3 by standard procedures. Slides were deparaffinized, rehydrated and incubated with peroxidase (0.3% H_2O_2) for 15 min. They were then incubated with 15% horse serum in TBS 1X for 1 h. After washing with TBS, slides were incubated overnight at 4ºC with the following primary antibodies: a rabbit polyclonal anti-human RORα (dilution 1:50, cat#ab60134; Abcam, Cambridge, UK); a rat monoclonal anti-human CD3 (dilution 1:50, cat#ab11089, Abcam); a mouse monoclonal anti- human CD31 (dilution 1:50, cat#ab187377, Abcam) and a rabbit monoclonal anti-phospho AKT (cat#4058, Cell Signaling). Alexa-Fluor® 488 goat anti-rabbit, Alexa-Fluor 594 goat anti-rat or an Alexa-Fluor 594 goat anti-mouse (dilution 1:1000; both from Molecular Probes, Eugene, OR) were used as secondary antibodies. Images were obtained with a Zeiss Axio Observer A1 microscope (Carl Zeiss Micro Imaging GmbH, Göttingen, Germany). Quantification of intracellular RORα expression in lymphocytes (CD3+) or endothelial cells (CD31+) was carried out by manually drawing a region of interest in each cell and measuring the fluorescence intensity in that area, as described [197, 198]. The mean pixel intensity was analysed in 6 different fields from omental AT sections from diabetic and non-diabetic patients (n=6 for each group) using ImageJ software. At least 20 cells were quantified for each condition. All acquisitions were obtained maintaining identical fluorescence parameters and thresholding was employed to delete the background signal. The results were expressed in arbitrary units (a.u.).

3.2.6 Western blot analysis

Protein was extracted from the AT as previously described in **Section 3.1.1.6**. and Bradford method [195] was employed to measure protein content. Next, samples diluted in Laemmli buffer 4X (**Table 14**) were denatured and proteins were separated by 10% SDS-PAGE electrophoresis (**Table 15**) and blotted onto polyvinylidene difluoride membranes. Then, non-specific binding sites were blocked with 5% BSA in TBS. Thereafter, membranes were incubated at 4ºC overnight with

primary antibodies against human RORα (dilution 1:200, cat#ab60134, Abcam), human phosphorylated-AKT (Ser473) (dilution 1:500, cat#4058), human AKT (dilution 1:500, cat#4685), human phosphorylated-p65 (Ser536) (dilution 1:500, cat# 3031) and human NF-κB p65 (dilution 1:500, cat#8242) (all purchased from Cell Signaling Technologies, Danvers, MA). Then, membranes were washed and incubated for 1 h with a secondary HRP-linked anti-rabbit antibody (dilution1:2000, cat#0448, Dako). The blots were developed using a chemiluminescence detection system. Signals were measured with ImageQuant LAS 500 Luminiscent Image Analyzer (Sweden).

3.2.7 Cell culture studies

Human umbilical vein endothelial cells (HUVEC) were cultured in human endothelial cell medium (EBM-2) supplemented with 10% fetal bovine serum (FBS) (all from Lonza, Barcelona, Spain). Cells were kept growing at constant conditions of temperature (37°C) and CO_2 concentration (5%).

3.2.8 Cytotoxicity assays

HUVEC were incubated in the presence of SR3335 (0.1–10 μM) or vehicle (0.1% DMSO) at 37 °C for 24 h in a 96-well plate. Assessment of viability was carried out by flow cytometry using annexin V-FITC and propidium iodide (PI) detection kit and analysed on a BD FACSVerse flow cytometer (both from BD Biosciences).

3.2.9 Leukocyte-HUVEC interactions under flow conditions

The flow chamber assay was run as described in **Section 3.1.2.2.3**. Briefly, confluent HUVEC were stimulated with TNFα (20 ng/ml) for 24 h. SR3335 (0.1-10 μM) was added to some plates 24 h prior to TNFα stimulation. Human mononuclear cells were isolated from the blood of healthy donors by Lymphoprep^{TM} density gradient as detailed in **Section 3.1.2.2.2**. The GlycoTech flow chamber (Gaithersburg, MD) was assembled and placed onto an inverted microscope stage, and freshly isolated human mononuclear cells (1×10^6 /ml) were perfused over the endothelial monolayers at a constant rate of 0.5 dyn/cm^2 using a syringe pump (Harvard Apparatus Inc., Holliston, MA). After 5 min of perfusion, adhered cells

were quantified by five selected fields (×20 objective, ×10 eyepiece) using a phase-contrast microscope (Axio Observer A1; Zeiss, Jena, Germany).

3.2.10 Determination of pro-inflammatory mediators in HUVEC

HUVEC were grown in 6-well plates until confluence and stimulated with TNFα (20 ng/mL) for 24 h. Some cells were pretreated with SR3335 (10 µM) or vehicle (0.1% DMSO) for 24 h before stimulus with TNFα. After treatments, supernatants were collected and CCL2/MCP-1 and CXCL8/IL-8 levels were determined using commercial ELISA kits (R&D Systems, Abingdon, United Kingdom) and following manufacturer´s instructions (**Table 19**).

3.2.11 Immunofluorescence assays in endothelial cells

Confluent HUVEC cultured on glass coverslips were treated for 24 h with SR3335 (10 µM) or vehicle (0.1% DMSO) and then stimulated for 24 h with TNFα (20 ng/ml). After washing with PBS, cells were fixed with 4% PFA and incubated with 1% BSA in PBS to prevent non-specific binding. Then, HUVEC were incubated at 4 °C overnight with the primary rabbit polyclonal antibodies: anti-human VCAM-1 (dilution 1:100, cat#ab106777; Abcam) and anti-human ICAM-1 (dilution 1:100, cat#ab53013; Abcam). An Alexa Fluor 488-conjugated goat anti-rabbit was used as a secondary antibody (1:1000, cat#11034; Molecular Probes). To evaluate NF-κB translocation, coverslips containing cells were treated for 24 h with SR3335 (10 µM) or vehicle (0.1% DMSO) and then stimulated for 30 min with TNFα (20 ng/ml). After washing with PBS, cells were fixed with methanol/acetone (1:1), and blocked with a 1% BSA/PBS. Cells were incubated at 4 °C overnight with a primary antibody against the NFκB p65 subunit (dilution 1:100; cat#610869, BD Transduction Laboratories, Lexington, KY). Immunofluorescence signals were detected using an Alexa Fluor 488-conjugated goat anti-rabbit secondary antibody (1:1000 dilution; Molecular Probes).

3.2.12 Western Blot analysis in HUVEC

HUVEC were grown in 6-well plates until confluence and stimulated with TNFα (20 ng/mL) for 30 min. Some cells were pretreated with SR3335 (10 µM) or vehicle (0.1% DMSO) for 24 h before the stimulus. After treatments, protein was

obtained as decribed in **Section 3.1.2.4** and quantified using the Bradford method [195]. Then, Western Blot was performed as detailed in **Section 3.1.1.6**, using a 10% running gel and the following primary antibodies: phosphorylated-p65 (Ser536) (dilution 1:500, cat# 3031) and NF-κB p65 (dilution 1:500, cat#8242) (all purchased from Cell Signaling Technologies, Danvers, MA). Then, membranes were washed and incubated for 1 h with a secondary HRP-linked anti-rabbit antibody (dilution1:2000, cat#0448, Dako). The blots were developed using a chemiluminescence detection system. Signals were measured with ImageQuant LAS 500 Luminiscent Image Analyzer (Sweden).

3.3 Statistical analysis

Values are expressed as individual data points, percentages or means±SEM when appropriate. Non-parametric data are expressed as the median and the interquartile range.

The normality of distribution of data was evaluated with Kolmogorov-Smirnov test. For comparisons between two groups, Student´s t test was used for data that passed both normality (Kolmogorov-Smirnov test) and equality of variance (Levene´s test); otherwise, the non-parametric Mann-Whitney U test was used. For comparisons between multiple groups, one-way analysis of variance followed by *post hoc* Bonferroni or Newman-Keuls analysis was used in data that passed both normality and equality of variance; otherwise, the non-parametric Kruskal-Wallis test followed by Dunn´s *post hoc* analysis was used.

Additional statistical studies include: $\chi 2$ analysis, which was used to assess statistical significance between qualitative variables; the log-rank test, performed to analyse survival data and Spearman correlation test, used to analyse the correlation between experimental findings and clinical features.

A significance level of 5% ($\alpha=0.05$) and 80% power ($\beta=0.20$) was established and data were considered statistically significant at $P<0.05$.

All graphics and statistical calculations were performed using GraphPad Prism 6 (GraphPad Software, La Jolla, CA).

4. RESULTS

4.1 Study of the effects of SGLT-2 inhibition in abdominal aortic aneurysm development and endothelial dysfunction

4.1.1 Ang II-induced dissecting aneurysm formation was inhibited in mice treated with empagliflozin for 28 days

Twelve-week-old male apoE$^{-/-}$ mice were infused subcutaneously with Ang II at a dose of 1000 ng/kg per minute (n=48) or with saline (n=10) for 28 days. Ang II–infused mice received orally vehicle (n=16) or empagliflozin administered daily at a dose of 1 mg/kg (n=16) or 3 mg/kg (n=16).

At the end of the study period, aortas were isolated and photographed. Images in **Figure 17A** show that Ang II induces AAA in apoE$^{-/-}$ mice but aneurysm formation seems to be reduced in mice treated with empagliflozin. According with these observations, morphometric analysis showed that the maximal external diameter of the ascending, thoracic and suprarenal aorta was greater in Ang II–infused apoE$^{-/-}$ than in saline-infused mice (P<0.001; **Figures 17B-D**). Empagliflozin cotreatment at the dose of 1 mg/kg did not affect any external diameters (P>0.05; **Figures 17B-D**); however, empagliflozin cotreatment at the dose of 3 mg/kg decreased significantly ascending aortic (P=0.047), thoracic (P=0.037), and suprarenal dilatations (Ang II, 2.3±0.1 mm versus Ang II + empagliflozin [3 mg/Kg] 1.4±0.1 mm; P=0.02) (**Figures 17B-D**).

Regarding mortality, within the initial 28 days of treatment, 7 (43%) Ang II–infused apoE$^{-/-}$ mice and 7 (43%) Ang II mice cotreated with the low dose of empagliflozin (1 mg/kg) died as a result of rupture of the aorta, whereas 4 deaths (25%) occurred in mice treated with empagliflozin at the higher dose (3 mg/kg; P=0.36; **Figure 17E**).

Additionally, according to the classification system of Daugherty et al, [191] the aneurysms induced by sole administration of Ang II were more severe than those with empagliflozin cotreatment (3 mg/kg; P<0.05; **Figure 17F**).

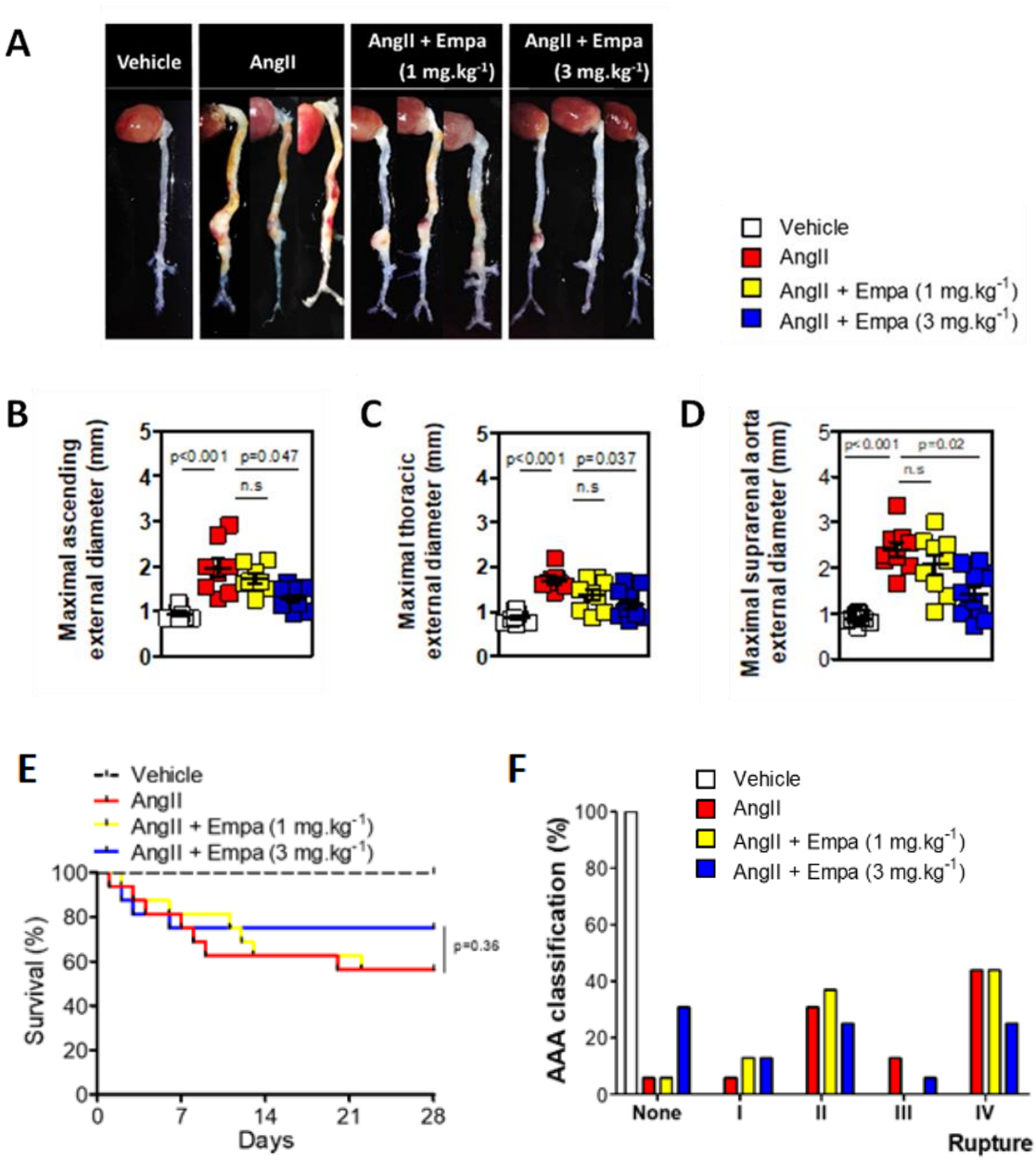

Figure 17. Effect of oral empagliflozin (Empa) treatment on Ang II–induced dissecting AAA in apoE$^{-/-}$ mice. (**A**) Representative images of aortas 28 days after surgery. Maximal ascending (**B**), thoracic (**C**) and suprarenal (**D**) external diameters (mm) of the aortas were measured by morphometry at day 28. Data represent the mean±SEM from vehicle (n=10), Ang II (n=9), Ang II+Empa 1 mg/kg (n=9), and Ang II+Empa 3 mg/kg (n=12). Statistical analysis was performed by Kruskal-Wallis (Dunn post hoc) test. (**E**) Kaplan-Meier curves of survival free from abdominal aneurysm rupture. Survival curves were analysed using the log-rank test (Mantel-Cox test). (**F**) Aneurysm severity (stages I–IV) was scored using a classification scheme similar to the one described previously [191]. Stage IV was attributed to ruptured aneurysms. n.s. indicates nonsignificant.

Furthermore, empagliflozin (3 mg/kg) significantly decreased body weight in apoE$^{-/-}$ mice infused with Ang II (vehicle, 28.6±0.2 g versus Ang II + empagliflozin [3 mg/Kg], 26.1±0.6 g; P=0.04; **Table 20**). By contrast, empagliflozin administration (1 or 3 mg/kg) did not affect glucose levels or the lipid profile (P>0.05; **Table 20**) and none of the treatments affected Ang II–induced elevation of blood pressure (P>0.05; **Table 20**).

	Weight (g)	SBP (mmHg)	Glucose (mg.dl^{-1})	Triglycerides (mg.dl^{-1})	TC (mg.dl^{-1})	HDL-C (mg.dl^{-1})
Vehicle (n=10)	28.6±0.2	114±4.1	91.7±6	139.1±7.4	532.1±20.9	44.8±1.8
AngII (n=9)	28.7±0.7 n.s	162.5±13.7 *p<0.05	93.8±9.9 n.s	136.0±10.9 n.s	497.8±19.2 n.s	44.0±1.7 n.s
AngII + Empa (1 mg.kg^{-1}) (n=9)	28.1±0.6 n.s	185.5±13.8 *p<0.05	94.0±8 n.s	123.5±12.7 n.s	495.7±19.1 n.s	42.6±1.4 n.s
AngII + Empa (3 mg.kg^{-1}) (n=12)	26.1±0.6 *p=0.04	165±8.1 *p=0.009	74.2±4.1 n.s	148.8±8.8 n.s	501±26.8 n.s	47.3±3.1 n.s

Table 20. Effects of empagliflozin (Empa) treatment on weight, systolic blood pressure (SBP), glucose, triglycerides, total cholesterol (TC) and HDL-cholesterol (HDL-C) in apoE$^{-/-}$ mice infused with Ang II for 28 days. Data represent the mean±SEM from vehicle (n=10), Ang II (n=9), Ang II + empagliflozin 1 mg/kg (n=9) and Ang II + empagliflozin 3 mg/kg (n=12). Statistical analysis was performed with non-parametric Kruskal-Wallis test followed by Dunn´s post hoc analysis. *p<0.05 vs vehicle. n.s. indicates nonsignificant.

4.1.2 Empagliflozin treatment reduced elastic fibers degradation and vascular smooth muscle cell destruction in suprarenal aortas of apoE$^{-/-}$ mice infused with Ang II for 28 days

Histological examination of serial sections of suprarenal aortic segments of Ang II-infused mice revealed a structural deformity within the adventitia of the abdominal aorta (**Figure 18A**) together with a marked degradation and disappearance of elastic laminae in the medial layer due to focal elastin destruction (P<0.001; **Figures 18B** and **D**). In addition, suprarenal aortas from Ang II-treated mice presented a loss of vascular smooth muscle α-actin cells (P<0.001; **Figures 18C** and **E**). Whereas empagliflozin at the dose of 1 mg/kg did not affect the changes induced by Ang II (P>0.05; **Figures 18A-E**), all of these parameters were

significantly improved in empagliflozin-cotreated mice at the dose of 3 mg/kg (P=0.007 and P=0.006, respectively; **Figures 18D** and **E**).

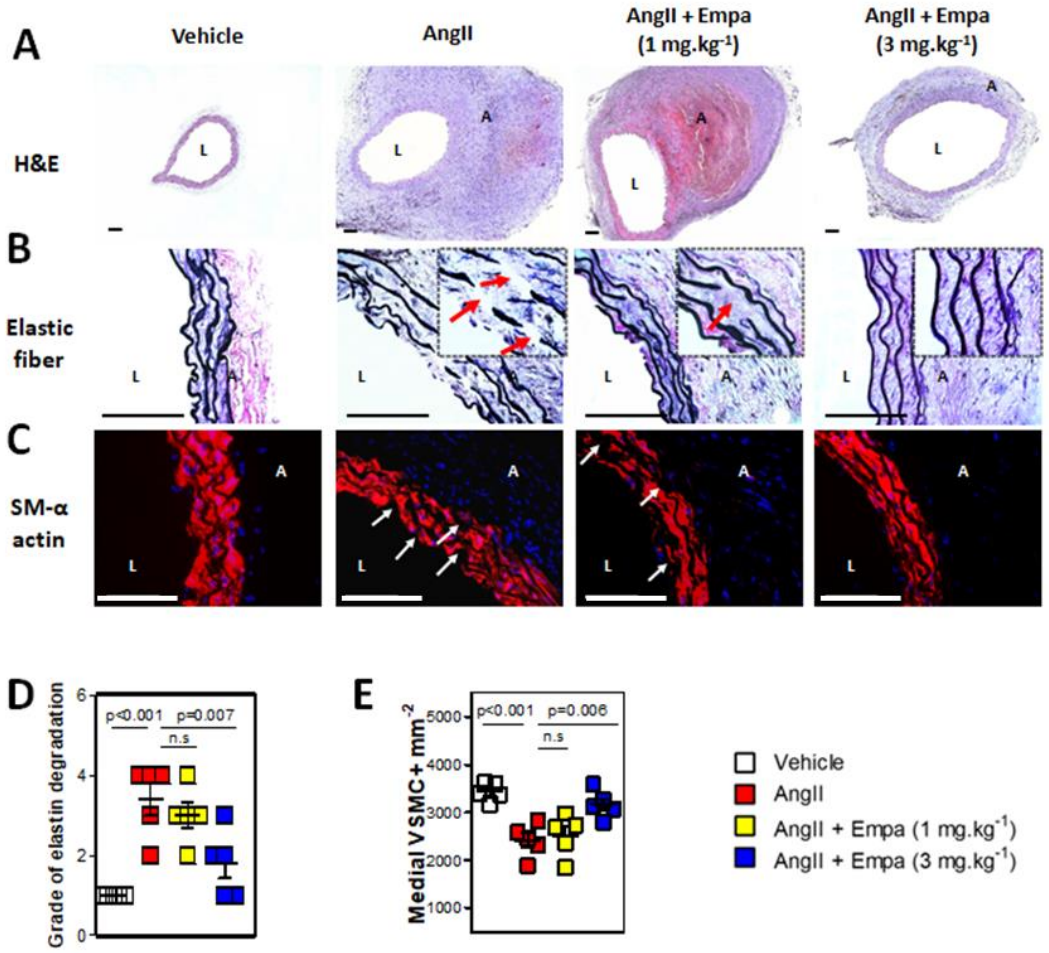

Figure 18. Effects of empagliflozin (Empa) on elastic fibers and medial vascular smooth muscle cells in the suprarenal aortas of apoE$^{-/-}$ mice infused with Ang II for 28 days. (**A**) Representative photomicrographs of hematoxylin and eosin (H&E) staining. Bars=200 µm. (**B**) Representative images of histological stainings for elastin fibers (Van Gieson); arrows show the sites of elastin destruction. Bars=100 µm. (**C**) Representative immunostaining for smooth muscle α-actin (SM-α actin; red). Nuclei were stained with DAPI (4′,6-diamidino-2-phenylindole; blue). Arrows show the sites of loss of medial smooth muscle (SM) cells. Bars=100 µm. (**D**) Severity of elastin degradation was semiquantified as following: grade 1, no degradation; grade 2, mild degradation; grade 3, severe degradation; and grade 4, the presence of aortic rupture. Data represent the mean±SEM from n=5 animals for each group. (**E**) Medial vascular smooth muscle cell (VSMC) positive per mm^2. Lumen (L) and adventitial (A) regions are indicated. Data represent the mean±SEM from vehicle (n=5), Ang II (n=5), Ang II+Empa 1 mg/kg (n=5) and Ang II+Empa 3 mg/kg (n=5). Statistical analysis was performed by 1-way ANOVA (Newman-Keuls post hoc test). n.s. indicates nonsignificant.

4.1.3 Empagliflozin reduces macrophage infiltration and neovascularization in dissecting AAA induced by infusion of Ang II for 28 days

Inflammation and angiogenesis are two processes associated to AAA pathogenesis [77, 199, 200]. As expected, a marked infiltration of macrophages, identified by positive Mac3 immunostaining, was detected in the media and adventitia of the suprarenal aortic aneurysms sections from Ang II–infused mice (P<0.001; **Figures 19A** and **B**). Empagliflozin cotreatment at the dose of 1 mg/kg did not affect macrophage infiltration(P>0.05; **Figures 19A** and **B**),but at the higher dose of 3 mg/kg, empagliflozin significantly decreased the number of infiltrated macrophages(P<0.001; **Figures 19A** and **B**).Additionally, a significant increase of CD31+ capillary microvessels was observed in the suprarenal aortas of Ang II–infused mice (P<0.001; **Figures 19A** and **C**) accompanied by a significant elevation in *Vegf* mRNA expression (P=0.02; **Figure 19D**). At the lower dose of 1 mg/kg, empagliflozin did not affect CD31+ capillary microvessels (P>0.05; **Figure 19A** and **C**) neither mRNA expression of *Vegf* (P>0.05; **Figure 19D**), although mice cotreated simultaneously with empagliflozin at the higher dose of 3 mg/kg showed a marked reduction in capillary formation(P<0.001; **Figures 19A** and **C**)and in *Vegf* mRNA expression (P=0.04; **Figure 19D**).

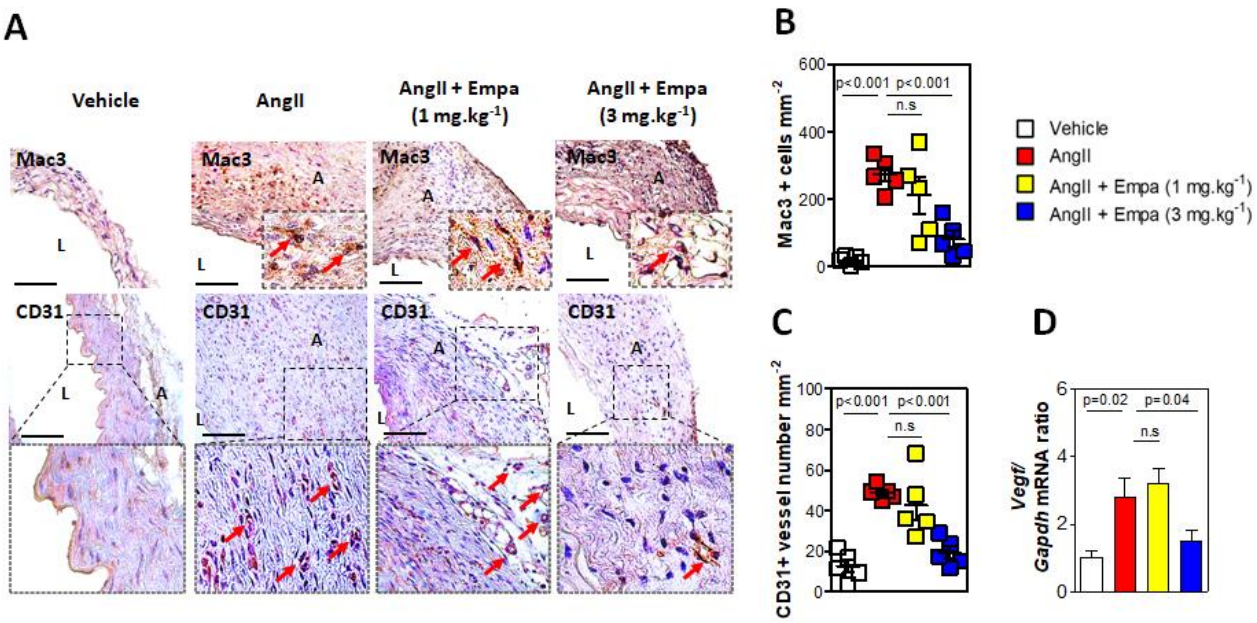

Figure 19. Effect of empagliflozin (Empa) treatment on macrophage infiltration and neovascularization in the suprarenal aortic wall of apoE$^{-/-}$ mice infused with Ang II for 28 days. (**A**) Representative immunohistochemical staining of Mac3+ cells and CD31+ microvessels in aortic cross sections. Bars=100 µm. Lumen (L) and adventitial (A) regions are indicated. (**B**) Quantitative data for Mac3+ cells and (**C**) CD31+ microvessels per mm^2 in suprarenal aortic sections. Data represent the mean±SEM from vehicle (n=5), Ang II (n=5), Ang II+Empa 1 mg/kg (n=5), and Ang II+Empa 3 mg/kg (n=5). (**D**) Gene expression of *Vegf* in the suprarenal aortas was analysed by real-time RT-PCR. Data represent mean±SEM of the ratio between the gene and *Gapdh* gene expression (n=5 each group). Statistical analysis was performed by one-way analysis of variance (ANOVA) followed by Newman-Keuls post hoc test. n.s. indicates nonsignificant.

4.1.4 Empagliflozin reduces chemokine expression in the suprarenal aortas of apoE$^{-/-}$ mice infused with Ang II for 28 days

Given that leukocyte infiltration is a process mediated by the generation of a chemoattractant gradient in which chemokines play a key role, the next step was to evaluate the effect of empagliflozin on the expression of CCL-2/MCP-1 and CCL-5/RANTES in the AAA lesion of apoE$^{-/-}$ mice infused with Ang II.

Immunohistochemistry assays showed that protein levels of CCL-2/MCP-1 and CCL-5/RANTES were significantly increased in the suprarenal aortas from Ang II–infused mice compared with those in vehicle-treated mice (P<0.001; **Figures 20A-C**) and were notably reduced by empagliflozin cotreatment (3 mg/kg; P<0.001 and P=0.02, respectively; **Figures 20A-C**). Similar results were obtained by qPCR

analysis. Ang II–infused mice showed higher levels of *Ccl-2/Mcp-1* and *Ccl-5/Rantes* mRNA expression than vehicle-treated mice (P=0.003 and P<0.001 respectively; **Figures 20D** and **E**) and this increase was significantly reduced in mice co-treated with empagliflozin at the dose of 3 mg/Kg (P=0.03 and P<0.001, respectively; **Figures 20D** and **E**) but not in mice treated with empagliflozin at the dose of 1 mg/Kg (P>0.05, **Figures 20D** and **E**).

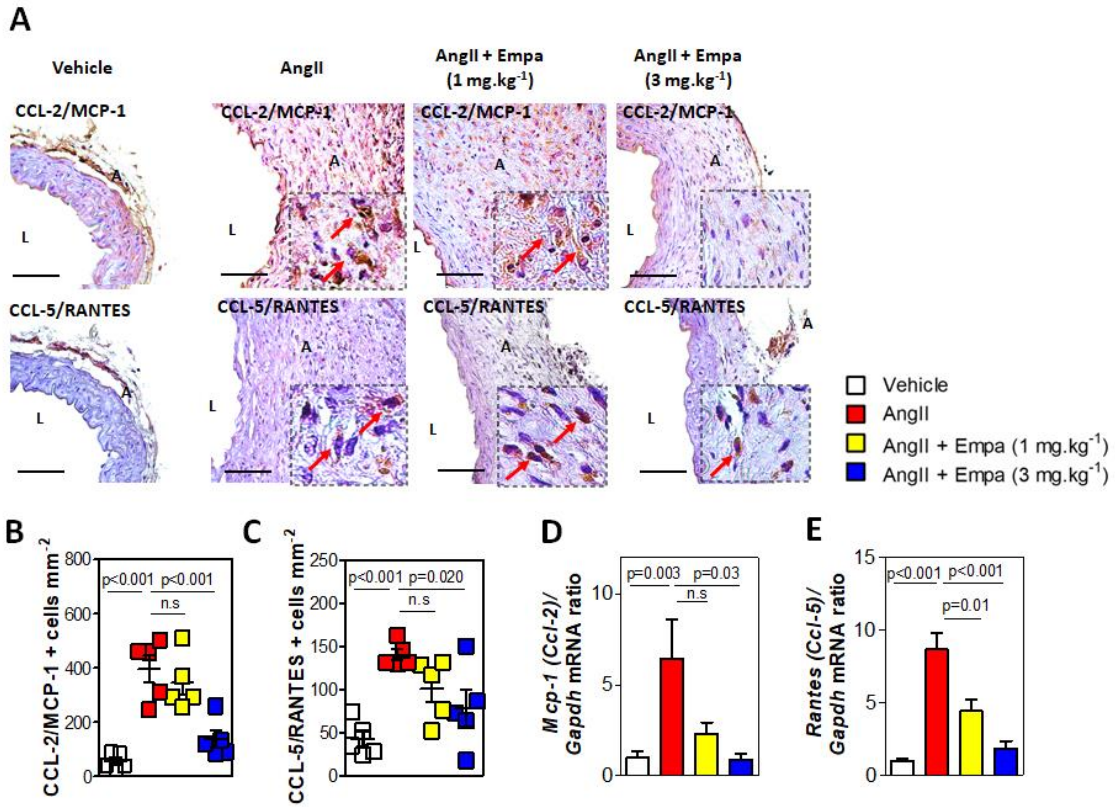

Figure 20. Effect of empagliflozin (Empa) treatment on chemokine expression in the suprarenal aortic wall of apoE$^{-/-}$ mice infused with Ang II for 28 days. (**A**) Representative immunohistochemical staining of CCL-2 (chemokine [C-C motif] ligand 2)/MCP-1 (monocyte chemoattractant protein-1), and CCL-5 (chemokine [C-C motif] ligand 5)/RANTES (regulated on activation, normal T cell-expressed and secreted) in aortic cross sections. Bars=100 µm. Lumen (L) and adventitial (A) regions are indicated. (**B**) Quantitative data for CCL-2/MCP-1+ cells, and (**C**) CCL-5/RANTES+ cells per mm^2 in suprarenal aortic sections. Data represent the mean±SEM from vehicle (n=5), Ang II (n=5), Ang II+Empa 1 mg/kg (n=5), and Ang II+Empa 3 mg/kg (n=5). Gene expression of *Mcp-1/Ccl-2* (**D**) and *Rantes/Ccl-5* (**E**) in the suprarenal aortas was analysed by real-time RT-PCR. Data represent mean±SEM of the ratio between each gene and *Gapdh* gene expression (n=5 for each group). Statistical analysis was performed by one-way analysis of variance (ANOVA) followed by Newman-Keuls post hoc test. n.s. indicates nonsignificant.

4.1.5 Empagliflozin treatment reduced extracellular matrix degradation in suprarenal aortas of apoE$^{-/-}$ mice infused with Ang II for 28 days

As it is known that matrix metalloproteinases (MMPs) are involved in extracellular matrix (ECM) destruction and aortic wall remodelling in AAA [201], the effects of empagliflozin on the expression of MMP-2, MMP-9 and the tissue inhibitor of metalloproteinases (TIMP)-1 in the suprarenal aortas of apoE$^{-/-}$ mice were then evaluated. Immunohistochemical analyses revealed that Ang II–infused mice had higher expression of MMP-2 and MMP-9 protein than vehicle-treated mice in the suprarenal aortas (P<0.001; **Figures 21A-C**), and these results correlated with a significant increase in mRNA expression of *Mmp-2* and *Mmp-9* (P<0.05; **Figures 22A** and **B**). It was also observed that emplagliflozin cotreatment at a dose of 1 mg/kg neither affected MMPs protein levels (P>0.05, **Figures 21A-C**) nor mRNA expression of *Mmp-2* or *Mmp-9* (P>0.05; **Figures 22A** and **B**). By contrast, oral empagliflozin administration at the higher dose (3 mg/kg) significantly decreased MMP-2 and MMP-9 protein levels (P<0.001 and P=0.01 respectively; **Figures 21A-C**) and their mRNA expression (P=0.03 and P=0.04 respectively; **Figures 22A** and **B**). Conversely, TIMP-1 protein levels were higher in the suprarenal aortas from mice cotreated with empagliflozin at a dose of 3 mg/kg than in those from Ang II-infused mice (P=0.01; **Figures 21A** and **D**) and also mRNA expression of *Timp-1* was significantly increased in the empagliflozin-treated group (3 mg/kg; P=0.02; **Figure 22C**).

Additionally, MMP enzymatic activity was also determined. As expected, suprarenal aortic extracts from Ang II–infused mice had higher MMP activity relative to vehicle-infused mice (P<0.05; **Figure 22D**) and this was significantly decreased by empagliflozin cotreatment at the dose of 3 mg/Kg (P<0.05; **Figure 22D**). However, empagliflozin at the dose of 1 mg/kg did not affect MMP enzymatic activity (P>0.05; **Figure 22D**).

Finally, a double immunofluorescence was carried out to evaluate the cellular localization of MMPs and TIMP-1 in the suprarenal aortic aneurysms (**Figure 23**). Both MMP-2/MMP-9 and TIMP-1 were detected mainly in macrophages (Mac3+) and endothelial cells (CD31+) from suprarenal aortic aneurysms (**Figures 23A** and **B** respectively).

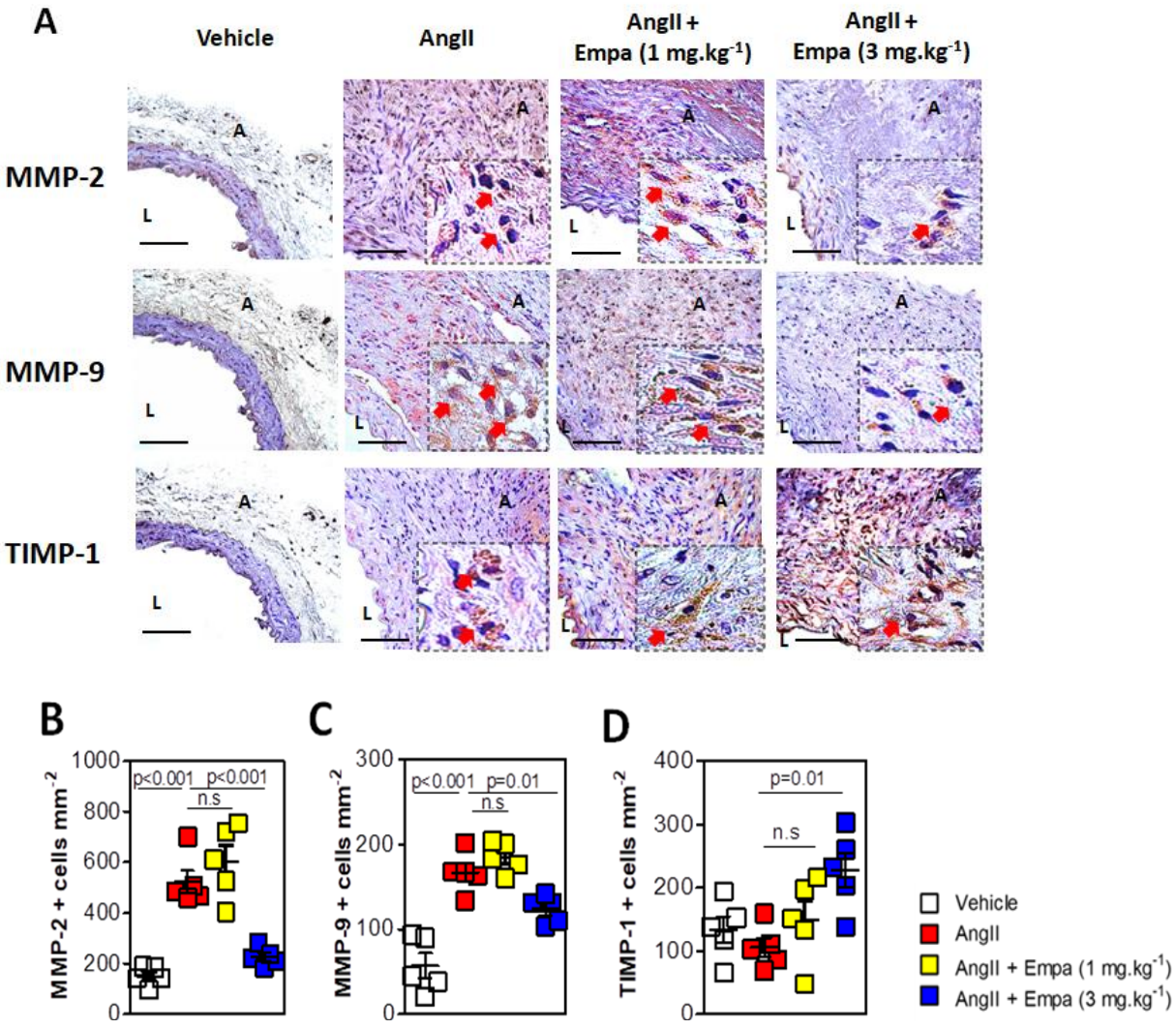

Figure 21. Effects of empagliflozin (Empa) administration on MMP (matrix metalloproteinase)-2, MMP-9, and TIMP-1 (tissue inhibitor of metalloproteinase) protein expression in the suprarenal aortas of apoE$^{-/-}$ mice infused with Ang II for 28 days. (**A**) Representative immunohistochemical staining of MMPs and TIMP-1 in the abdominal aorta of apoE$^{-/-}$ mice. Bars=100 μm. Lumen (L) and adventitial (A) regions are indicated. Quantification of (**B**) MMP-2+, (**C**) MMP-9+, and (**D**) TIMP-1+ cells per mm^2 in the suprarenal aortas. Data represent the mean±SEM from n=5 animals per group. Data analysis was performed by one-way analysis of variance (ANOVA) followed by post hoc Newman-Keuls analysis.

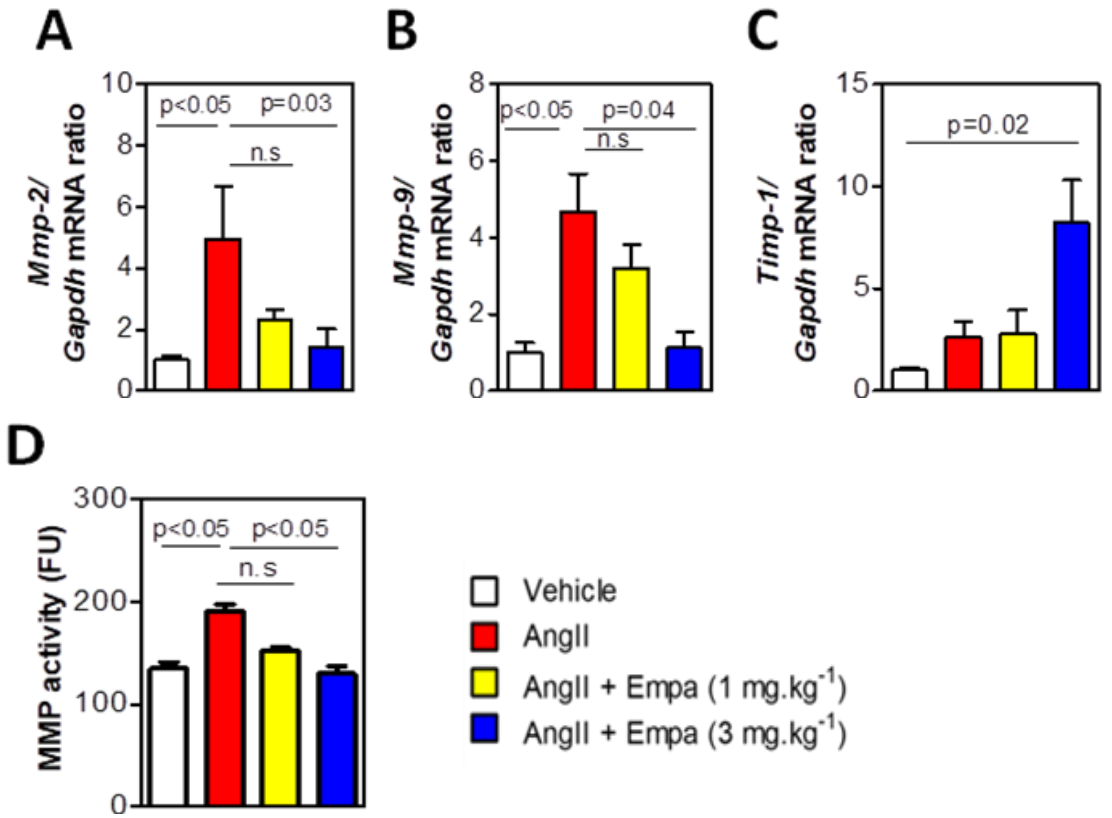

Figure 22. Effects of empagliflozin (Empa) administration on *Mmp* (matrix metalloproteinase)-*2*, *Mmp-9*, and *Timp-1* (tissue inhibitor of metalloproteinase) mRNA expression and protease activity in the suprarenal aortas of apoE$^{-/-}$ mice infused with Ang II for 28 days. Gene expression of (**A**) *Mmp-2*, (**B**) *Mmp-9* and (**C**) *Timp-1* in the suprarenal aortas was analysed by real-time RT-PCR. Data represent mean±SEM of the ratio between each gene and *Gapdh* gene expression (n=5 for each group). Statistics were performed by one-way ANOVA followed by post hoc Newman-Keuls analysis. (**D**) MMP activity was measured in protein abdominal aorta extracts by fluorometry. FU indicates fluorescence units. Data represent the mean±SEM from n=5 animals per group. Statistical analysis was performed by one-way ANOVA (Newman-Keuls post hoc test). n.s. indicates nonsignificant.

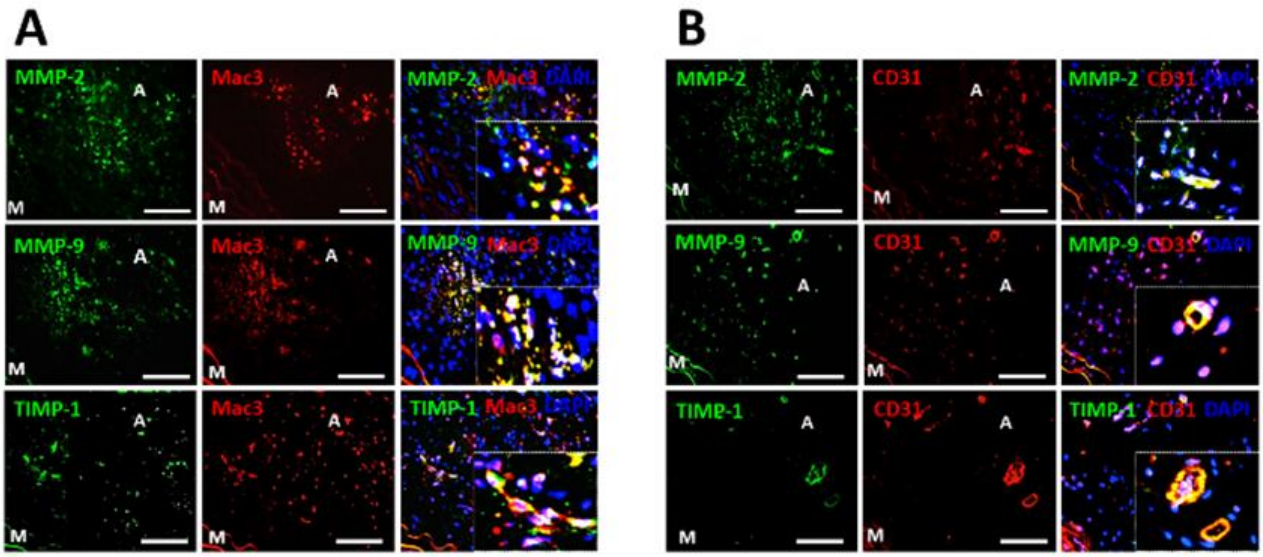

Figure 23. Cellular localization of both MMP-2/MMP-9 and TIMP-1 in suprarenal aortic aneurysms. Representative immunofluorescence images showing colocalization of MMP-2, MMP-9 and TIMP-1 with (**A**) Mac3 (macrophages) and (**B**) CD31 (endothelial cells) in the suprarenal aorta of apoE$^{-/-}$ mice infused with Ang II for 28 days. Immunofluorescence was visualised using Alexa Fluor 633 secondary antibody (CD31 or Mac3, red) and Alexa Fluor 488 secondary antibody (MMP-2 or MMP-9, TIMP-1 green). Nuclei were stained with DAPI (blue). A, adventitia and M, media regions are indicated. Bars, 100 µm.

4.1.6 Empagliflozin inhibits the activation of p38 MAPK and NF-κB in AAA induced by Ang II infusion for 28 days

Activation of p38 MAPK and NF-κB signalling is known to be associated with AAA pathogenesis [202, 203]. For this reason, the next objective was to analyse the impact of empagliflozin cotreatment on these pathways in suprarenal aneurysmal tissue. As shown in **Figure 24**, suprarenal aortas from Ang II-infused mice presented a higher phosphorylation level of p38 MAPK ($P<0.001$; **Figure 24A**) and p65 ($P<0.05$; **Figure 24B**) than in the vehicle-treated mice. However, this activation was significantly dampened in equivalent tissue from empagliflozin-cotreated mice at a dose of 3 mg/kg ($P<0.05$; **Figures 24A** and **B**) whereas this reduction was not observed in mice cotreated with empagliflozin at a dose of 1 mg/kg ($P>0.05$; **Figures 24A** and **B**).

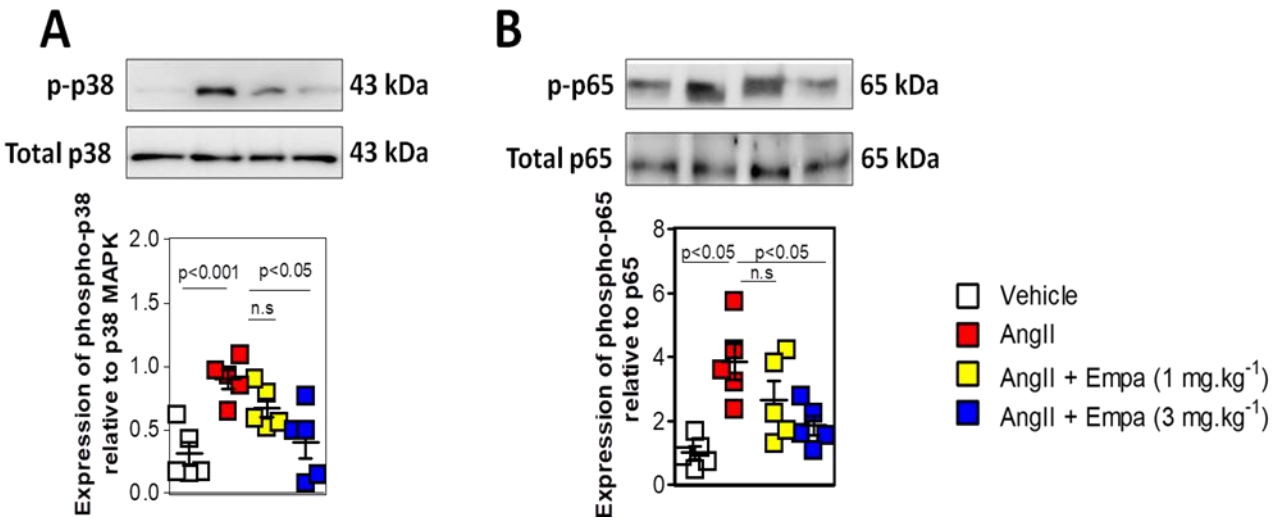

Figure 24. Effect of empagliflozin treatment on the activation of NF-κB and p38 MAPK signalling pathways in suprarenal abdominal aortic tissue. (**A**) Representative Western blot of phospho p38/total p38 and (**B**) phospho p65/total p65 in the suprarenal aortas. Data represent the mean±SEM from n=5 animals per each group. Statistical analysis was performed by one-way ANOVA (Newman-Keuls post hoc test). MAPK, mitogen-activated protein kinase; and n.s. indicates nonsignificant.

4.1.7 SGLT-2 is expressed in the suprarenal aorta of apoE$^{-/-}$ mice

SGLT-2 has been reported to be expressed in kidney [204], adipose tissue [205], aorta [194] and endothelial cells [206]. In order to assess SGLT-2 expression in the aorta of the apoE$^{-/-}$ mice used in the present study, Western Blot assays were performed. The obtained results confirmed the expression of SGLT-2 in the suprarenal aorta of mice infused with Ang II for 28 days. Although a modest increase was observed in Ang II–treated animals, none of the treatments significantly altered SGLT-2 expression (P>0.05; **Figure 25A**). In addition, immunohistochemical analysis showed positive SGLT-2 expression in suprarenal aortic cross sections (**Figure 25B**).

To detect which type of cells expressed SGLT-2 in AAA, a double immunofluorescence was performed. Images shown in **Figure 25C** revealed that SGLT-2 protein expression was mainly localised in endothelial cells (CD31+ cells) but also in macrophages (Mac3+ cells). In addition, *Sglt-2* mRNA expression was detected in the suprarenal aortas from all treatment groups (**Figure 25D**). Although a weak increase was observed in Ang II–infused animals, none of the treatments significantly altered *Sglt-2* mRNA expression (P>0.05; **Figure 25D**). Similarly, the

analysis of thoracic regions from the same mice showed that *Sglt-2* mRNA expression did not differ between the investigated groups (P>0.05; **Figure 25D**). Finally, when suprarenal and thoracic aorta tissues were compared, the pattern of *Sglt-2* mRNA expression was apparently uniform throughout the aorta.

4.1.8 Ang II-induced dissecting aneurysm formation was undetectable in the acute phase of AAA

To study the effect of empagliflozin (3 mg/kg) in the early phase of Ang II–induced vascular dysfunction, twelve-week-old male apoE$^{-/-}$ mice were infused subcutaneously with Ang II at a dose of 1000 ng/kg per minute (n=10) or with saline (n=5) for 5 days. Ang II–infused mice received orally vehicle (n=5) or empagliflozin administered daily at a dose of 3 mg/kg (n=5).

At day 5, aortas were isolated and photographed. Macroscopic images showed that Ang II did not induce AAA in apoE$^{-/-}$ mice and no aneurysms were detected in mice treated with empagliflozin 3 mg/kg (**Figure 26A**). Additionally, morphometric analysis showed that the maximal external diameter of the suprarenal aortas did not significantly differ between the different groups of treatment (P>0.05; **Figure 26B**).

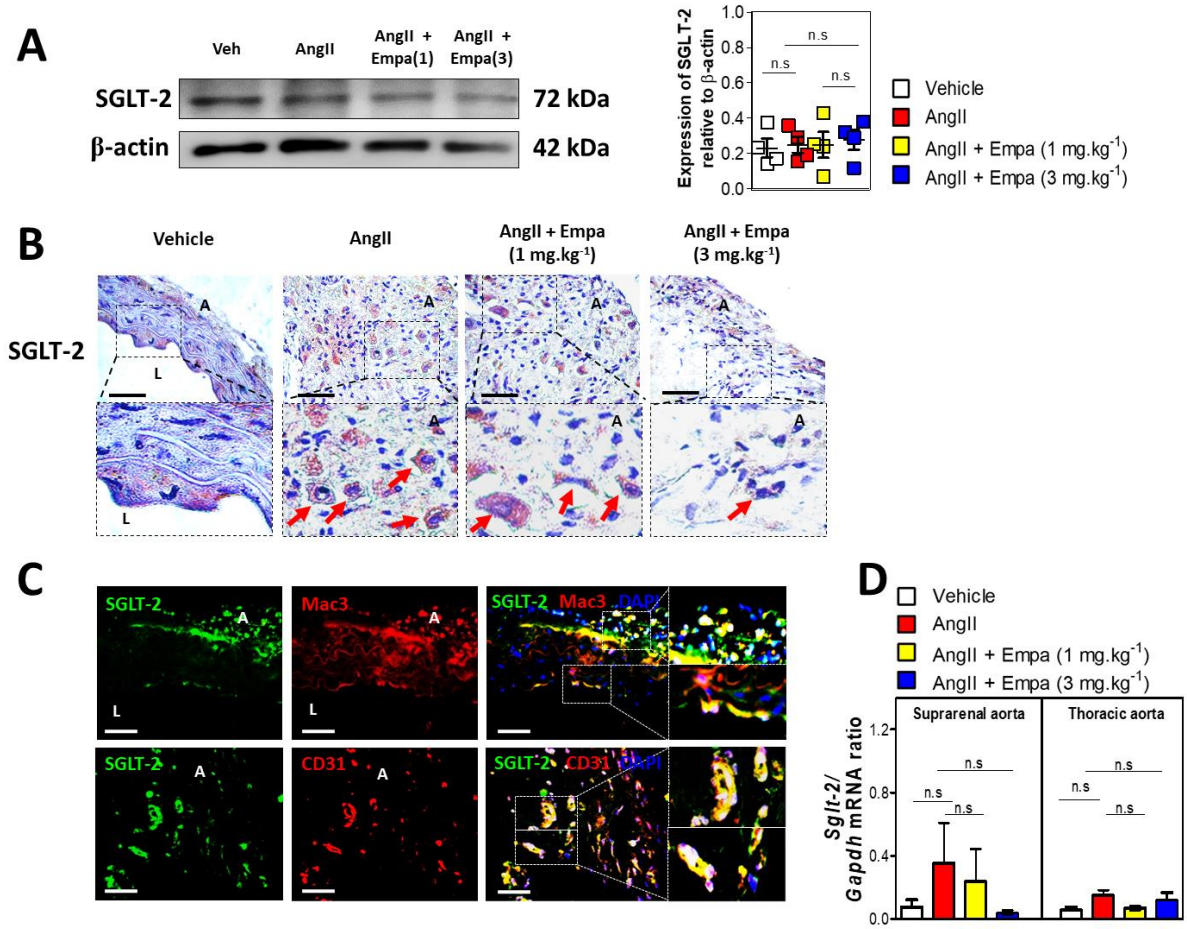

Figure 25. SGLT-2 (sodium-glucose cotransporter type 2) is expressed in the suprarenal aortas of apoE$^{-/-}$ mice. (**A**) SGLT-2 protein expression was evaluated by Western blot analysis. A representative Western blot of SGLT-2 expression is shown. Data represent the mean±SEM from n=4 animals per each treatment group. Statistical analysis was performed by one-way ANOVA (Newman-Keuls post hoc test). (**B**) Representative immunohistochemical staining of SGLT-2 in aortic cross sections. Bars=100 μm. Lumen (L) and adventitial (A) regions are indicated. (**C**) Representative immunofluorescence images showing colocalization of SGLT-2/Mac3 or SGLT-2/CD31 in the aneurysmal tissue. Immunoreactivity was visualised using Alexa Fluor 633 secondary antibody (CD31 or Mac3, red) and Alexa Fluor 488 antibody (SGLT-2, green). Nuclei were stained with DAPI (4′,6-diamidino-2-phenylindole; blue). (**D**) Gene expression of *Sglt-2* was also analysed by real-time RT-PCR in suprarenal and thoracic aortas. Data represent the mean±SEM from n=4 animals per each group. Statistical analysis was performed by one-way ANOVA (Newman-Keuls post hoc test). Empa indicates empagliflozin; n.s., nonsignificant.

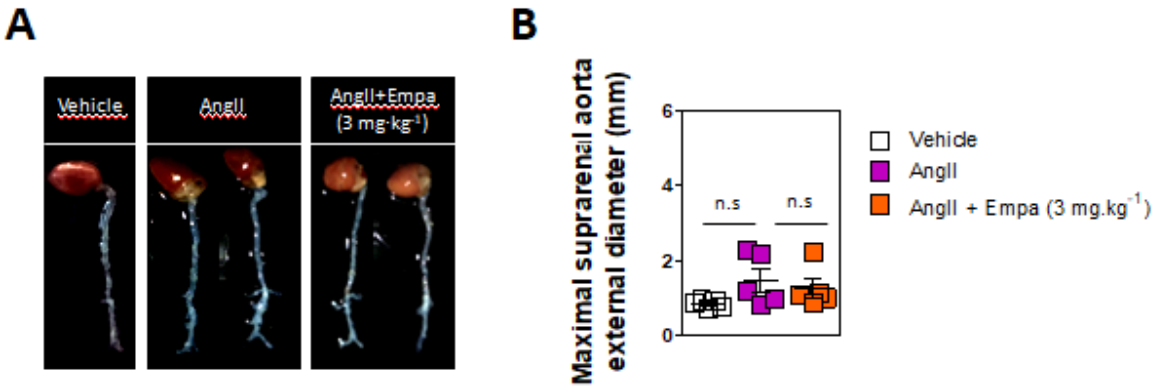

Figure 26. Effect of oral empagliflozin (Empa) treatment on Ang II–induced dissecting AAA in apoE$^{-/-}$ mice. (**A**) Representative images of aortas 5 days after surgery. (**B**) Maximal suprarenal external diameter (mm) of the aortas was measured by morphometry at day 5. Data represent the mean±SEM from n=5 animals in each group. Statistical analysis was performed by Kruskal-Wallis (Dunn post hoc) test.

4.1.9 Effect of oral empagliflozin administration on the elastic fibers and vascular smooth muscle cells in the early phase of dissecting AAA formation

Elastin degradation and loss of smooth muscle (SM)-α actin cells are two pathological features associated with AAA pathology. In order to evaluate the effect of empagliflozin (3 mg/kg) on the integrity of the medial layer of the suprarenal aorta of apoE$^{-/-}$ mice infused with Ang II for 5 days, histological analysis was carried out. Images obtained from elastic fibers, which were visualised with Van Gieson staining, revealed no elastin degradation after Ang II infusion (**Figure 27A**). Similar results were obtained when immunofluorescence assays were performed to evaluate the effect of the empagliflozin treatment (3 mg/kg) on vascular SM α-actin cells. No loss of medial SM-α actin cells was detected in the suprarenal aorta of apoE$^{-/-}$ mice after Ang II infusion for 5 days (**Figure 27B**).

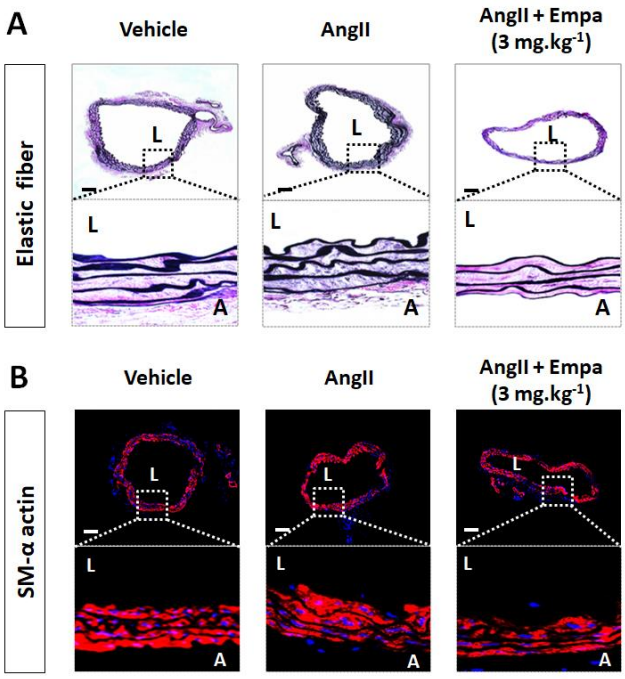

Figure 27. Effects of empagliflozin (3 mg/kg) on suprarenal aortas of apoE$^{-/-}$ mice infused with Ang II for 5 days. (**A**) Histological staining of elastic fibers (Verhoeff–van Gieson staining) (**B**) Immunofluorescence staining of smooth muscle-α actin cells in the suprarenal aorta of apoE$^{-/-}$ mice. L, lumen and A, adventitia regions are indicated. Bars, 200 µm.

4.1.10 Effect of empagliflozin treatment on macrophage infiltration, neovascularization and chemokine expression in the suprarenal aortic wall of apoE$^{-/-}$ mice infused with Ang II for 5 days

Given that leukocyte recruitment and macrophage infiltration are processes associated with the pathogenesis of AAA, we next evaluated the effect of empagliflozin (3 mg/kg) on the infiltrated macrophages in the abdominal aorta of apoE$^{-/-}$ mice during the early phase of AAA formation. Immunohistochemical assays against the macrophage marker Mac3 were performed, however, no positive staining was detected in suprarenal aortas of apoE$^{-/-}$ mice infused with Ang II (**Figure 28A**). Similarly, empagliflozin (3 mg/kg) treatment showed no effect on new vessel formation, which is another pathological feature of AAA. The mRNA expression of *Vegf* did not significantly increase in suprarenal aortas of apoE$^{-/-}$ mice after Ang II infusion for 5 days (P>0.05; **Figure 28B**). However, *Ccl-2/Mcp-1* and *Ccl-5/ Rantes* mRNA expression was significantly increased in the suprarenal aortas of Ang II–infused apoE$^{-/-}$ mice (P=0.01 and P=0.02, respectively; **Figures 28C** and **D**) but not in empagliflozin-cotreated mice (P=0.02 and P=0.03, respectively; **Figures 28C** and **D**).

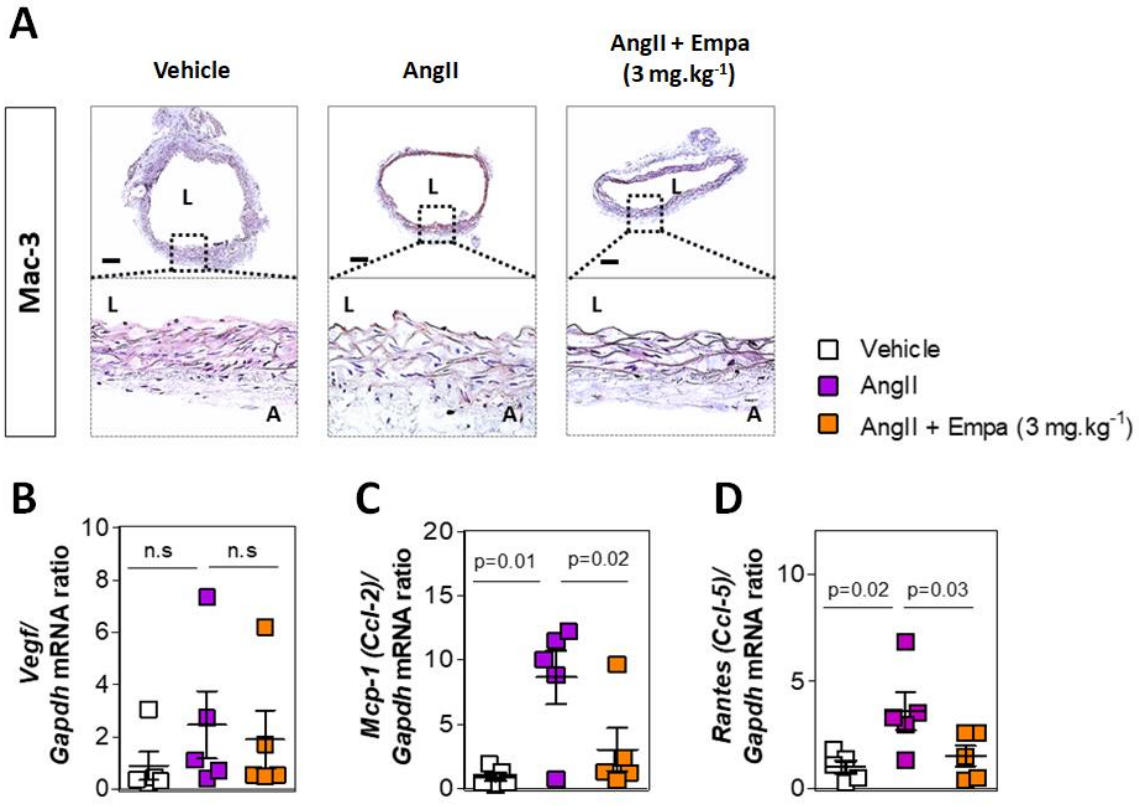

Figure 28. Effect of empagliflozin treatment on macrophage infiltration, neovascularization, and chemokine expression in the suprarenal aortas of apoE$^{-/-}$ mice infused with Ang II for 5 days. (**A**) Immunohistochemical staining of macrophages (Mac3) in the suprarenal aorta of apoE$^{-/-}$ mice. L, lumen and A, adventitia regions are indicated. Bars, 200 µm. Gene expression of (**B**), *Vegf*; (**C**), *Mcp-1* and (**D**), *Rantes* was analysed by real-time RT-PCR. Data represent the mean±SEM of the ratio between each gene and *Gapdh* expression (n=5 animals per each group). Data analysis was performed by one-way analysis of variance followed by post hoc Newman-Keuls test.

4.1.11 Effect of empagliflozin treatment on the expression of matrix metalloproteinases in the suprarenal aorta of apoE$^{-/-}$ mice infused with Ang II for 5 days

Since MMPs play an important role in ECM degradation and aortic wall remodelling in AAA [201], we questioned wether empagliflozin (3 mg/kg) treatment may affect the expression of MMP-2 and MMP-9 in the suprarenal aortic tissue of apoE$^{-/-}$ mice in the early phase of AAA formation. Immunohistochemical assays showed positive MMP-2 and MMP-9 staining in the aortas from Ang-II–infused mice (**Figure 29A**). Additionally, qPCR assays showed higher mRNA expression levels

of *Mmp-9* (P=0.01; **Figure 29C**) but not of *Mmp-2* (P>0.05; **Figure 29B**) in the suprarenal aortas of mice infused with Ang II for 5 days than those detected in the aortas from vehicle-treated mice. Furthermore, the increase of *Mmp-9* mRNA expression was significantly reduced when mice were cotreated with empagliflozin (3 mg/kg) (P=0.02; **Figure 29C)**

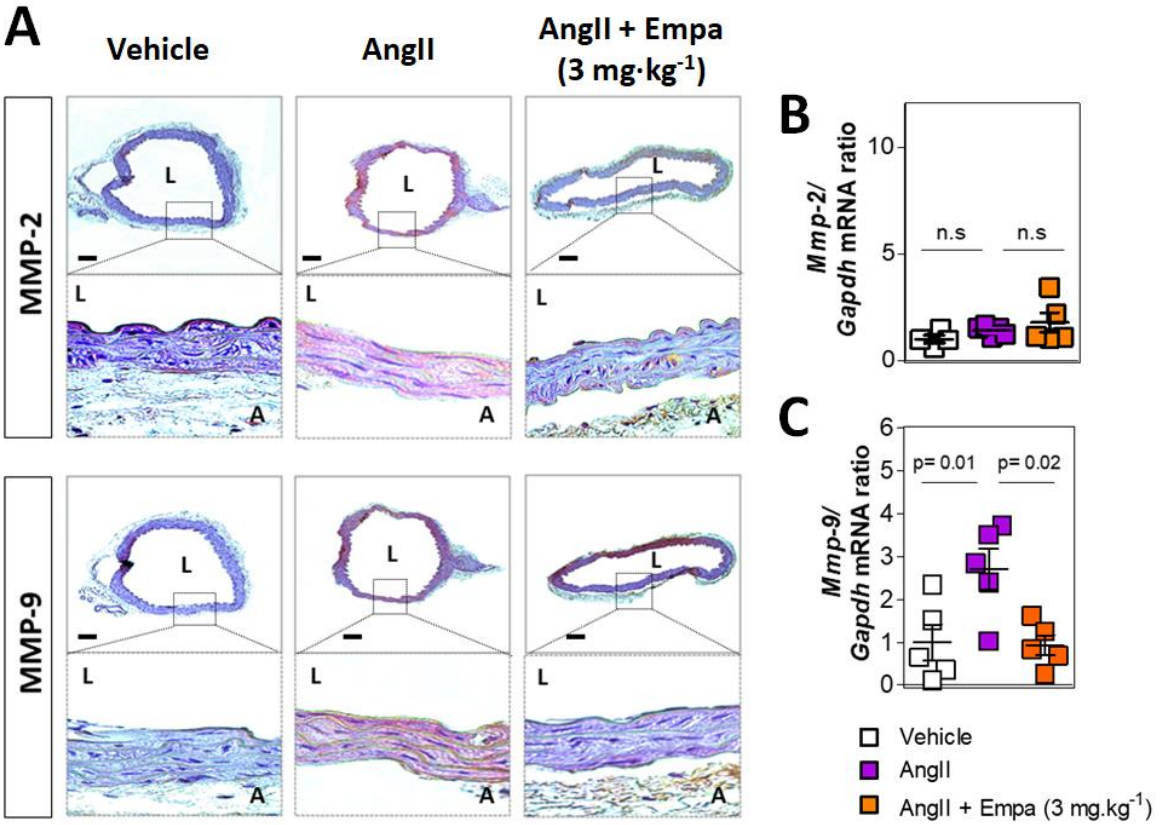

Figure 29. Effects of empagliflozin on MMPs expression in the suprarenal aorta of mice infused with Ang II for 5 days. (**A**) Immunohistochemical staining of MMP-2 and MMP-9 expression in the suprarenal aorta of apoE$^{-/-}$ mice. L, lumen and A, adventitia regions are indicated. Bars, 200 µm. Gene expression of (**B**) *Mmp-2*, and (**C**) *Mmp-9* was analysed by real-time RT-PCR. Data represent mean ± SEM of the ratio between each gene and *Gapdh* expression (n=5 animals per each group). Data analysis was performed by one-way analysis of variance followed by post hoc Newman-Keuls test.

4.1.12 Empagliflozin reduces the activation of p38 MAPK and NF-κB in the in the early phase of dissecting AAA formation

As previously mentioned, p38 MAPK and NF-κB signalling pathways are activated in AAA pathogenesis. According with these observations, Western Blot assays were carried out to study wether empagliflozin may affect the activation of these two pathways in suprarenal aortas of mice infused with Ang II for 5 days. Images and densitometric analysis showed an increase in the phosphorylation levels of p38 MAPK (P<0.05; **Figure 30A**) and p65 (P<0.05; **Figure 30B**) in the aortas of Ang II-infused mice compared with those detected in the aortas from vehicle mice. When mice were cotreated with empagliflozin (3 mg/kg), phosphorylation levels of p38 MAPK and p65 were significantly reduced (P<0.05; **Figures 30A** and **B** respectively).

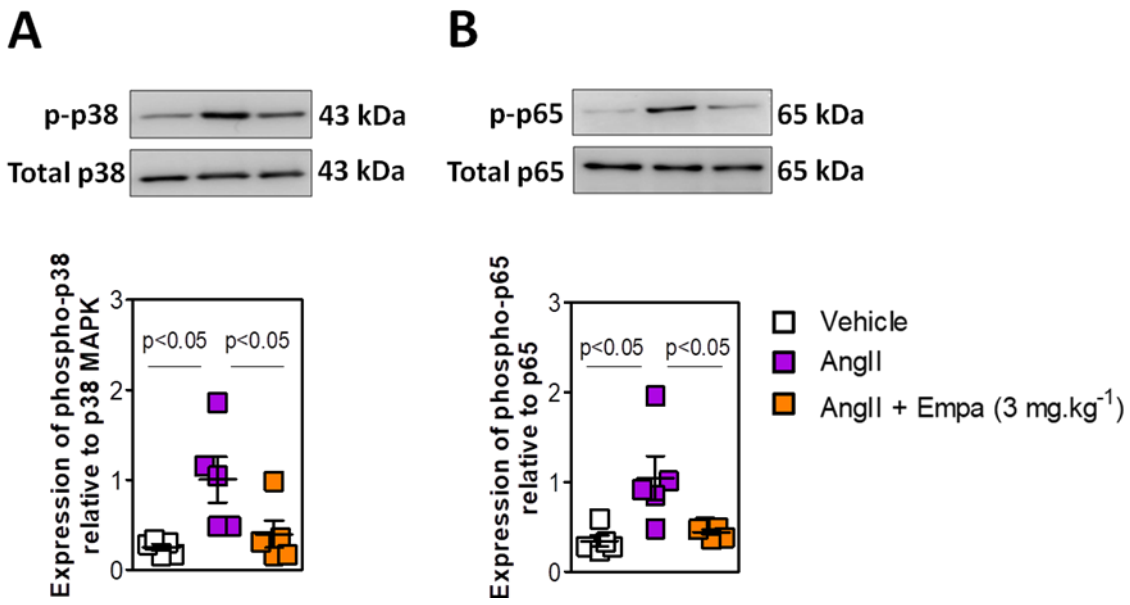

Figure 30. Effect of empagliflozin on the activation of p38 MAPK and NF-κB in the suprarenal aorta of mice infused with Ang II for 5 days. (**A**) Densitometric analysis of phospho p38/total p38 and (**B**), phospho p65/total p65 in the suprarenal aortic tissues. Data represent mean±SEM (n=5 animals per each group) of protein densitometry. Data analysis was performed by one-way analysis of variance followed by post hoc Newman-Keuls test.

4.1.13 Effect of empagliflozin on Human Aortic Endothelial Cells (HAEC) after stimulation with Ang II

In an attempt to extrapolate the results obtained in mice to humans, primary Human Aortic Endothelial Cells (HAEC) were used as an *in vitro* model to study the impact of empagliflozin in vascular inflammation induced by Ang II. First of all, the expression levels of SGLT-2 in HAEC whole-cell lysates were investigated (**Figure 31A**). Western blot analysis revealed that SGLT-2 is expressed in HAEC, however, neither Ang II (1 μM) nor empagliflozin (3 μM) cotreatment affected the expression of SGLT-2 in these cells (P>0.05; **Figure 31A**).

As reported in previous studies, vascular inflammation and macrophage infiltration are two processes that play an important role in AAA development [207, 208]. Therefore, the effect of empagliflozin on mononuclear leukocyte-endothelial cell interactions was analysed under flow conditions. To perform this *in vitro* study, HAEC were pretreated with empagliflozin at different concentrations (0.1 – 3 μM; 24 h) before stimulation with Ang II (1 μM; 24 h). Then, mononuclear cell adhesion was determined using a dynamic model of the flow chamber [209]. Human mononuclear cells (10^6 cells/mL) were isolated from peripheral blood of healthy volunteers and then perfused across the pretreated HAEC monolayers for 5 min at 0.5 dynes/cm^2. Next, mononuclear cells attached to the endothelium were quantified. Stimulation with Ang II 1 μM for 24 h significantly increased mononuclear cell adhesion compared to vehicle treated cells (P<0.001, **Figure 31B**). By contrast, empagliflozin treatment significantly reduced mononuclear leukocyte-endothelium interactions (P<0.05; **Figure 31B**).

Furthermore, since the interaction between Ang II and its receptor, AT_1, promotes the production and secretion of different chemokines such as CCL-2/MCP-1 [210] and CCL-5/RANTES [211], ELISA assays were performed. CCL-2/MCP-1 and CCL-5/RANTES levels were measured in supernatants of HAEC cultures subjected to the different treatments. Interestingly, CCL-2/MCP-1 and CCL-5/RANTES levels were significantly increased in the culture medium of HAEC stimulated with Ang II for 24 h (P<0.05; **Figures 31C** and **D**) and they were diminished by preincubation of the cells with empagliflozin (3 μM) for 24 h (P<0.05; Figures **31C** and **D**).

Endothelial dysfunction induced by Ang II promotes the extravasation of leukocytes from blood vessels to the inflammatory loci. This process is mediated by the adhesion molecules VCAM-1 and ICAM-1 expressed by the activated endothelium [212]. As expected, HAEC stimulated with Ang II (1 μM) for 24 h showed a marked increase in the expression of VCAM-1 and ICAM-1 (**Figure 31E**) and this increase was significantly diminished by empagliflozin treatment (3 μM, 24 h; **Figure 31E**).

Since p38 MAPK and NF-κB signalling pathways play a key role in vascular inflammation given that they regulate the expression of genes encoding pro-inflammatory chemokines and CAMs, we next evaluated the effect of empagliflozin on the activation of p38 MAPK and NF-κB in HAEC. Western blot analysis revealed that Ang II (1 μM, 24 h) induced the activation of both signalling pathways by increasing the phosphorylation of p38 MAPK ($P<0.05$; **Figure 32A**) and NF-κB ($P<0.05$; **Figure 32B**). However, this effect was significantly reduced in HAEC pretreated with empagliflozin 3 μM for 24 h ($P<0.05$; **Figures 32A** and **B**).

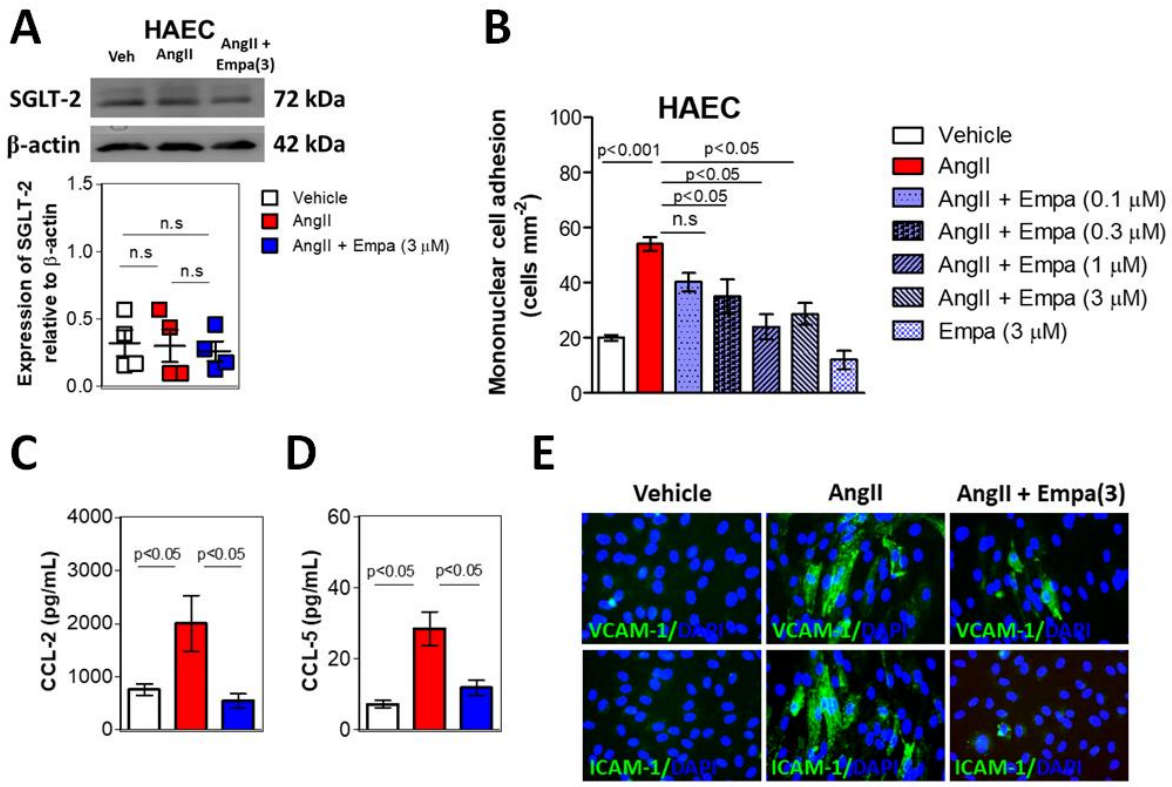

Figure 31. ***In vitro*** **effects of empagliflozin (Empa) in human aortic endothelial cells (HAEC).** (**A**) Western blot analysis of SGLT-2 protein expression in HAEC treated with Empa. Data are the mean±SEM from vehicle, Ang II and Ang II+Empa 3 μM (n=4 for each group). A representative Western blot of SGLT-2 expression is shown. Statistical analysis was performed by Kruskal-Wallis (Dunn post hoc) test. (**B**) Effect of Empa on leukocyte-endothelial cell interactions. Data are the mean±SEM (n=5 for each group). Statistical analysis was performed by one-way ANOVA (Newman-Keuls post hoc test). (**C**) CCL-2 (chemokine [C-C motif] ligand 2) and (**D**) CCL-5 (chemokine [C-C motif] ligand 5) were determined by ELISA in cell-free supernatants of HAEC. Results are expressed as mean±SEM (n=5 for each group). Statistical analysis was performed by 1-way ANOVA (Newman-Keuls post hoc test). (**E**) Effect of Empa on endothelial cell adhesion molecule expression. Cells were treated with Empa (3 μM) for 24 h and then stimulated with Ang II (1 μM, 24 h). VCAM-1 (vascular cell adhesion molecule 1) and ICAM-1 (intercellular adhesion molecule 1) expression was determined by immunofluorescence using an Alexa Fluor 488 antibody (green). Nuclei were counterstained with DAPI (4′,6-diamidino-2-phenylindole; blue). n.s. indicates nonsignificant.

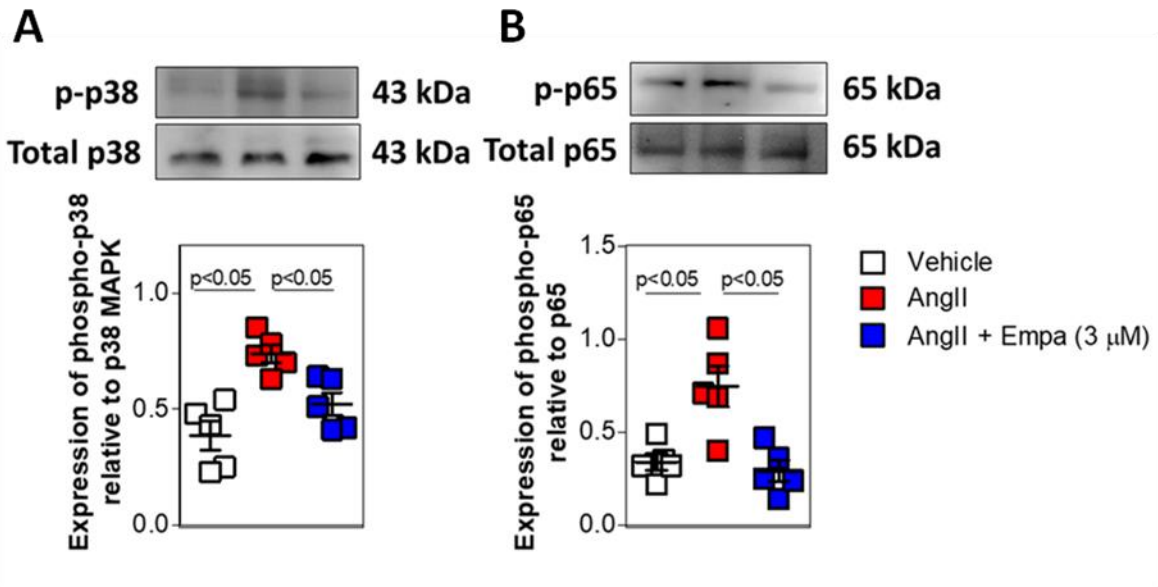

Figure 32. Effects of empagliflozin (Empa) on p38 MAPK and p65 NF-κB signalling in human aortic endothelial cells (HAEC). Representative Western blots of (**A**) phospho p38/total p38 and (**B**) phospho p65/total p65 in vehicle-treated, Ang II–treated, and Ang II+Empa–treated HAEC. Data represent mean±SEM of protein densitometry (n=5 for each group). Statistical analysis was performed by one-way ANOVA (Newman-Keuls post hoc test). n.s. indicates nonsignificant.

4.1.14 Empagliflozin reduced the secretion of CCL-2/MCP-1 and CCL-5/RANTES and decreased the release of metalloproteinases from human macrophages

Macrophages play a critical role in vascular inflammation and extracellular matrix degradation during AAA progression and development [63]. First, the effect of empagliflozin on chemokine release in human THP-1 macrophages was evaluated by ELISA. Results revealed that supernatants from Ang II-stimulated cells (1 μM, 24 h) had a higher concentration of CCL-2/MCP-1 and CCL-5/RANTES than vehicle-treated cells (P<0.05; **Figures 33A** and **B**). This effect was counteracted when THP-1 cells were pretreated with empagliflozin (3 μM, 24 h) (P<0.05; **Figures 33A** and **B**). Similar effects were observed in MMP-2, MMP-9 and VEGF release. As shown in **Figures 33C, D** and **E**, cells stimulated with Ang II (1 μM, 24 h) increased MMPs and VEGF secretion compared with vehicle-treated cells (P<0.05) and this increase was significantly reduced in cells pretreated with empagliflozin (3 μM, 24 h; P<0.05; **Figures 33C, D** and **E**). As expected, no differences in

chemokine release, MMPs or VEGF secretion were found when cells were only pretreated with empagliflozin (3 µM, 24h) compared with vehicle-treated cells.

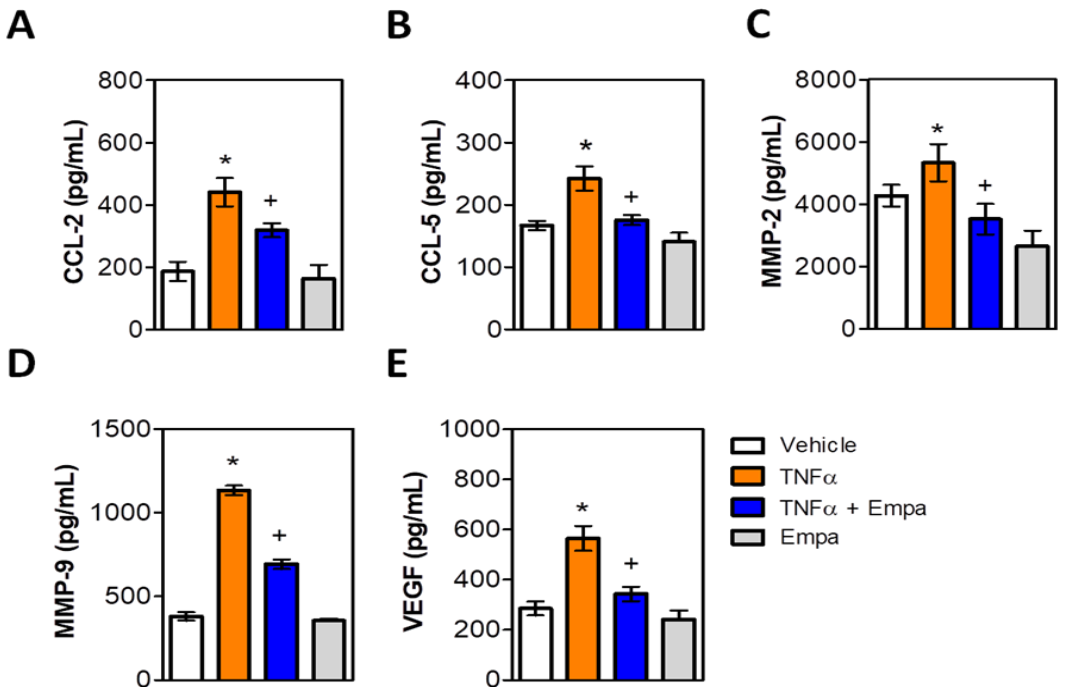

Figure 33. ***In vitro*** **effects of empagliflozin (Empa) in human THP-1 macrophages.** Cells were preincubated with empagliflozin (3 µM, 24 h) and then stimulated with TNFα (20 ng/mL) for 24 h. (**A**) CCL-2; (**B**) CCL-5; (**C**) MMP-2; (**D**) MMP-9 and (**E**) VEGF release was determined by ELISA in the cell-free supernatants of THP-1 cells. Data represent mean±SEM (n=5 each group). Statistical analysis was performed by one-way ANOVA (Newman-Keuls post-hoc test). *p<0.05 vs vehicle; +p<0.05 vs TNFα treated THP-1 cells.

4.2 Study of the role of RORα in adipose tissue from morbid obese patients with or without diabetes

4.2.1 Expression of RORα is higher in omental than in subcutaneous adipose tissue from patients with morbid obesity

AT from 41 morbidly obese patients subjected to Roux-en-Y bariatric surgery was collected to study the role of RORα in obesity. The group was composed by 30 women (73% of total obese patients) and 11 men (27% of total obese patients), aged 43 ± 2 years and with a mean body mass index (BMI) of 43.34 ± 0.8 kg/m^2 (**Table 21**). Among the total number of obese patients, 11 of them had a diagnosis of T2DM. Clinical and anthropometric determinations were also carried out. Data are shown in **Table 21**.

Table 21. Clinical and biochemical characteristics of the patients included in the study.

	All obese patients (n=41)	Non-diabetics (n=30)	Diabetics (n=11)
Age, years	43 ± 2	41.8 ± 1.9	46.8 ± 2.7
Female sex, %	73	80	54
BMI (kg/m^2)	43.34 ± 0.8	44.10 ± 1	41.2 ± 1.3
Weight (kg)	121 ± 3	123 ± 4	116.9 ± 5
Waist circumference (cm)	128 ± 2	126.1 ± 2.8	131.1 ± 3
Fasting glucose (mg/dL)	94.4 ± 3.7	86.1 ± 2.2	116.5 ± 10
Plasma insulin (mIU/mL)	19.6 ± 1.6	18.8 ± 1.4	21.9 ± 4.7
HOMA-IR index	4.7 ± 0.6	3.9 ± 0.3	6.8 ± 2.0
Triglycerides (mg/dL)	109.2 ± 5.4	104.9± 6	120.5 ± 12
Total cholesterol (mg/dL)	157.2 ± 5.1	164.5 ± 5	139.3± 12
LDL cholesterol (mg/dL)	104.7 ± 5	113.3 ± 4	82.1 ± 10
HDL cholesterol (mg/dL)	40.4 ± 1.2	38.9 ± 2	44.2 ± 2
CRP (mg/dL)	7.1 ± 1	7.4 ± 1.3	6.2 ± 1.3
HbA1c (%)	5.9 ± 0.2	5.5 ± 0.1	6.9 ± 0.4
Systolic blood pressure (mmHg)	128 ± 3	126 ± 3	132 ± 4
Diastolic blood pressure (mmHg)	79.6 ± 1.6	78.4 ± 1.9	82.6 ± 3.1

Values are expressed as mean ± SEM. Abbreviations: BMI, Body Mass Index; HOMA-IR, homeostasis model assessment of insulin resistance; LDL, Low Density Lipoprotein; HDL, High Density Lipoprotein; CRP, C-reactive protein; HbA1c, glycated haemoglobin.

In order to evaluate the involvement of RORα in obesity, the expression of RORα in paired subcutaneous and omental AT samples was determined. Results from qPCR and Western blot revealed that both *RORA* mRNA (**Figure 34A**) and RORα protein (**Figure 34B**) levels were significantly higher in omental AT than in subcutaneous AT (P = 0.031 and P = 0.034 for mRNA and protein, respectively). To corroborate this data, immunofluorescence assays were also performed. As expected, the number of RORα-positive cells was significantly higher in omental AT than in subcutaneous AT (**Figure 34C**, P = 0.009).

According with the previous findings, it was interesting to evaluate whether the changes in *RORA* mRNA expression were associated with metabolic parameters. As illustrated in **Table 22**, Spearman correlation analysis revealed that *RORA* mRNA expression levels correlated positively with BMI (*r* = 0.344, P = 0.027) and HOMA-IR index (*r* = 0.319, P = 0.041). No correlations were found between *RORA* expression and other metabolic parameters (**Table 22**). In regards to patient treatments, no correlations were found between *RORA* expression and hypoglycemic drugs (r = -0.013; P = 0.93) or statins (r = 0.073; P = 0.66) (**Table 23**).

Given that type 2 diabetes mellitus is commonly linked to obesity [213, 214], RORα protein in omental AT samples from patients with and without diabetes was compared. In line with previous results, RORα protein expression in omental AT was significantly higher in patients with diabetes than in non-diabetics (**Figure 35A**, P=0.04). Likewise, immunofluorescence analysis revealed that the number of RORα-positive cells was higher in omental fat from diabetic patients than in nondiabetic peers (**Figure 35B** and **C**, P=0.002). Double-labeling immunofluorescence analysis showed that RORα expression was mainly localised in CD3+ cells and CD31+ endothelial cells in omental fat (**Figure 35D**). While the number of RORα-CD31+ endothelial cells was similar in both groups (**Figure 35E**, P > 0.05), the number of RORα-CD3-positive cells was higher in omental fat from diabetic patients than in non-diabetic peers (**Figure 35F**, P = 0.003). Additionally, intracellular analysis of RORα expression revealed a significant up-regulation of RORα in both endothelial and CD3+ cells in omental fat from diabetic patients (**Figure 35G** and **H**, P = 0.02 and P = 0.031, respectively).

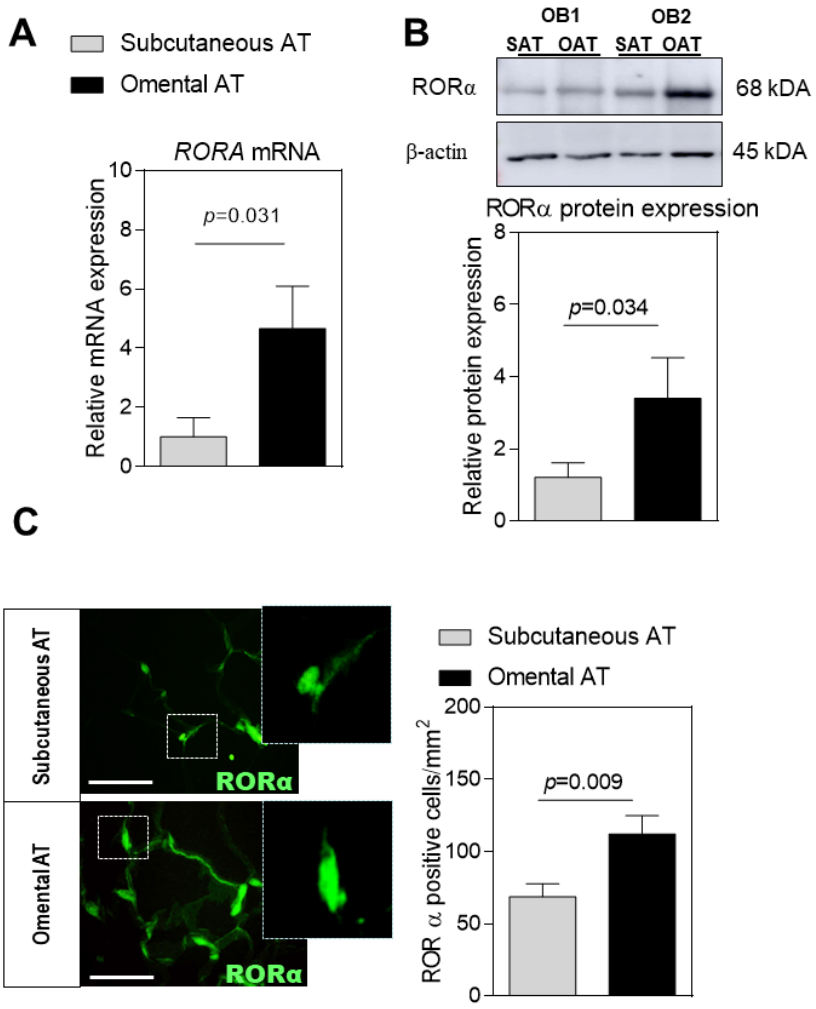

Figure 34. RORα expression in paired subcutaneous and omental adipose tissue from morbid obese subjects. (**A**) Columns show fold increase of *RORA mRNA* expression in omental adipose tissue (AT) relative to subcutaneous AT. Values are expressed as mean ± SEM. (n=41) Comparisons between groups were made with Student´s two-tailed test (**B**) Representative westerns blots of RORα protein expression from two obese patients (OB1&2). Values are expressed as mean ± SEM. (n=7). Comparisons between groups were made with Student´s two-tailed test (**C**) Images showing the expression of RORα in omental and subcutaneous AT from morbid obese patients. Immunoreactivity was visualised using an Alexa Fluor 488 secondary antibody (RORα, green). Columns show RORα-positive cells/mm^2 in subcutaneous and omental AT. Scale bar: 50 µm. Values are expressed as mean ± SEM (n=7). Comparisons between groups were made with Student´s two-tailed test.

Table 22. Spearman test correlations between *RORA* mRNA expression and clinical metabolic parameters in patients with morbid obesity.

Clinical - Metabolic marker	Correlation coeficient r	P values
BMI	0.344	0.027*
HOMA -IR	0.319	0.041*
Glucose	0.101	0.535
HbA1c	0.266	0.090
SBP	0.104	0.513
DBP	0.159	0.320
Total Cholesterol	−0.064	0.691
LDL Cholesterol	−0.048	0.766
HDL Cholesterol	−0.144	0.374
Triglycerides	0.128	0.431

Abbreviations: BMI, body mass index; SBP, Systolic blood pressure; DBP, Diastolic blood pressure; HbA1c, haemoglobin A1c; LDL, Low-density lipoprotein; HDL, High-density lipoprotein. *P < 0.05.

Table 23. Treatment of morbid obese subjects.

	Non-diabetics (n=30)	Diabetics (n=11)
Current therapy, n (%)		
Statins	6 (20)	4 (27)
Oral hypoglycemic drugs	1 (3)	10 (90)
Insulin	0 (0)	2 (18)
Beta-blockers	0 (0)	1 (9)
ARA II/ACE I	2 (7)	2 (18)
Diuretics	2 (7)	0 (0)

Abbreviations: ARAII: Angiotensin II receptor antagonist; ACEI: Angiotensin converting enzyme inhibitor.

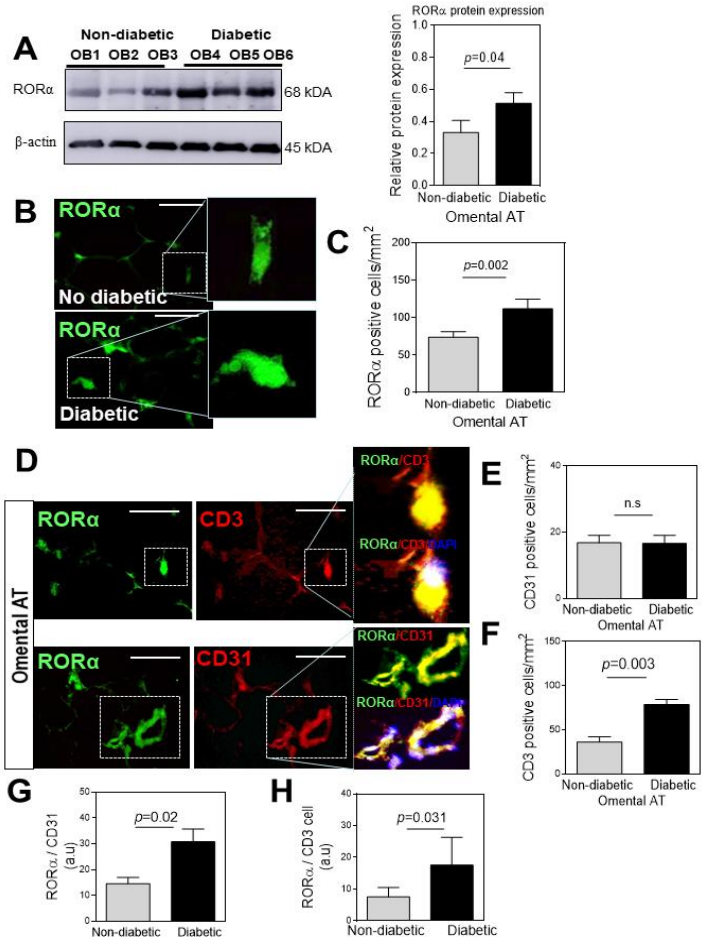

Figure 35. RORα expression in morbidly obese subjects with or without diabetes. (A) RORα protein expression was determined by western blotting of omental fat from non-diabetic and diabetic patients. Representative western blots are shown from three different non-diabetic patients (OB1–3) and three different diabetic patients (OB4–6). Data represent the mean ± SEM of protein densitometry (n=11 each group). (**B**) Representative images showing RORα-positive cells in omental adipose tissue (AT) from diabetic and non-diabetic obese subjects. Immunoreactivity was visualised using an Alexa Fluor 488 (RORα, green) secondary antibody. Scale bar: 50 µm. (**C**) Columns show RORα-positive cells/mm^2. Values are expressed as mean ± SEM. Comparisons between groups were made with Student´s two-tailed test. (**D**) Representative images showing colocalization of RORα with CD3 or CD31 in omental AT from morbid obese patients. Immunoreactivity was visualised using an Alexa Fluor 488 (RORα, green) and Alexa Fluor 594 (CD31 or CD3, red) secondary antibodies. Scale bar: 50 µm. Nuclei were counterstained with DAPI (blue). (**E**) Columns show RORα/CD31 positive cells/ mm^2 in omental AT. Values are expressed as mean ± SEM. Comparisons between groups were made with Student´s two-tailed test. (**F**) Columns show RORα/CD3 positive cells/ mm^2 in omental AT. Values are expressed as mean ± SEM. Comparisons between groups were made with Student´s two-tailed test. (**G**) Quantification of RORα intracellular fluorescence intensity in endothelial cells (CD31+) and (**H**) lymphocytes (CD3+) from omental AT of diabetic and non-diabetic obese patients (n=6 for each group). Fluorescence intensity is expressed in arbitrary units (a.u.). Values are expressed as mean ± SEM. Comparisons between groups were made with Student´s two-tailed test.

4.2.2 Pharmacological inhibition of RORα blocks chemokine release in omental adipose tissue from morbid obese patients with diabetes

Prompted by the previous observations, and given that visceral fat can produce inflammatory cytokines/chemokines [143], the role of RORα in chemokine production triggered by obesity- and diabetes-related factors was next investigated. For this purpose, functional *ex vivo* studies were performed. As shown in **Figure 36**, CXCL-8/IL-8 and CCL-2/MCP-1 release into conditioned medium after 48 h of culture was significantly higher in omental fat depots from diabetic patients than in equivalent samples from non-diabetic peers (**Figures 36A** and **B**, P = 0.003). Notably, treatment of AT explants from diabetic patients with the RORα inverse agonist SR3335 (10 µM) led to a significant decrease in CXCL-8/IL-8 and CCL-2/MCP-1 secretion into the conditioned medium (**Figure 36A** and **B**, P = 0.02 and P = 0.01, respectively).

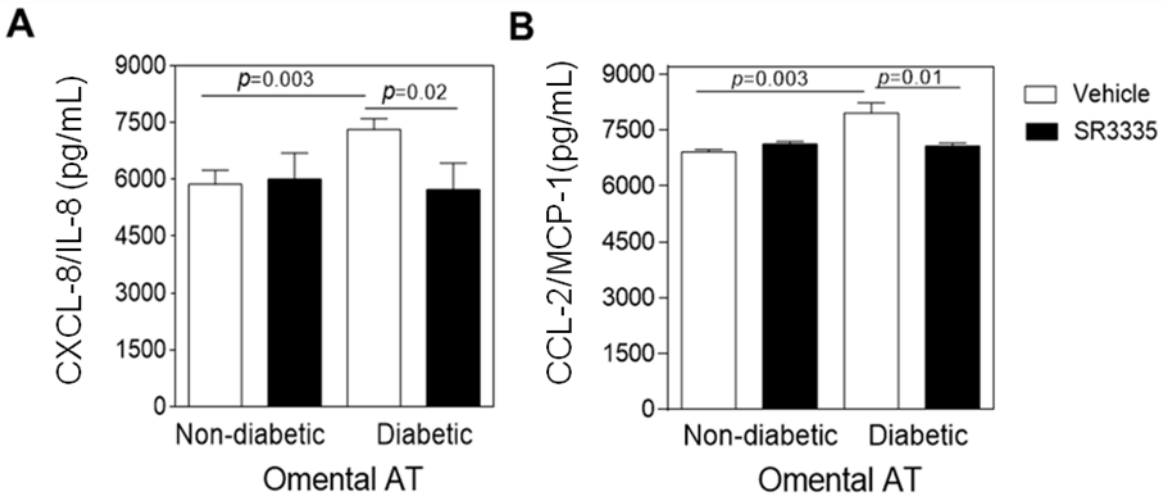

Figure 36. Chemokine release in adipose tissue explants from diabetic and non-diabetic morbid obese subjects. Omental adipose tissue (AT) explants from non-diabetic and diabetic obese patients were cultured for 48 h. AT explants were treated either with the inverse agonist of RORα, SR3335 (10 µM) or vehicle. (**A**) CXCL-8/IL-8 and (**B**) CCL-2/MCP-1 secretion into conditioned media was measured by ELISA. Chemokine secretion is expressed as a pg/ml/mg of tissue. Values are expressed as mean ± SEM (n=6 each group). Comparisons between groups were made with Student´s two-tailed test.

4.2.3 Pharmacological inhibition of RORα promotes AKT phosphorylation in visceral fat explants from morbid obese patients with diabetes

Because AKT (also known as protein kinase B) is involved in cell growth, metabolism and survival downstream of insulin sigalling [215], AKT activation was examined *ex vivo* in omental AT depots from diabetic and non-diabetic patients. Furthermore, the effect of pharmacological RORα blockade in this signalling pathway was also explored. Western blot analysis revealed that basal phosphorylation levels of AKT were significantly lower in omental AT from diabetic than from non-diabetic patients (**Figure 37A**, P = 0.04). Treatment of omental AT with SR3335 (10 µM) resulted in a significant increase in AKT activation in samples from diabetic patients (**Figure 37A**, P = 0.03), whereas it was unchanged in samples from non-diabetics (**Figure 37A**, P > 0.05). To confirm these observations, immunofluorescence studies were performed. As shown in **Figure 37B**, compared with vehicle-treated AT explants, SR3335 (10 µM) treatment markedly increased AKT phosphorylation in samples from diabetic patients. Double immunofluorescence analysis indicated that AKT phosphorylation was mainly in endothelial cell-positive microvessels (**Figure 37B**).

Given that the transcription factor NF-κB is highly associated with AT inflammation and dysfunction, [216, 217] the phosphorylation status of the NF-κB subunit p65 in omental fat was then investigated. Basal p65 NF-κB phosphorylation was significantly higher in omental AT from diabetic patients than in non-diabetics (**Figure 37C**, P = 0.01). Notably, treatment of omental AT with SR3335 (10 µM) significantly reduced p65 NF-κB activation in samples from diabetic patients (**Figure 37C**, P = 0.007), whereas it remained unchanged in samples from non-diabetic patients (**Figure 37C**, P > 0.05).

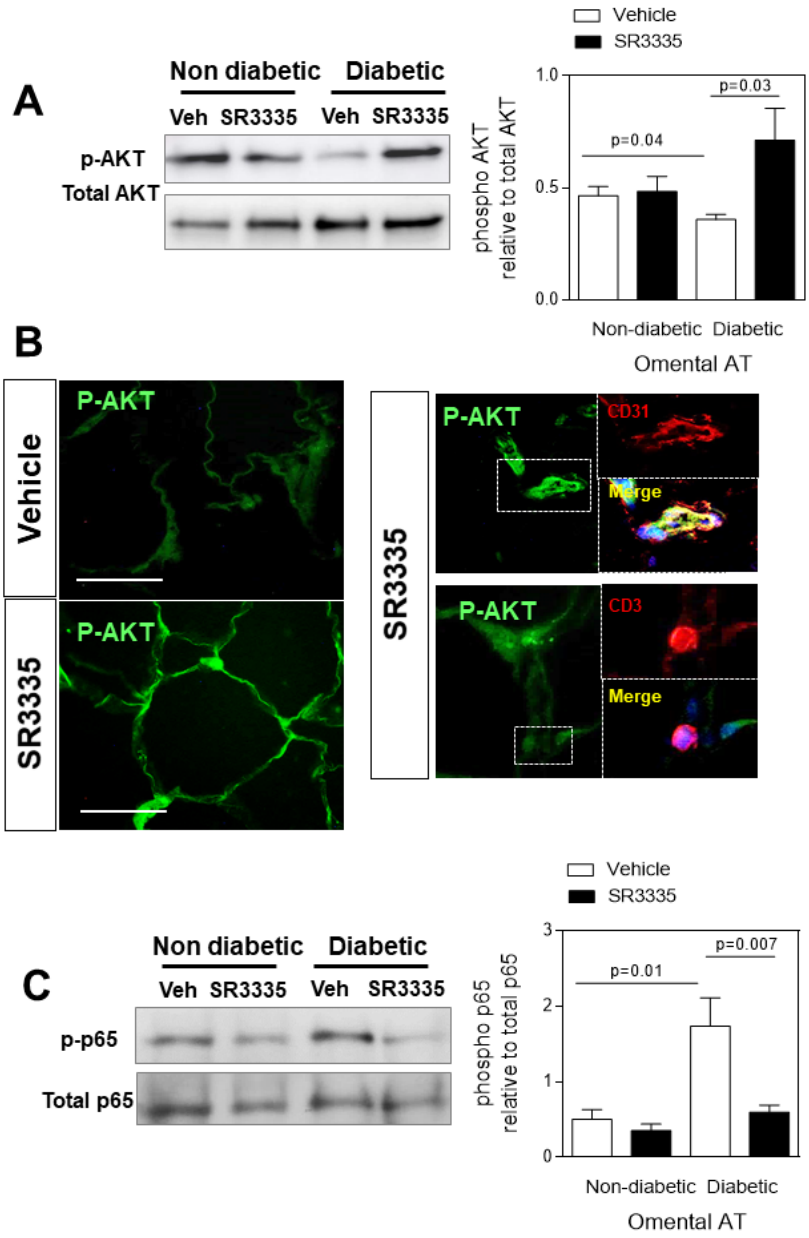

Figure 37. Effects of RORα inhibition on AKT and p65 NF-κB signalling in omental fat from diabetic and non-diabetic morbid obese patients. Omental adipose tissue (AT) explants were incubated with vehicle or SR3335 (10 μM) for 48 h. (**A**) Western blot of phospho-AKT in samples from non-diabetic and diabetic morbid obese patients. Columns show the mean ± SEM (n=5 independent experiments) and are expressed as phosphorylated relative to nonphosphorylated protein. (**B**) Representative images showing colocalization of phospho-AKT with CD3 or CD31 in omental AT from diabetic morbid obese patients. Immunoreactivity was visualised using an Alexa Fluor 488 (phospho-AKT, green) and Alexa Fluor 594 (CD31 or CD3, red) secondary antibodies. Scale bar: 50 μm. (**C**) Western blot of phospho-p65-NFκB in samples from non-diabetic and diabetic morbid obese patients. Columns show the mean ± SEM (n=5 independent experiments) and are expressed phosphorylated relative the nonphosphorylated protein. Comparisons between groups were made with Student´s two-tailed test.

4.2.4 Effects of SR3335 on endothelial cell viability

Since RORα staining was detected in microvessels, the effects of RORα blockade in human endothelial cells were evaluated. HUVEC were incubated with increasing concentrations of SR3335 (0.1 to 10 µM) for 24 h to assess cell viability. Flow cytometry analysis showed that viability of human endothelial cells was unaffected by SR3335 treatment (**Figure 38**).

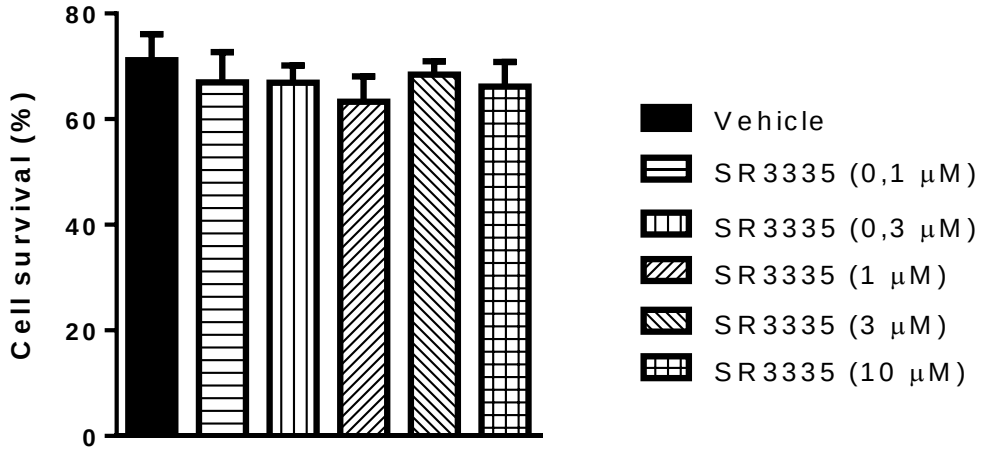

Figure 38. Effect of SR3335 on the viability of human endothelial cells. HUVEC were incubated for 24 h with vehicle (DMSO 0.1%) or SR3335 at different concentrations (0.1–10 µM). Data are presented as means ± SEM of *n* = 5 independent experiments. Comparisons between groups were made with one-way ANOVA.

4.2.5 Pharmacological inhibition of RORα reduces TNFα-induced mononuclear cell-endothelial cell interactions and chemokine release in human endothelial cells.

Endothelial dysfunction is an early hallmark of atherogenesis in obesity and induces a prothrombotic and pro-inflammatory state of the endothelium that increases the adhesion and subsequent migration of mononuclear cells. The effects of pharmacological RORα suppression on leukocyte-endothelial cell interactions were determined using the dynamic model of the parallel flow chamber. TNFα was employed as an inflammatory stimulus to mimic endothelial dysfunction since it is released by AT [180, 183], and its circulating levels are notably increased in obese patients [180, 181]. Freshly isolated human mononuclear cells were perfused across HUVEC monolayers stimulated or not with TNFα (20

ng/mL) for 24 h. Results showed that leukocyte adhesion to endothelial cells was significantly higher in TNFα-stimulated HUVEC than in vehicle-treated cells (**Figure 39A**, $P < 0.05$). Pre-treatment of endothelial cells for 24 h with SR3335 (0.1–10 μM) significantly reduced the increase in the TNFα-induced mononuclear leukocyte adhesion to endothelial cells in a concentration-dependent manner (**Figure 39A**, $P < 0.05$).

TNFα stimulation of endothelial cells can induce the release of several chemokines that collectively contribute to mononuclear leukocyte recruitment. Thus, we next evaluated the consequences of functional RORα blockade on chemokine release in human endothelial cells. As anticipated, CXCL-8/IL-8 and CCL-2/MCP-1 release was significantly higher in HUVEC stimulated for 24 h with TNFα than with vehicle (**Figure 39B** and **C**, $P < 0.05$). Pre-treatment of HUVEC for 24 h with SR3335 (0.1 – 10 μM) inhibited, in a concentration-dependent manner, both IL-8/CXCL8 and MCP-1/CCL2 secretion induced by TNFα (Figure **39B** and **C**, $P < 0.05$).

4.2.6 The inverse agonist SR3335 diminishes TNFα-induced increased adhesion molecule expression and NF-kB activation in human endothelial cells

To investigate whether the anti-inflammatory effects of SR3335 are mediated by the modulation of cellular adhesion molecule expression, immunofluorescence studies for VCAM-1 and ICAM-1 were performed in HUVEC. As shown in **Figure 40A**, TNFα stimulation resulted in an up-regulation of VCAM-1 and ICAM-1 expression in endothelial cells when compared with unstimulated HUVEC (**Figure 40A**). Pre-treatment of HUVEC with SR3335 before TNFα stimulation diminished VCAM-1 and ICAM-1 expression (**Figure 40A**).

Finally, given that NF-κB signalling has a critical role in mediating TNFα-induced chemokine release and cellular adhesion molecule expression, we evaluated the effects of RORα inhibition on NF-κB activation in HUVEC. As shown in **Figure 40A**, SR3335 decreased the nuclear translocation of NF-κB induced by TNFα. In support of this finding, western blot analysis showed that SR3335 treatment diminished the TNFα-induced p-65 phosphorylation in human endothelial cells (**Figure 40B**, $P < 0.05$).

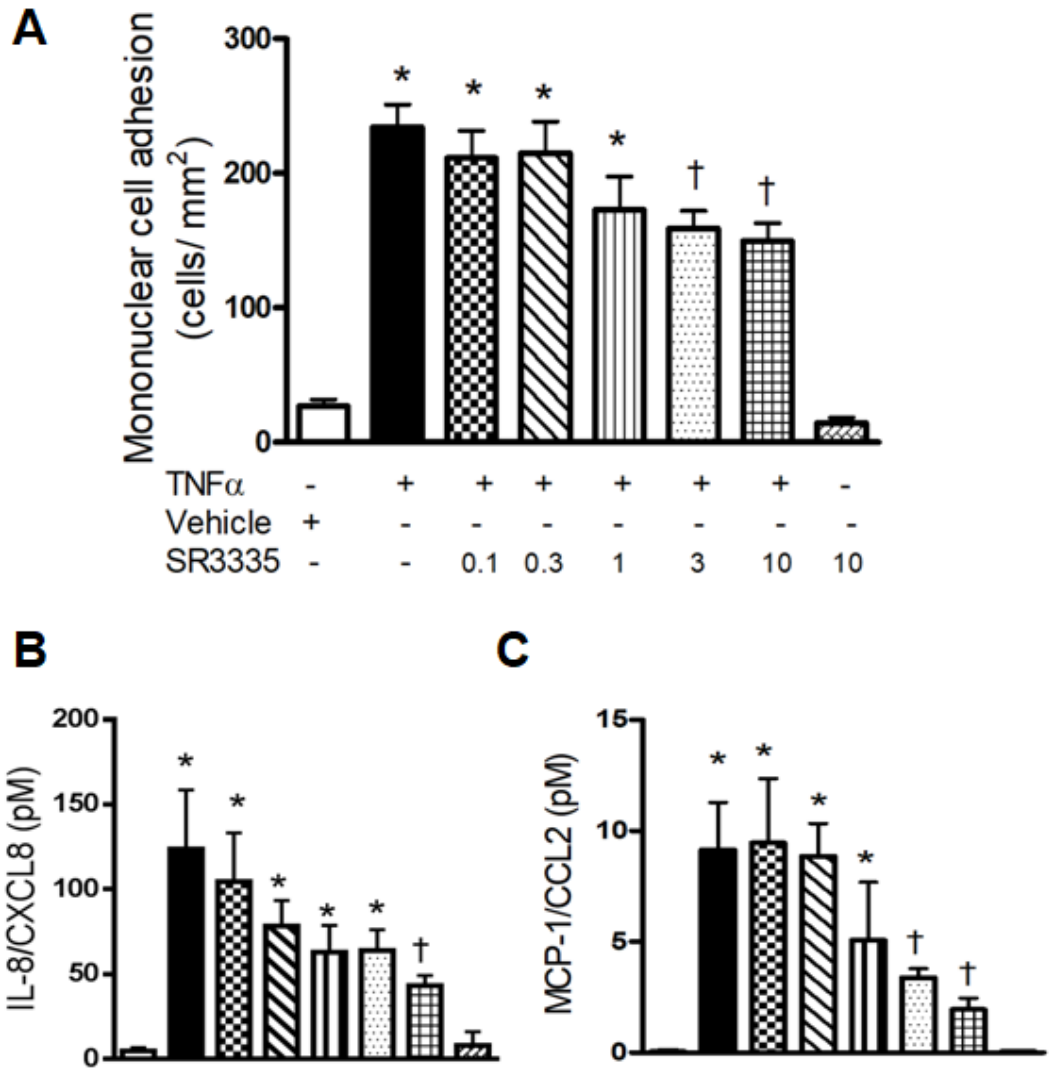

Figure 39. Effects of RORα inhibition on mononuclear cell-endothelium recruitment under physiological flow conditions. HUVEC were incubated for 24 h with vehicle (DMSO 0.1%) or SR3335 (0.1–10 μM) prior to TNFα stimulation (20 ng/ml, 24 h). Freshly isolated human mononuclear cells were perfused across the endothelial monolayers for 5 min at 0.5 dyn/cm^2 and leukocyte attachment (**A**) was determined. Data show the mean ± SEM of n=5 independent experiments. *$p < 0.05$ relative to the vehicle group; † $p < 0.05$ relative to TNFα-stimulated cells. Comparisons between groups were made by one-way ANOVA. (**B**) CXCL-8/IL-8 and (**C**) CCL-2/MCP-1 secretion from endothelial cells stimulated with TNFα are decreased by SR3335 treatment. Results are expressed as pM concentration and are presented as mean ± SEM (n=5 independent experiments). *$p < 0.05$ relative to the vehicle group; † $p < 0.05$ relative to the TNFα-stimulated cells. Comparisons between groups were made by one-way ANOVA.

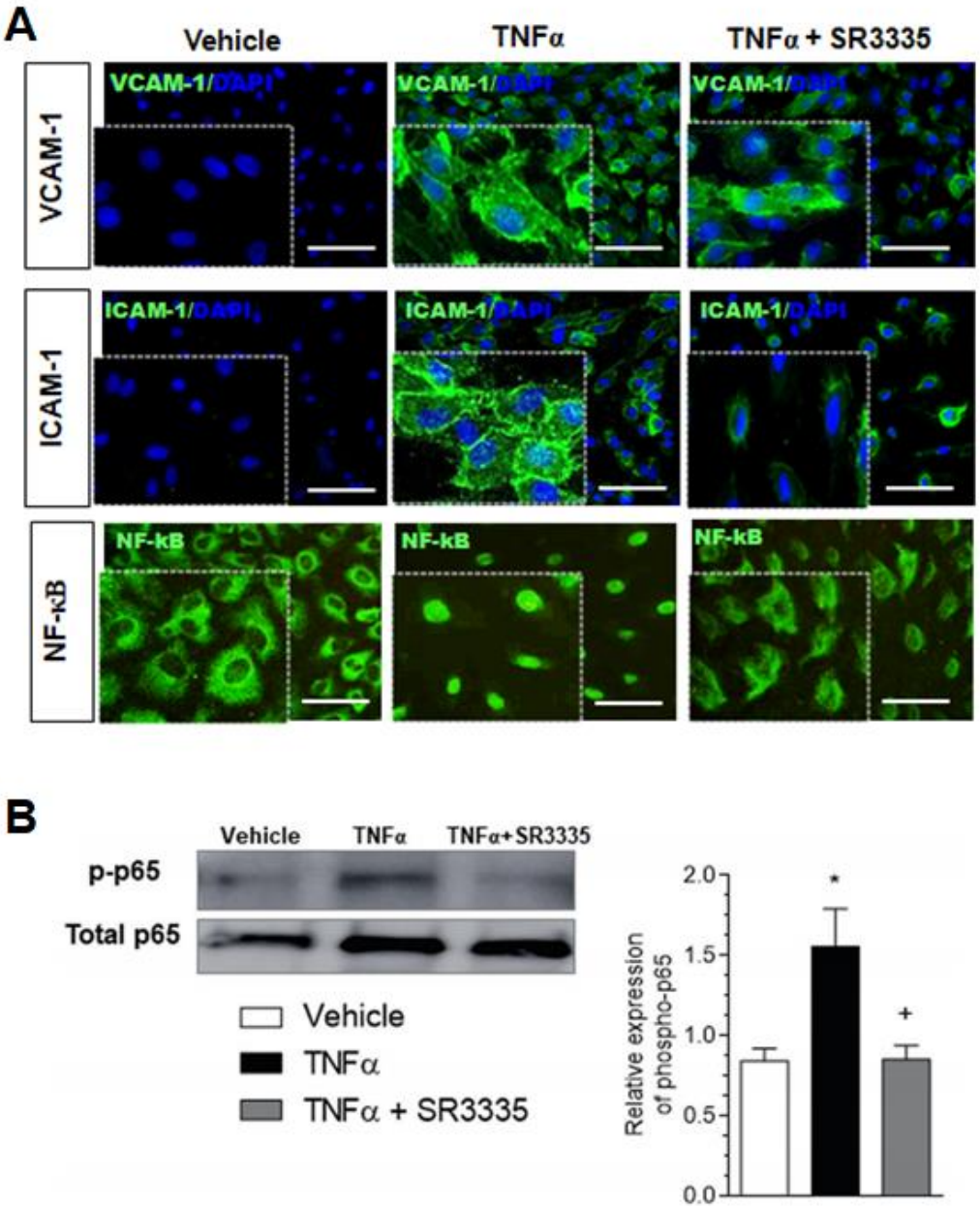

Figure 40. Effects of RORα inhibition on VCAM-1 and ICAM-1 expression and NF-κB activation. (**A**) SR3335 (10 µM) inhibits VCAM-1 and ICAM-1 expression and NF-κB activation induced by TNFα (20 ng/mL) in HUVEC. VCAM-1 and ICAM-1 expression and NF-κB translocation (green) to the nucleus were visualised by indirect immunofluorescence. Representative images from n=4 independent experiments. Scale bar: 100 µm. (**B**) Western blot analysis of phospho-p65-NFκB in HUVEC. Data are presented as mean ± SEM of n=5 independent experiments. *P < 0.05 relative to the vehicle group; + P < 0.05 relative to TNFα-stimulated cells. Comparisons between groups were made by one-way ANOVA.

5. Discussion

5.1 Study of the effects of SGLT-2 inhibition in abdominal aortic aneurysm development and endothelial dysfunction

SGLT-2 inhibitors are the newest class of available glucose-lowering drugs, and empagliflozin has recently demonstrated impressive beneficial effects in patients with T2DM and established atherosclerotic disease [120, 218]. Empagliflozin has been reported to reduce cardiovascular events, especially with regard to heart failure [120], making it the preferred agent to treat T2DM in patients with or at high risk for this condition. Further, recent studies have reported positive effects of SGLT-2 inhibitors in several cardiovascular disorders such as obesity [110-112], myocardial infarct [219, 220], and atherosclerosis [106, 122].

In the present Thesis, we provide evidence that oral administration of empagliflozin reduces Ang II–induced AAA development. We found that suprarenal aortic expression of the proinflammatory chemokines CCL-2 and CCL-5 was increased in response to Ang II infusion in both the acute (5 days) and chronic (28 days) phases. The attenuation of aneurysm formation by empagliflozin was accompanied by a reduction in macrophage infiltration within the lesions and a downregulation of CCL-2 and CCL-5 in the aorta, which are reported to be upregulated in the microenvironment of the AAA wall in humans [221, 222], and in animal models of AAA [200]. Moreover, the CCR2 (C-C chemokine receptor type 2)/CCL-2 axis is known to be involved in AAA development [223], and infiltration of macrophages is reduced by dual blockade of RANTES and CCR1/CCR5 (C-C chemokine receptor type 1/C-C chemokine receptor type 5) receptors within the experimental aortic aneurysm lesion, leading also to the inhibition of matrix-degrading protease release and angiogenesis [221, 224]. In line with our findings, a recent study by Han et al [122] reported that empagliflozin treatment in apoE$^{-/-}$ mice fed with a Western diet reduced atheromatous plaque formation and lowered the levels of inflammatory markers (*Tnf-α, Il-6, and Ccl-2*) and macrophage infiltration in the aortic arch [122]. Similarly, in atherosclerosis-prone mouse models, administration of other SGLT-2 inhibitors such as dapagliflozin [225] or ipragliflozin [226] reduced atheroma burden and inflammation. Our results highlight the benefits of empagliflozin for attenuating AAA and provide further support for the protective role of SGLT-2 blockade in reducing the immune/inflammatory profile in the vascular wall.

The differences among the clinical doses of empagliflozin used for humans (10 and 25 mg per day) and the experimental doses used for mice (1 and 3 mg/kg per day) in the present study reflect differences in the pharmacokinetic parameters between humans and rodents. A number of species-specific differences have been demonstrated regarding pharmacokinetics properties of SGLT-2 inhibitors, particularly with respect to the elimination half-life of the drug in plasma between humans and rodents including mice [185-187]. Accordingly, mice are stronger and faster empagliflozin metabolizers: whereas the half-life of empagliflozin is ≈10 to 12 hours in humans, in mice, it is ≈1 to 2 hours. We would note that the doses and regimen of empagliflozin used in the present study were based on pharmacokinetics studies of mice [185-187] and also studies that reported to be efficient in animal models of obesity [227, 228], diabetes mellitus [185-187], and atherosclerosis [122, 125].

SGLT-2 is highly expressed in kidney [204] but is also found in other tissues and vascular cells, including adipose tissue [205], aorta [194], and endothelial cells [206]. In agreement with previous studies [194], SGLT-2 was detected in the vascular aortic wall. Our findings also demonstrate that SGLT-2 is mainly localised in endothelial cells, but also in macrophages, and remained unchanged after Ang II infusion or empagliflozin cotreatment. In addition to the salutary effects of SGLT-2 inhibitors on glycemic control, several studies have demonstrated beneficial effects of SGLT-2 inhibitors on vascular dysfunction. For example, empagliflozin [229] or dapagliflozin [230-232] treatment was associated with a decline in arterial stiffness in patients with T2DM. Moreover, in preclinical models, chronic empagliflozin treatment improved vascular function in diabetic rats by reducing oxidative stress and inflammation in the aortic wall [233]. The underlying mechanisms involved in beneficial actions of SGLT-2 inhibition are believed to be associated with glucose lowering, weight reduction, and antihypertensive effects but also anti-inflammatory and antioxidative actions [234-237].

SGLT-2 inhibitors reduce hyperglycemia in T2DM by reducing renal glucose reabsorption. In the present study, we did not detect significant differences in glucose levels between mice treated or not with empagliflozin, suggesting that SGLT-2 inhibitors may have cardioprotective effects independently of glucose status and that empagliflozin does not increase the risk of hypoglycemia in nondiabetic states. In agreement with our observations, empagliflozin improved

diastolic function in a nondiabetic rodent model of heart failure with preserved ejection fraction [219]. Additionally, a recent study by Lim et al [220] has shown that chronic SGLT-2 inhibition by canagliflozin reduces myocardial ischemia/reperfusion injury in both diabetic and nondiabetic rats [220] and canagliflozin did not cause hypoglycemia in nondiabetic animals [220].

Regarding blood pressure effects, evidence from clinical studies on T2DM and hypertension demonstrates improvements in systolic blood pressure with empagliflozin treatment [238]. By contrast, in our model, empagliflozin administration had no noticeable effects on the elevated blood pressure induced by Ang II infusion, which leads us to hazard that the protective effects of SGLT-2 inhibition on aneurysmal formation are blood pressure independent. Although we do not have a clear explanation, these results could be related to divergent species-dependent effects of SGLT-2 inhibitor treatment on reducing blood pressure. For instance, recent experimental studies by Habibi et al [239] found that empagliflozin administered for 5 weeks at a higher dose of 10 mg/kg per day improved glycemic indices along with diastolic relaxation in a db/db mice model, in the absence of any changes to the increased blood pressure [239]. The same authors showed that reductions in aortic and micro vascular stiffness in db/db mice by empagliflozin were not associated with improvements in blood pressure [240]. Finally, another study found that oral administration of the selective SGLT-2 inhibitor TA-1887 (10 mg/kg per day) for 10 weeks failed to decrease blood pressure in a nondiabetic chronic kidney disease model of nephrectomized rats [241]. Given these findings, further studies are warranted to fully elucidate species-dependent different responses in blood pressure after SGLT-2 inhibitor treatment.

There is growing evidence that angiogenesis within the wall of an aortic aneurysm might play key roles in aneurysm progression and rupture [242]. Inflammatory cells that infiltrate the aneurysmal wall release growth factors and pro-angiogenic chemokines that contribute to neovascularisation [242]. Of interest, suprarenal aortic VEGF levels and neovascularization were unchanged during the acute phase of dissecting AAA formation; however, during the chronic phase of Ang II–induced dissecting AAA, a marked increase in angiogenesis and VEGF levels was detected. Also, there are data showing that CCL-2, CCL-5, and VEGF are likely important molecules in the angiogenic activity elicited by Ang II [200]. Against this background, a recent study reported that SGLT-2 inhibition has

angiostatic effects [243]. Accordingly, SGLT-2 blockade by canagliflozin suppressed endothelial proliferation and tubule formation in human endothelial cells [243]. Consistent with these observations, we detected a marked reduction in neovascularization and VEGF levels in the suprarenal aortas of chronic empagliflozin-cotreated mice. A possible explanation for this might be the reduction in the number of inflammatory cells including macrophages, which are an important source of VEGF during aortic aneurysm development [244].

MMPs are also key players in the pathogenesis of AAA [245] and are secreted not only by endothelial cells and smooth muscle cell but also by infiltrating immune cells (predominantly macrophages) and drive medial smooth muscle cell apoptosis, elastin degradation, and consequently, AAA progression [245]. MMP activity is regulated by TIMPs, and the MMP/TIMP ratio is critical for the control of tissue damage [246]. In accord with previous studies [247], we detected an increase in MMP-9 in suprarenal aortas before dissecting AAA formation and 28 days after Ang II infusion; however, MMP-2 expression was prominent only at the later stages of dissecting AAA development. Empagliflozin-cotreated mice had less medial elastin destruction together with a decrease in MMP-2 and MMP-9 and an increase in TIMP-1 levels in suprarenal aortas. Consistent with our data, inhibition of SGLT-2 with luseogliflozin was shown to downregulate MMP-2 and MMP-9 and reduce atherosclerosis [106]. Overall, these findings suggest that SGLT-2 blockade may play an important role in the preservation of vessel wall integrity.

Another important finding was that empagliflozin decreased chemokine (CCL-2 and CCL-5), MMP (MMP-2 and MMP-9), and VEGF release from TNFα-stimulated human THP-1 macrophages. In line with our studies, other groups have demonstrated anti-inflammatory effects in vitro with SGLT-2 inhibitors in several type of cells. For instance, canagliflozin inhibited IL (interleukin)-1β–stimulated CCL-2 and IL-6 in human endothelial cells [206], and dapagliflozin reduced high glucose-induced CCL-2 and ICAM-1 in human proximal tubular epithelial cells [248]. Additionally, we found that empagliflozin treatment diminished the adhesion of mononuclear leukocytes to dysfunctional endothelium and also decreased Ang II–induced CCL-5 and CCL-2 release and VCAM-1 and ICAM-1 expression on HAECs. However, because of the limitation of these in vitro findings in human cells, further preclinical and clinical studies are needed to understand how empagliflozin affects AAA development *in vivo*.

Finally, we investigated the mechanistic basis for the protective role of SGLT-2 inhibition in AAA formation by examining NF-κB and p38 MAPK signalling. It is well known that p38 MAPK is associated with MMP upregulation, inflammation, and AAA progression [199]. Additionally, NF-κB activation promotes the upregulation of cytokines/chemokines in the vascular wall [199, 249]. In a previous study, inhibition of endothelial NF-κB signalling attenuated Ang II–induced AAA development, which was associated with the downregulation of endothelial adhesion molecules (VCAM-1 and ICAM-1), MMPs (MMP-2 and MMP-9) and with macrophage arrest in the abdominal aorta wall [202]. We found that the increased phosphorylation of p38 MAPK and p65 NF-κB was weakened in the suprarenal aortas of apoE$^{-/-}$ mice cotreated with empagliflozin for 28 days. Additionally, diminished activation of p65 NF-kB and p38 MAPK was detected after acute empagliflozin treatment. In line with our findings, dapagliflozin decreased NF-κB activation induced by hyperglycemia in cultured human proximal tubular epithelial cells [248]. Overall, the beneficial vascular effects exhibited by empagliflozin indicate that the impaired activation of NF-κB pathway limits the release of inflammatory/proangiogenic molecules, resulting in blunted endothelial activation.

As mentioned, in clinical studies, empagliflozin has demonstrated benefit for a 3-point major cardiovascular event outcome of cardiovascular death, nonfatal myocardial infarction, or nonfatal stroke [121]. The mechanisms by which SGLT-2 inhibition improves cardiovascular outcomes remain poorly understood. Several mechanisms have been postulated including effects such as decreased arterial stiffness and vascular resistance [250], improvements in weight and visceral adiposity [251], decreases in uric acid and oxidative stress [252, 253], and a shift in myocardial fuel energetics [254]. Our experimental findings should, therefore, be interpreted with caution due to empagliflozin off target effects. Future studies with SGLT-2 knockout mice are warranted to clarify the anti-AAA effects of SGLT-2 inhibitors and might aid translation to clinical settings.

In conclusion, the present findings provide evidence that chronic oral treatment with empagliflozin reduces Ang II–induced dissecting AAA formation in mice. The pleiotropic beneficial effects that empagliflozin exerts to reduce AAA pathology (vascular inflammation, neovascularization, and MMP dysregulation) suggest that therapeutic inhibition of SGLT-2 could be a viable strategy to limit AAA growth. The interplay between SGLT-2 inhibitors and abdominal aneurysm

formation in humans remains an open question and requires further clinical research.

5.2 Study of the role of RORα in adipose tissue from morbid obese patients with or without diabetes

Morbid obesity is characterised by pathological remodelling of AT. Expansion of omental AT is associated with the development of insulin resistance, while subcutaneous fat has a minor contribution [255-258]. Accordingly, identifying inflammatory factors and molecular pathways involved in AT dysfunction should be a promising strategy to manage and/or prevent the development of metabolic diseases.

Remarkably little is known about the role of RORα in human obesity. Here, we show that RORα is overexpressed in omental AT in morbid obesity, suggesting that up-regulation of RORα might contribute to the AT dysfunction in this fat depot. Interestingly, the correlation between RORα expression and BMI could be explained by the association between adiposity and metabolic alterations in morbid obese patients. In this context, we found that up-regulation of RORα correlated with greater insulin resistance in obesity, which is in line with a preclinical report showing the up-regulation of RORα in epididymal AT from obese mice but not lean mice [259]. Furthermore, Lau and colleagues [260] showed that RORα-deficient staggerer mice had improved insulin sensitivity and increased glucose uptake in skeletal muscle [260]. Additionally, recent studies have shown that the RORα inverse-agonist SR3335 up-regulates UCP1 expression in adipose tissue, and promotes fat loss by increasing thermogenesis in mice [261, 262]. In additional studies, Kang et al. [175] showed that compared with wild-type mice, RORα-deficient mice fed a high-fat diet presented lower adiposity, reduced hepatic triglyceride levels and were resistant to the development of hepatic steatosis and AT-associated inflammation [175]. It is well known that AT dysfunction contributes to chronic low-grade inflammation and insulin resistance owing to the over-production of inflammatory factors released by adipocytes and other cells present in fat. Interestingly, we observed that omental fat depots from patients with morbid obesity and type 2 diabetes mellitus secreted higher levels of IL-8/CXCL8 and MCP-1/CCL2 chemokines than those from non-diabetic peers, and this correlated with a higher expression of RORα in endothelial cells and CD3+ lymphocytes in visceral fat. IL-8/CXCL8 and MCP-1/CCL2 have been previously associated with obesity,

metabolic inflammation and insulin resistance [263-265], and are known to be involved in the progression of atherosclerotic lesions [266].

The data presented here on the relationship between RORα and AT inflammation in morbid obesity supports previous studies that have been performed in preclinical animal models. For instance, a study by Liu et al. [259] demonstrated that lipopolysaccharide treatment markedly increased the expression of RORα in macrophages and in 3T3-L1 adipocytes. The authors observed RORα overexpression in AT from obese mice, and treatment with the RORα-specific agonist SR1078 increased the expression of inflammatory cytokines (*Tnf*-α, *Il-6*, *Ccl-2/Mcp-1*) and the numbers of infiltrated macrophages into AT [259]. Using different approaches, the authors also showed that RORα induces an endoplasmic reticulum (ER) stress response that contributes to AT inflammation [259]. Based on these previous findings and the data presented here, it is tempting to speculate that RORα in obesity induces ER stress and promotes the up-regulation of several inflammatory factors that may have additive effects in driving AT dysfunction.

SR3335 has been shown to directly bind RORα, but not other RORs, and functions as a selective partial inverse agonist of RORα [267]. Kumar et al. [267] showed in a cell-based chimeric receptor Gal4 DNA-binding domain-nuclear receptor ligand-binding domain cotransfection assay that SR3335 significantly inhibited the constitutive transactivation activity of RORα (IC_{50} = 480 nM) (partial inverse agonist activity) but had no effect on the activity of LXRα and RORγ, even at 10 μM. These authors indicated that SR3335 also displays no activity on RORβ (radioligand binding or co-transfection assays), FXR (co-transfection assays) or any other receptors in a selectivity panel for human nuclear receptors [267]. More recently, Wang et al [268] carried out a larger study that corroborates these findings. The authors tested the activity of SR3335 (10 μM) against 48 human nuclear receptors in HEK293 cells subjected to a Gal4-RORα ligand binding domain cotransfection. Results revealed that SR3335 poorly modulates the activity of other nuclear receptors [268], a fact that proves the high specificity of the inverse agonist SR3335 for RORα.

In a recent study, dual inhibition of RORα/γ activity was found to diminish the occurrence of a leukocyte inflammatory infiltrate and also atherosclerotic plaque development in LDL-deficient mice [177]. Furthermore, SR3335 suppressed gluconeogenesis in a diet-induced mouse model of obesity [267], and RORα

blockade was found to decrease insulitis and prevent hyperglycemia in a preclinical model of type 1 diabetes [269]. However, little is known regarding the impact of RORα suppression on chemokine release in human AT. Here, we observed that increased CXCL-8/IL-8 and CCL-2/MCP-1 release in omental fat explants from diabetic patients was diminished by RORα inhibition. We hypothesise that the downregulation of these chemokines, and likely other pro-inflammatory factors, may have additive beneficial effects in promoting insulin sensitivity. That being said, because our experimental conditions are *ex vivo,* our findings should be interpreted with some caution and the interplay *in vivo* between the RORα and AT dysfunction in humans remains an open question that requires further investigation.

Insulin is known to exert critical control over anabolic responses in AT through activation of AKT signalling and, consequently, stimulating the uptake of glucose and free fatty acids [215]. In line with previous findings [270], we found that AKT signalling in visceral AT was downregulated in morbid obese patients with diabetes relative to non-diabetic peers. Our finding that pharmacological blockade of RORα activity increases AKT activation mainly in endothelial cells from AT explants points to a potential treatment approach to blunt abnormal insulin signalling in obesity. Indeed, activation of AKT in skeletal muscle has been observed in RORα-deficient staggerer mice [260]. Additionally, adipocytes of RORα-deficient mice are highly sensitive to the action of insulin and can increase their lipid storage capacity in response to high-fat diet [271]. As mentioned earlier, RORα-deficient staggerer mice are protected from high-fat diet-induced obesity [176, 260] and related systemic insulin resistance, and are resistant to the development of hyperlipidemia and liver steatosis [175].

NF-kB signalling is involved in multiple downstream pathways linked to cytokine/chemokine synthesis and endothelial cell dysfunction, and is a known mediator of obesity-induced inflammation [216, 217]. Indeed, NF-kB activity has been proposed as a potential treatment target for obesity, insulin resistance and type 2 diabetes [216, 270, 272]. Based on our findings, it is tempting to speculate that RORα might be a major regulator of exacerbated NF-kB signalling and of the increased production of CXCL-8/IL-8 and CCL-2/MCP-1 chemokines in visceral fat. Additionally, given that CXCL-8/IL-8 and CCL-2/MCP-1 overexpression in inflamed AT is mainly mediated through activation of NF-κB [273] and these chemokines further could activate NF-κB in AT, it is possible that the reduced phosphorylation

of p65 NF-κB observed in AT explants could be due to the decreased chemokine levels, but also due to an indirect effect of RORα on NF-κB. Liu et al. [259] showed that the PERK (an endoplasmic reticulum transmembrane protein sensor) pathway was activated by RORα in AT from *ob/ob* mice. It has also been reported that PERK signalling activates NF-κB [274]. Based on our findings, and these aforementioned studies, we can also contemplate that activation of PERK and its downstream translation initiation factor eIF2α by RORα in human AT could activate NF-κB and thus promote the expression of these inflammatory chemokines; however, further studies regarding those signalling pathways in human AT are necessary.

Endothelial dysfunction is a pathogenic feature of obesity, which might explain the higher incidence of cardiovascular disease in these patients [178, 179]. TNFα is a key adipokine in the endothelial dysfunction associated with obesity and is a known potential risk factor in the early progression of atherosclerotic lesions through the stimulation of different leukocyte-recruiting chemokines and cellular adhesion molecule expression in endothelium [180-183]. We characterised the consequences of RORα suppression in human endothelial dysfunction *ex vivo* using dynamic flow assays. We found that the increased adhesion of mononuclear cells to TNFα-triggered dysfunctional endothelium was notably reduced by pharmacological inhibition of RORα, and was accompanied by a concomitant reduction of CXCL-8/IL-8 and CCL-2/MCP-1 chemokine secretion from HUVEC. This decrease in leukocyte-endothelial adhesive interactions promoted by RORα blockade might involve the modulation of different cellular adhesion molecules that participate in atherogenesis. Indeed, RORα inhibition diminished TNFα-induced VCAM-1 and ICAM-1 expression in human endothelial cells. Along this line, a recent animal study showed that treatment of mice with an inverse RORα agonist suppressed atherosclerosis development [177].

Overall, our findings suggest that up-regulation of RORα may be important in human morbid obesity, leading us to propose that the activation of RORα in this setting might promote inflammation during AT expansion, resulting in metabolic dysfunction. Indeed, our *ex vivo* results point in this direction. However, a limitation of the present study is that we did not have access to AT from non-obese subjects, and thus we could not study RORα expression in this particular group. Accordingly, replication of these findings in a larger cohort of obese and lean subjects is needed

as a next step in evaluating the functional relevance of RORα and its potential relationship with metabolic complications associated with obesity.

6. CONCLUSIONS

1. Pharmacological blockade of SGLT-2 by empagliflozin reduced the severity and incidence of AAA induced by Ang II in apoE$^{-/-}$ mice. Empagliflozin treatment reduced macrophage infiltration, chemokine expression (MCP-1 and RANTES), ECM degradation and neovascularization in the vascular wall. Therefore, pharmacological modulation of SGLT-2 may prevent or even delay the progression of this cardiovacular disorder linked to RAS activation.

2. SGLT-2 was expressed in human aortic endothelial cells and its pharmacological inhibition with empagliflozin counteracted the pro-inflammatory status induced by Ang II. Empagliflozin prevented mononuclear cell adhesion to the endothelium by inhibiting VCAM-1 and ICAM-1 expression and chemokine release (MCP-1 and RANTES) in Ang II-stimulated HAEC. These studies suggest that SGLT-2 inhibition might represent a novel promising therapeutic strategy to prevent endothelial dysfunction.

3. Compared to subcutaneous AT, RORα was overexpressed in omental AT from morbidly obese patients and even more in omental AT from obese diabetic individuals leading to suggest that the upregulation of RORα is associated with insulin resistance and metabolic alterations in morbid obesity. Pharmacological inhibition of RORα with the inverse agonist SR3335 blocked cytokine/chemokine secretion in omental fat from morbid obese diabetic patients through the inhibition of p65 NFκB phosphorylation and the activation of AKT signalling pathway. These findings suggest that RORα could represent a new pharmacological target in morbid obesity and its metabolic comorbidities.

4. Pharmacological inhibition of RORα reduced chemokine (CXCL-8/IL-8 and CCL-2/MCP-1) secretion, CAM expression and NFκB activation induced by TNFα in human endothelial cells. These effects lead to a decreased mononuclear leukocyte interaction, a key step in atherogenesis. Therefore, RORα inhibition could represent a new potential therapeutic strategy to prevent cardiovacular complications in morbid obesity.

7. REFERENCES

1. Mccomb S, Thiriot A, Akache B, Krishnan L,Stark F. Introduction to the Immune System. Methods Mol Biol. 2019; 2024: 1-24.
2. Germolec DR, Shipkowski KA, Frawley RP,Evans E. Markers of Inflammation. Methods Mol Biol. 2018; 1803: 57-79.
3. Serhan CN. Treating inflammation and infection in the 21st century: new hints from decoding resolution mediators and mechanisms. Faseb j. 2017; 31(4): 1273-88.
4. Hoda SA,Ginter PS. Robbins and cotran pathologic basis of disease. American Journal of Clinical Pathology. 2015; 144(1): 172.
5. Libby P. Inflammatory Mechanisms: The Molecular Basis of Inflammation and Disease. Nutrition Reviews. 2007; 65(12): 140-46.
6. Rao RM, Yang L, Garcia-Cardena G,Luscinskas FW. Endothelial-dependent mechanisms of leukocyte recruitment to the vascular wall. Circ Res. 2007; 101(3): 234-47.
7. Rius C,Sanz MJ. Intravital Microscopy in the Cremaster Muscle Microcirculation for Endothelial Dysfunction Studies. Methods Mol Biol. 2015; 1339: 357-66.
8. Konukoglu D,Uzun H. Endothelial Dysfunction and Hypertension. Adv Exp Med Biol. 2017; 956: 511-40.
9. Abdal Dayem A, Lee S, H YC,Cho SG. The Impact of Adhesion Molecules on the In Vitro Culture and Differentiation of Stem Cells. Biotechnol J. 2018; 13(2).
10. Schnoor M, Alcaide P, Voisin MB,Van Buul JD. Crossing the Vascular Wall: Common and Unique Mechanisms Exploited by Different Leukocyte Subsets during Extravasation. Mediators Inflamm. 2015; 2015: 946509.
11. Libby P. Inflammation in atherosclerosis. Arterioscler Thromb Vasc Biol. 2012; 32(9): 2045-51.
12. Granger DN, Vowinkel T,Petnehazy T. Modulation of the inflammatory response in cardiovascular disease. Hypertension. 2004; 43(5): 924-31.
13. Wettschureck N, Strilic B,Offermanns S. Passing the Vascular Barrier: Endothelial Signaling Processes Controlling Extravasation. Physiol Rev. 2019; 99(3): 1467-525.
14. Mcever RP. Selectins: initiators of leucocyte adhesion and signalling at the vascular wall. Cardiovasc Res. 2015; 107(3): 331-9.
15. Ley K, Laudanna C, Cybulsky MI,Nourshargh S. Getting to the site of inflammation: the leukocyte adhesion cascade updated. Nat Rev Immunol. 2007; 7(9): 678-89.
16. Mcever RP,Zhu C. Rolling cell adhesion. Annu Rev Cell Dev Biol. 2010; 26: 363-96.
17. Muller WA. How endothelial cells regulate transmigration of leukocytes in the inflammatory response. Am J Pathol. 2014; 184(4): 886-96.
18. Nourshargh S,Alon R. Leukocyte migration into inflamed tissues. Immunity. 2014; 41(5): 694-707.
19. Stone MJ, Hayward JA, Huang C, Z EH,Sanchez J. Mechanisms of Regulation of the Chemokine-Receptor Network. Int J Mol Sci. 2017; 18(2): 342.
20. Gerhardt T,Ley K. Monocyte trafficking across the vessel wall. Cardiovasc Res. 2015; 107(3): 321-30.
21. Kufareva I. Chemokines and their receptors: insights from molecular modeling and crystallography. Curr Opin Pharmacol. 2016; 30: 27-37.
22. Chen K, Bao Z, Tang P, Gong W, Yoshimura T,Wang JM. Chemokines in homeostasis and diseases. Cell Mol Immunol. 2018; 15(4): 324-34.
23. Cardona SM, Garcia JA,Cardona AE. The fine balance of chemokines during disease: trafficking, inflammation, and homeostasis. Methods Mol Biol. 2013; 1013: 1-16.
24. Hughes CE,Nibbs RJB. A guide to chemokines and their receptors. 2018; 285(16): 2944-71.

25. Balakin KV, Ivanenkov YA, Tkachenko SE, Kiselyov AS,Ivachtchenko AV. Regulators of chemokine receptor activity as promising anticancer therapeutics. Curr Cancer Drug Targets. 2008; 8(4): 299-340.
26. Marques RE, Guabiraba R, Russo RC,Teixeira MM. Targeting CCL5 in inflammation. Expert Opin Ther Targets. 2013; 17(12): 1439-60.
27. Li H, Bai S, Ao Q, Wang X, Tian X, Li X*, et al.* Modulation of Immune-Inflammatory Responses in Abdominal Aortic Aneurysm: Emerging Molecular Targets. J Immunol Res. 2018; 2018: 7213760.
28. Jones GT, Phillips LV, Williams MJ, Van Rij AM,Kabir TD. Two C-C Family Chemokines, Eotaxin and RANTES, Are Novel Independent Plasma Biomarkers for Abdominal Aortic Aneurysm. J Am Heart Assoc. 2016; 5(5): e002993.
29. Dimitrov S, Shaikh F, Pruitt C, Green M, Wilson K, Beg N,Hong S. Differential TNF production by monocyte subsets under physical stress: blunted mobilization of proinflammatory monocytes in prehypertensive individuals. Brain Behav Immun. 2013; 27(1): 101-8.
30. Mehta AK, Gracias DT,Croft M. TNF activity and T cells. Cytokine. 2018; 101: 14-18.
31. Wakefield PE, James WD, Samlaska CP,Meltzer MS. Tumor necrosis factor. J Am Acad Dermatol. 1991; 24(5 Pt 1): 675-85.
32. Gao W, Liu H, Yuan J, Wu C, Huang D, Ma Y*, et al.* Exosomes derived from mature dendritic cells increase endothelial inflammation and atherosclerosis via membrane TNF-α mediated NF-κB pathway. J Cell Mol Med. 2016; 20(12): 2318-27.
33. Ballanti E, Perricone C, Di Muzio G, Kroegler B, Chimenti MS, Graceffa D,Perricone R. Role of the complement system in rheumatoid arthritis and psoriatic arthritis: relationship with anti-TNF inhibitors. Autoimmun Rev. 2011; 10(10): 617-23.
34. Adamy C, Le Corvoisier P, Candiani G, Kirsch M, Pavoine C, Defer N*, et al.* Tumor necrosis factor alpha and glutathione interplay in chronic heart failure. Arch Mal Coeur Vaiss. 2005; 98(9): 906-12.
35. Bennet AM, Van Maarle MC, Hallqvist J, Morgenstern R, Frostegård J, Wiman B*, et al.* Association of TNF-alpha serum levels and TNFA promoter polymorphisms with risk of myocardial infarction. Atherosclerosis. 2006; 187(2): 408-14.
36. Alzamil H. Elevated Serum TNF-α Is Related to Obesity in Type 2 Diabetes Mellitus and Is Associated with Glycemic Control and Insulin Resistance. J Obes. 2020; 2020: 5076858.
37. Mirhafez SR, Pasdar A, Avan A, Esmaily H, Moezzi A, Mohebati M*, et al.* Cytokine and growth factor profiling in patients with the metabolic syndrome. Br J Nutr. 2015; 113(12): 1911-9.
38. Popa C, Netea MG, Van Riel PL, Van Der Meer JW,Stalenhoef AF. The role of TNF-alpha in chronic inflammatory conditions, intermediary metabolism, and cardiovascular risk. J Lipid Res. 2007; 48(4): 751-62.
39. Mussbacher M, Salzmann M, Brostjan C, Hoesel B, Schoergenhofer C, Datler H*, et al.* Cell Type-Specific Roles of NF-kappaB Linking Inflammation and Thrombosis. Front Immunol. 2019; 10: 85.
40. Yang Y,Kim SC. Functional roles of p38 mitogen-activated protein kinase in macrophage-mediated inflammatory responses. Mediators Inflamm. 2014; 2014: 352371.
41. Sprague AH,Khalil RA. Inflammatory cytokines in vascular dysfunction and vascular disease. Biochem Pharmacol. 2009; 78(6): 539-52.
42. Rose DM, Alon R,Ginsberg MH. Integrin modulation and signaling in leukocyte adhesion and migration. Immunol Rev. 2007; 218: 126-34.

43. Zarbock A, Kempf T, Wollert KC,Vestweber D. Leukocyte integrin activation and deactivation: novel mechanisms of balancing inflammation. J Mol Med (Berl). 2012; 90(4): 353-9.
44. Chakraborty S, Hu SY, Wu SH, Karmenyan A,Chiou A. The interaction affinity between vascular cell adhesion molecule-1 (VCAM-1) and very late antigen-4 (VLA-4) analyzed by quantitative FRET. PLoS One. 2015; 10(3): e0121399.
45. Khunkaewla P, Schiller HB, Paster W, Leksa V, Cermák L, Andera L*, et al.* LFA-1-mediated leukocyte adhesion regulated by interaction of CD43 with LFA-1 and CD147. Mol Immunol. 2008; 45(6): 1703-11.
46. Bednarczyk M, Stege H, Grabbe S,Bros M. β2 Integrins-Multi-Functional Leukocyte Receptors in Health and Disease. Int J Mol Sci. 2020; 21(4): 1402.
47. Hu M, Zhang H, Liu Q,Hao Q. Structural Basis for Human PECAM-1-Mediated Trans-homophilic Cell Adhesion. Sci Rep. 2016; 6: 38655.
48. Lertkiatmongkol P, Liao D, Mei H, Hu Y,Newman PJ. Endothelial functions of platelet/endothelial cell adhesion molecule-1 (CD31). Curr Opin Hematol. 2016; 23(3): 253-9.
49. Arcangeli ML, Frontera V,Aurrand-Lions M. Function of junctional adhesion molecules (JAMs) in leukocyte migration and homeostasis. Arch Immunol Ther Exp (Warsz). 2013; 61(1): 15-23.
50. Muller WA. Getting leukocytes to the site of inflammation. Vet Pathol. 2013; 50(1): 7-22.
51. Mitroulis I, Alexaki VI, Kourtzelis I, Ziogas A, Hajishengallis G,Chavakis T. Leukocyte integrins: role in leukocyte recruitment and as therapeutic targets in inflammatory disease. Pharmacol Ther. 2015; 147: 123-35.
52. Filippi MD. Mechanism of Diapedesis: Importance of the Transcellular Route. Adv Immunol. 2016; 129: 25-53.
53. Muller WA. Mechanisms of leukocyte transendothelial migration. Annu Rev Pathol. 2011; 6: 323-44.
54. Sage PT,Carman CV. Settings and mechanisms for trans-cellular diapedesis. Front Biosci (Landmark Ed). 2009; 14: 5066-83.
55. Schulte D, Küppers V, Dartsch N, Broermann A, Li H, Zarbock A*, et al.* Stabilizing the VE-cadherin-catenin complex blocks leukocyte extravasation and vascular permeability. Embo j. 2011; 30(20): 4157-70.
56. Kummer D,Ebnet K. Junctional Adhesion Molecules (JAMs): The JAM-Integrin Connection. Cells. 2018; 7(4): 25.
57. Sakalihasan N, Michel JB, Katsargyris A, Kuivaniemi H, Defraigne JO, Nchimi A*, et al.* Abdominal aortic aneurysms. Nat Rev Dis Primers. 2018; 4(1): 34.
58. Carino D, Sarac T, Ziganshin B,Elefteriades J. Abdominal Aortic Aneurysm: Evolving Controversies and Uncertainties. Int J of Angiol. 2018; 27(2): 58-80.
59. Davis FM, Daugherty A,Lu HS. Updates of Recent Aortic Aneurysm Research. Arterioscler Thromb Vasc Biol. 2019; 39(3): e83-e90.
60. Keisler B,Carter C. Abdominal aortic aneurysm. Am Fam Physician. 2015; 91(8): 538-43.
61. Jana S, Hu M,Shen M. Extracellular matrix, regional heterogeneity of the aorta, and aortic aneurysm. 2019; 51(12): 1-15.
62. Sun J, Deng H, Zhou Z, Xiong X,Gao L. Endothelium as a Potential Target for Treatment of Abdominal Aortic Aneurysm. Oxid Med Cell Longev. 2018; 2018: 6306542.
63. Raffort J, Lareyre F, Clement M, Hassen-Khodja R, Chinetti G,Mallat Z. Monocytes and macrophages in abdominal aortic aneurysm. Nat Rev Cardiol. 2017; 14(8): 457-71.
64. Quintana RA,Taylor WR. Cellular Mechanisms of Aortic Aneurysm Formation. Circ Res. 2019; 124(4): 607-18.
65. Li J, Krishna SM,Golledge J. The Potential Role of Kallistatin in the Development of Abdominal Aortic Aneurysm. Int J Mol Sci. 2016; 17(8): 1312.

66. Fahey E,Doyle SL. IL-1 Family Cytokine Regulation of Vascular Permeability and Angiogenesis. Front Immunol. 2019; 10: 1426.
67. Melincovici CS, Boşca AB, Şuşman S, Mărginean M, Mihu C, Istrate M*, et al.* Vascular endothelial growth factor (VEGF) - key factor in normal and pathological angiogenesis. Rom J Morphol Embryol. 2018; 59(2): 455-67.
68. Davis FM, Rateri DL,Daugherty A. Abdominal aortic aneurysm: novel mechanisms and therapies. Curr Opin Cardiol. 2015; 30(6): 566-73.
69. Santos RaS, Sampaio WO, Alzamora AC,Motta-Santos D. The ACE2/Angiotensin-(1-7)/MAS Axis of the Renin-Angiotensin System: Focus on Angiotensin-(1-7). Physiol Rev. 2018; 98(1): 505-53.
70. Benigni A, Cassis P,Remuzzi G. Angiotensin II revisited: new roles in inflammation, immunology and aging. EMBO Mol Med. 2010; 2(7): 247-57.
71. Chang Y,Wei W. Angiotensin II in inflammation, immunity and rheumatoid arthritis. Clin Exp Immunol. 2015; 179(2): 137-45.
72. Forrester SJ, Booz GW,Sigmund CD. Angiotensin II Signal Transduction: An Update on Mechanisms of Physiology and Pathophysiology. 2018; 98(3): 1627-738.
73. Muniyappa R,Yavuz S. Metabolic actions of angiotensin II and insulin: a microvascular endothelial balancing act. Mol Cell Endocrinol. 2013; 378(1-2): 59-69.
74. Paulis L, Foulquier S, Namsolleck P, Recarti C, Steckelings UM,Unger T. Combined Angiotensin Receptor Modulation in the Management of Cardio-Metabolic Disorders. Drugs. 2016; 76(1): 1-12.
75. Wu CH, Mohammadmoradi S, Chen JZ, Sawada H, Daugherty A,Lu HS. Renin-Angiotensin System and Cardiovascular Functions. Arterioscler Thromb Vasc Biol. 2018; 38(7): e108-e16.
76. Bitker L,Burrell LM. Classic and Nonclassic Renin-Angiotensin Systems in the Critically Ill. Crit Care Clin. 2019; 35(2): 213-27.
77. Varela ML, Mogildea M, Moreno I,Lopes A. Acute Inflammation and Metabolism. Inflammation. 2018; 41(4): 1115-27.
78. Ames MK, Atkins CE,Pitt B. The renin-angiotensin-aldosterone system and its suppression. J Vet Intern Med. 2019; 33(2): 363-82.
79. Guang C, Phillips RD, Jiang B,Milani F. Three key proteases--angiotensin-I-converting enzyme (ACE), ACE2 and renin--within and beyond the renin-angiotensin system. Arch Cardiovasc Dis. 2012; 105(6-7): 373-85.
80. Zhang H,Baker A. Recombinant human ACE2: acing out angiotensin II in ARDS therapy. Crit Care. 2017; 21(1): 305.
81. Sparks MA, Crowley SD, Gurley SB, Mirotsou M,Coffman TM. Classical Renin-Angiotensin system in kidney physiology. Compr Physiol. 2014; 4(3): 1201-28.
82. Su JB. Different cross-talk sites between the renin-angiotensin and the kallikrein-kinin systems. J Renin Angiotensin Aldosterone Syst. 2014; 15(4): 319-28.
83. Ferrario CM,Mullick AE. Renin angiotensin aldosterone inhibition in the treatment of cardiovascular disease. Pharmacol Res. 2017; 125(Pt A): 57-71.
84. Kawai T, Forrester SJ, O'brien S, Baggett A, Rizzo V,Eguchi S. AT1 receptor signaling pathways in the cardiovascular system. Pharmacol Res. 2017; 125(Pt A): 4-13.
85. Liang B, Wang X, Zhang N, Yang H, Bai R, Liu M*, et al.* Angiotensin-(1-7) Attenuates Angiotensin II-Induced ICAM-1, VCAM-1, and MCP-1 Expression via the MAS Receptor Through Suppression of P38 and NF-κB Pathways in HUVECs. Cell Physiol Biochem. 2015; 35(6): 2472-82.
86. Piqueras L,Sanz MJ. Angiotensin II and leukocyte trafficking: New insights for an old vascular mediator. Role of redox-signaling pathways. Free Radic Biol Med. 2020; 157: 38-54.

87. Li XC, Zhu D, Zheng X, Zhang J,Zhuo JL. Intratubular and intracellular renin-angiotensin system in the kidney: a unifying perspective in blood pressure control. Clin Sci (Lond). 2018; 132(13): 1383-401.
88. Nishiyama A,Kobori H. Independent regulation of renin-angiotensin-aldosterone system in the kidney. Clin Exp Nephrol. 2018; 22(6): 1231-39.
89. Lu Q, Ma Z, Ding Y, Bedarida T, Chen L, Xie Z,Song P. Circulating miR-103a-3p contributes to angiotensin II-induced renal inflammation and fibrosis via a SNRK/NF-κB/p65 regulatory axis. Nat Commun. 2019; 10(1): 2145.
90. Yasue S, Masuzaki H, Okada S, Ishii T, Kozuka C, Tanaka T*, et al.* Adipose tissue-specific regulation of angiotensinogen in obese humans and mice: impact of nutritional status and adipocyte hypertrophy. Am J Hypertens. 2010; 23(4): 425-31.
91. Kalupahana NS,Moustaid-Moussa N. The renin-angiotensin system: a link between obesity, inflammation and insulin resistance. Obes Rev. 2012; 13(2): 136-49.
92. Azushima K, Ohki K, Wakui H, Uneda K, Haku S, Kobayashi R*, et al.* Adipocyte-Specific Enhancement of Angiotensin II Type 1 Receptor-Associated Protein Ameliorates Diet-Induced Visceral Obesity and Insulin Resistance. J Am Heart Assoc. 2017; 6(3): e004488.
93. Flaten HK,Monte AA. The Pharmacogenomic and Metabolomic Predictors of ACE Inhibitor and Angiotensin II Receptor Blocker Effectiveness and Safety. Cardiovasc Drugs Ther. 2017; 31(4): 471-82.
94. Momoniat T, Ilyas D,Bhandari S. ACE inhibitors and ARBs: Managing potassium and renal function. Cleve Clin J Med. 2019; 86(9): 601-07.
95. Montezano AC, Nguyen Dinh Cat A, Rios FJ,Touyz RM. Angiotensin II and vascular injury. Curr Hypertens Rep. 2014; 16(6): 431.
96. Kortekaas KE, Meijer CA, Hinnen JW, Dalman RL, Xu B, Hamming JF,Lindeman JH. ACE inhibitors potently reduce vascular inflammation, results of an open proof-of-concept study in the abdominal aortic aneurysm. PLoS One. 2014; 9(12): e111952.
97. Van Thiel BS, Van Der Pluijm I, Te Riet L, Essers J,Danser AH. The renin-angiotensin system and its involvement in vascular disease. Eur J Pharmacol. 2015; 763(Pt A): 3-14.
98. Zhao G, Chang Z, Zhao Y, Guo Y, Lu H, Liang W*, et al.* KLF11 protects against abdominal aortic aneurysm through inhibition of endothelial cell dysfunction. JCI Insight. 2021; 6(5): e141673.
99. Daugherty A, Manning MW,Cassis LA. Angiotensin II promotes atherosclerotic lesions and aneurysms in apolipoprotein E-deficient mice. J Clin Invest. 2000; 105(11): 1605-12.
100. Daugherty A,Cassis L. Chronic angiotensin II infusion promotes atherogenesis in low density lipoprotein receptor -/- mice. Ann N Y Acad Sci. 1999; 892: 108-18.
101. Manning MW, Cassi LA, Huang J, Szilvassy SJ,Daugherty A. Abdominal aortic aneurysms: fresh insights from a novel animal model of the disease. Vasc Med. 2002; 7(1): 45-54.
102. Mahaffey KW, Neal B, Perkovic V, De Zeeuw D, Fulcher G, Erondu N*, et al.* Canagliflozin for Primary and Secondary Prevention of Cardiovascular Events: Results From the CANVAS Program (Canagliflozin Cardiovascular Assessment Study). Circulation. 2018; 137(4): 323-34.
103. Scheen AJ. Cardiovascular Effects of New Oral Glucose-Lowering Agents: DPP-4 and SGLT-2 Inhibitors. Circ Res. 2018; 122(10): 1439-59.
104. Verma S,Mcmurray JJV. SGLT2 inhibitors and mechanisms of cardiovascular benefit: a state-of-the-art review. Diabetologia. 2018; 61(10): 2108-17.
105. Scott R, Morgan J, Zimmer Z, Lam RLH, O'neill EA, Kaufman KD,Engel SS. A randomized clinical trial of the efficacy and safety of sitagliptin compared with

dapagliflozin in patients with type 2 diabetes mellitus and mild renal insufficiency: The CompoSIT-R study. Diabetes Obes Metab. 2018; 20(12): 2876-84.
106. Nakatsu Y, Kokubo H, Bumdelger B, Yoshizumi M, Yamamotoya T, Matsunaga Y*, et al.* The SGLT2 Inhibitor Luseogliflozin Rapidly Normalizes Aortic mRNA Levels of Inflammation-Related but Not Lipid-Metabolism-Related Genes and Suppresses Atherosclerosis in Diabetic ApoE KO Mice. Int J Mol Sci. 2017; 18(8): 1704.
107. Kosiborod M, Cavender MA, Fu AZ, Wilding JP, Khunti K, Holl RW*, et al.* Lower Risk of Heart Failure and Death in Patients Initiated on Sodium-Glucose Cotransporter-2 Inhibitors Versus Other Glucose-Lowering Drugs: The CVD-REAL Study (Comparative Effectiveness of Cardiovascular Outcomes in New Users of Sodium-Glucose Cotransporter-2 Inhibitors). Circulation. 2017; 136(3): 249-59.
108. Honda Y, Imajo K, Kato T, Kessoku T, Ogawa Y, Tomeno W*, et al.* The Selective SGLT2 Inhibitor Ipragliflozin Has a Therapeutic Effect on Nonalcoholic Steatohepatitis in Mice. PLoS One. 2016; 11(1): e0146337.
109. Ohki T, Isogawa A, Toda N,Tagawa K. Effectiveness of Ipragliflozin, a Sodium-Glucose Co-transporter 2 Inhibitor, as a Second-line Treatment for Non-Alcoholic Fatty Liver Disease Patients with Type 2 Diabetes Mellitus Who Do Not Respond to Incretin-Based Therapies Including Glucagon-like Peptide-1 Analogs and Dipeptidyl Peptidase-4 Inhibitors. Clin Drug Investig. 2016; 36(4): 313-9.
110. Bolinder J, Ljunggren Ö, Kullberg J, Johansson L, Wilding J, Langkilde AM*, et al.* Effects of dapagliflozin on body weight, total fat mass, and regional adipose tissue distribution in patients with type 2 diabetes mellitus with inadequate glycemic control on metformin. J Clin Endocrinol Metab. 2012; 97(3): 1020-31.
111. Ji W, Zhao M, Wang M, Yan W, Liu Y, Ren S*, et al.* Effects of canagliflozin on weight loss in high-fat diet-induced obese mice. PLoS One. 2017; 12(6): e0179960.
112. Xu L,Ota T. Emerging roles of SGLT2 inhibitors in obesity and insulin resistance: Focus on fat browning and macrophage polarization. Adipocyte. 2018; 7(2): 121-28.
113. Sasaki M, Sasako T, Kubota N, Sakurai Y, Takamoto I, Kubota T*, et al.* Dual Regulation of Gluconeogenesis by Insulin and Glucose in the Proximal Tubules of the Kidney. Diabetes. 2017; 66(9): 2339-50.
114. Ghezzi C, Loo DDF,Wright EM. Physiology of renal glucose handling via SGLT1, SGLT2 and GLUT2. Diabetologia. 2018; 61(10): 2087-97.
115. Scott RP,Quaggin SE. Review series: The cell biology of renal filtration. J Cell Biol. 2015; 209(2): 199-210.
116. Kalra S, Singh V,Nagrale D. Sodium-Glucose Cotransporter-2 Inhibition and the Glomerulus: A Review. Adv Ther. 2016; 33(9): 1502-18.
117. Chawla G,Chaudhary KK. A complete review of empagliflozin: Most specific and potent SGLT2 inhibitor used for the treatment of type 2 diabetes mellitus. Diabetes Metab Syndr. 2019; 13(3): 2001-08.
118. Sizar O, Podder V,Talati R. Empagliflozin, in StatPearls. 2020: Treasure Island (FL).
119. Gerich JE. Role of the kidney in normal glucose homeostasis and in the hyperglycaemia of diabetes mellitus: therapeutic implications. Diabet Med. 2010; 27(2): 136-42.
120. Zinman B, Wanner C, Lachin JM, Fitchett D, Bluhmki E, Hantel S*, et al.* Empagliflozin, Cardiovascular Outcomes, and Mortality in Type 2 Diabetes. N Engl J Med. 2015; 373(22): 2117-28.
121. Zinman B, Inzucchi SE, Lachin JM, Wanner C, Ferrari R, Fitchett D*, et al.* Rationale, design, and baseline characteristics of a randomized, placebo-

controlled cardiovascular outcome trial of empagliflozin (EMPA-REG OUTCOME™). Cardiovasc Diabetol. 2014; 13: 102.
122. Han JH, Oh TJ, Lee G, Maeng HJ, Lee DH, Kim KM*, et al.* The beneficial effects of empagliflozin, an SGLT2 inhibitor, on atherosclerosis in ApoE (-/-) mice fed a western diet. Diabetologia. 2017; 60(2): 364-76.
123. Dimitriadis GK, Nasiri-Ansari N, Agrogiannis G, Kostakis ID, Randeva MS, Nikiteas N*, et al.* Empagliflozin improves primary haemodynamic parameters and attenuates the development of atherosclerosis in high fat diet fed APOE knockout mice. Mol Cell Endocrinol. 2019; 494: 110487.
124. Liu Y, Xu J, Wu M, Xu B,Kang L. Empagliflozin protects against atherosclerosis progression by modulating lipid profiles and sympathetic activity. Lipids Health Dis. 2021; 20(1): 5.
125. Pennig J, Scherrer P, Gissler MC, Anto-Michel N, Hoppe N, Füner L*, et al.* Glucose lowering by SGLT2-inhibitor empagliflozin accelerates atherosclerosis regression in hyperglycemic STZ-diabetic mice. 2019; 9(1): 17937.
126. Ganbaatar B, Fukuda D, Shinohara M, Yagi S, Kusunose K, Yamada H*, et al.* Empagliflozin ameliorates endothelial dysfunction and suppresses atherogenesis in diabetic apolipoprotein E-deficient mice. Eur J Pharmacol. 2020; 875: 173040.
127. Park SH, Farooq MA, Gaertner S, Bruckert C, Qureshi AW, Lee HH*, et al.* Empagliflozin improved systolic blood pressure, endothelial dysfunction and heart remodeling in the metabolic syndrome ZSF1 rat. Cardiovasc Diabetol. 2020; 19(1): 19.
128. Climent E, Benaiges D, Goday A, Villatoro M, Julià H, Ramón JM*, et al.* Morbid obesity and dyslipidaemia: The impact of bariatric surgery. Clin Investig Arterioscler. 2020; 32(2): 79-86.
129. Tchernof A,Després JP. Pathophysiology of human visceral obesity: an update. Physiol Rev. 2013; 93(1): 359-404.
130. Abdelaal M, Le Roux CW,Docherty NG. Morbidity and mortality associated with obesity. Ann Transl Med. 2017; 5(7): 161.
131. Goossens GH. The Metabolic Phenotype in Obesity: Fat Mass, Body Fat Distribution, and Adipose Tissue Function. Obes Facts. 2017; 10(3): 207-15.
132. Arroyo-Johnson C,Mincey KD. Obesity Epidemiology Worldwide. Gastroenterol Clin North Am. 2016; 45(4): 571-79.
133. Marangoni RG, Korman B,Varga J. Adipocytic Progenitor Cells Give Rise to Pathogenic Myofibroblasts: Adipocyte-to-Mesenchymal Transition and Its Emerging Role in Fibrosis in Multiple Organs. Curr Rheumatol Rep. 2020; 22(11): 79.
134. Wright SM,Aronne LJ. Causes of obesity. Abdom Imaging. 2012; 37(5): 730-2.
135. Webb VL,Wadden TA. Intensive Lifestyle Intervention for Obesity: Principles, Practices, and Results. Gastroenterology. 2017; 152(7): 1752-64.
136. Fock KM,Khoo J. Diet and exercise in management of obesity and overweight. J Gastroenterol Hepatol. 2013; 28 Suppl 4: 59-63.
137. Narayanaswami V,Dwoskin LP. Obesity: Current and potential pharmacotherapeutics and targets. Pharmacol Ther. 2017; 170: 116-47.
138. Mccafferty BJ, Hill JO,Gunn AJ. Obesity: Scope, Lifestyle Interventions, and Medical Management. Tech Vasc Interv Radiol. 2020; 23(1): 100653.
139. Stolarczyk E. Adipose tissue inflammation in obesity: a metabolic or immune response? Curr Opin Pharmacol. 2017; 37: 35-40.
140. Unamuno X,Gómez-Ambrosi J. Adipokine dysregulation and adipose tissue inflammation in human obesity. Eur J Clin Invest. 2018; 48(9): e12997.
141. Crewe C, An YA,Scherer PE. The ominous triad of adipose tissue dysfunction: inflammation, fibrosis, and impaired angiogenesis. J Clin Invest. 2017; 127(1): 74-82.

142. Liu F, He J, Wang H, Zhu D,Bi Y. Adipose Morphology: a Critical Factor in Regulation of Human Metabolic Diseases and Adipose Tissue Dysfunction. Obes Surg. 2020; 30(12): 5086-100.
143. Guzik TJ, Skiba DS, Touyz RM,Harrison DG. The role of infiltrating immune cells in dysfunctional adipose tissue. Cardiovasc Res. 2017; 113(9): 1009-23.
144. Longo M, Zatterale F, Naderi J, Parrillo L, Formisano P, Raciti GA*, et al.* Adipose Tissue Dysfunction as Determinant of Obesity-Associated Metabolic Complications. Int J Mol Sci. 2019; 20(9): 2358.
145. Ibrahim MM. Subcutaneous and visceral adipose tissue: structural and functional differences. Obes Rev. 2010; 11(1): 11-8.
146. Morigny P, Houssier M, Mouisel E,Langin D. Adipocyte lipolysis and insulin resistance. Biochimie. 2016; 125: 259-66.
147. Nandipati KC, Subramanian S,Agrawal DK. Protein kinases: mechanisms and downstream targets in inflammation-mediated obesity and insulin resistance. Mol Cell Biochem. 2017; 426(1-2): 27-45.
148. Awasthee N, Rai V, Chava S, Nallasamy P, Kunnumakkara AB, Bishayee A*, et al.* Targeting lκappaB kinases for cancer therapy. Semin Cancer Biol. 2019; 56: 12-24.
149. Blanchett S, Boal-Carvalho I, Layzell S,Seddon B. NF-κB and Extrinsic Cell Death Pathways - Entwined Do-or-Die Decisions for T cells. Trends Immunol. 2021; 42(1): 76-88.
150. Feng J, Lu S,Ou B. The Role of JNk Signaling Pathway in Obesity-Driven Insulin Resistance. Diabetes Metab Syndr Obes. 2020; 13: 1399-406.
151. Ringseis R, Eder K, Mooren FC,Krüger K. Metabolic signals and innate immune activation in obesity and exercise. Exerc Immunol Rev. 2015; 21: 58-68.
152. Payankaulam S, Raicu AM,Arnosti DN. Transcriptional Regulation of INSR, the Insulin Receptor Gene. Genes (Basel). 2019; 10(12): 984.
153. Rachdaoui N. Insulin: The Friend and the Foe in the Development of Type 2 Diabetes Mellitus. Int J Mol Sci. 2020; 21(5): 1770.
154. Arneth B, Arneth R,Shams M. Metabolomics of Type 1 and Type 2 Diabetes. Int J Mol Sci. 2019; 20(10): 2467.
155. Czech MP. Mechanisms of insulin resistance related to white, beige, and brown adipocytes. Mol Metab. 2020; 34: 27-42.
156. Fazakerley DJ,Krycer JR. Muscle and adipose tissue insulin resistance: malady without mechanism? J Lipid Res. 2019; 60(10): 1720-32.
157. Gancheva S, Jelenik T, Álvarez-Hernández E,Roden M. Interorgan Metabolic Crosstalk in Human Insulin Resistance. Physiol Rev. 2018; 98(3): 1371-415.
158. Montgomery MK, De Nardo W,Watt MJ. Impact of Lipotoxicity on Tissue "Cross Talk" and Metabolic Regulation. Physiology (Bethesda). 2019; 34(2): 134-49.
159. Bandet CL, Tan-Chen S, Bourron O, Le Stunff H,Hajduch E. Sphingolipid Metabolism: New Insight into Ceramide-Induced Lipotoxicity in Muscle Cells. Int J Mol Sci. 2019; 20(3): 479.
160. Lair B,Laurens C. Novel Insights and Mechanisms of Lipotoxicity-Driven Insulin Resistance. Int J Mol Sci. 2020; 21(17): 6358.
161. Oguntibeju OO. Type 2 diabetes mellitus, oxidative stress and inflammation: examining the links. Int J Physiol Pathophysiol Pharmacol. 2019; 11(3): 45-63.
162. Kojetin DJ,Burris TP. REV-ERB and ROR nuclear receptors as drug targets. Nat Rev Drug Discov. 2014; 13(3): 197-216.
163. Zhang Y, Luo XY, Wu DH,Xu Y. ROR nuclear receptors: structures, related diseases, and drug discovery. Acta Pharmacol Sin. 2015; 36(1): 71-87.
164. Liu K, Zou C,Qin B. The association between nuclear receptors and ocular diseases. Oncotarget. 2017; 8(16): 27603-15.
165. Feng S, Xu S, Wen Z,Zhu Y. Retinoic acid-related orphan receptor RORβ, circadian rhythm abnormalities and tumorigenesis (Review). Int J Mol Med. 2015; 35(6): 1493-500.

166. Jetten AM, Kang HS,Takeda Y. Retinoic acid-related orphan receptors α and γ: key regulators of lipid/glucose metabolism, inflammation, and insulin sensitivity. Front Endocrinol (Lausanne). 2013; 4: 1.
167. Solt LA, Griffin PR,Burris TP. Ligand regulation of retinoic acid receptor-related orphan receptors: implications for development of novel therapeutics. Curr Opin Lipidol. 2010; 21(3): 204-11.
168. Fan J, Lv Z, Yang G, Liao TT, Xu J, Wu F*, et al.* Retinoic Acid Receptor-Related Orphan Receptors: Critical Roles in Tumorigenesis. Front Immunol. 2018; 9: 1187.
169. Hirose T, Smith RJ,Jetten AM. ROR gamma: the third member of ROR/RZR orphan receptor subfamily that is highly expressed in skeletal muscle. Biochem Biophys Res Commun. 1994; 205(3): 1976-83.
170. Besnard S, Heymes C, Merval R, Rodriguez M, Galizzi JP, Boutin JA*, et al.* Expression and regulation of the nuclear receptor RORalpha in human vascular cells. FEBS Lett. 2002; 511(1-3): 36-40.
171. Gulec C, Coban N, Ozsait-Selcuk B, Sirma-Ekmekci S, Yildirim O,Erginel-Unaltuna N. Identification of potential target genes of ROR-alpha in THP1 and HUVEC cell lines. Exp Cell Res. 2017; 353(1): 6-15.
172. Zhang Y, Liu Y, Liu Y, Zhang Y,Su Z. Genetic Variants of Retinoic Acid Receptor-Related Orphan Receptor Alpha Determine Susceptibility to Type 2 Diabetes Mellitus in Han Chinese. Genes (Basel). 2016; 7(8): 54.
173. Coban N, Gulec C, Ozsait-Selcuk B,Erginel-Unaltuna N. CYP19A1, MIF and ABCA1 genes are targets of the RORα in monocyte and endothelial cells. Cell Biol Int. 2017; 41(2): 163-76.
174. Kadiri S, Monnier C, Ganbold M, Ledent T, Capeau J,Antoine B. The nuclear retinoid-related orphan receptor-α regulates adipose tissue glyceroneogenesis in addition to hepatic gluconeogenesis. Am J Physiol Endocrinol Metab. 2015; 309(2): E105-14.
175. Kang HS, Okamoto K, Takeda Y, Beak JY, Gerrish K, Bortner CD*, et al.* Transcriptional profiling reveals a role for RORalpha in regulating gene expression in obesity-associated inflammation and hepatic steatosis. Physiol Genomics. 2011; 43(13): 818-28.
176. Lau P, Fitzsimmons RL, Raichur S, Wang SC, Lechtken A,Muscat GE. The orphan nuclear receptor, RORalpha, regulates gene expression that controls lipid metabolism: staggerer (SG/SG) mice are resistant to diet-induced obesity. J Biol Chem. 2008; 283(26): 18411-21.
177. Billon C, Sitaula S,Burris TP. Inhibition of RORα/γ suppresses atherosclerosis via inhibition of both cholesterol absorption and inflammation. Mol Metab. 2016; 5(10): 997-1005.
178. Engin A. Endothelial Dysfunction in Obesity. Adv Exp Med Biol. 2017; 960: 345-79.
179. Marques P,Collado A. Systemic Inflammation in Metabolic Syndrome: Increased Platelet and Leukocyte Activation, and Key Role of CX(3)CL1/CX(3)CR1 and CCL2/CCR2 Axes in Arterial Platelet-Proinflammatory Monocyte Adhesion. J Clin Med. 2019; 8(5): 708.
180. Catalán V, Gómez-Ambrosi J, Ramirez B, Rotellar F, Pastor C, Silva C*, et al.* Proinflammatory cytokines in obesity: impact of type 2 diabetes mellitus and gastric bypass. Obes Surg. 2007; 17(11): 1464-74.
181. Cartier A, Côté M, Bergeron J, Alméras N, Tremblay A, Lemieux I,Després JP. Plasma soluble tumour necrosis factor-alpha receptor 2 is elevated in obesity: specific contribution of visceral adiposity. Clin Endocrinol (Oxf). 2010; 72(3): 349-57.
182. Weber KS, Von Hundelshausen P, Clark-Lewis I, Weber PC,Weber C. Differential immobilization and hierarchical involvement of chemokines in

monocyte arrest and transmigration on inflamed endothelium in shear flow. Eur J Immunol. 1999; 29(2): 700-12.
183. Hotamisligil GS, Shargill NS,Spiegelman BM. Adipose expression of tumor necrosis factor-alpha: direct role in obesity-linked insulin resistance. Science. 1993; 259(5091): 87-91.
184. Robinet P, Milewicz DM, Cassis LA, Leeper NJ, Lu HS,Smith JD. Consideration of Sex Differences in Design and Reporting of Experimental Arterial Pathology Studies-Statement From ATVB Council. Arterioscler Thromb Vasc Biol. 2018; 38(2): 292-303.
185. Tahara A, Takasu T, Yokono M, Imamura M,Kurosaki E. Characterization and comparison of SGLT2 inhibitors: Part 3. Effects on diabetic complications in type 2 diabetic mice. Eur J Pharmacol. 2017; 809: 163-71.
186. Tahara A, Takasu T, Yokono M, Imamura M,Kurosaki E. Characterization and comparison of sodium-glucose cotransporter 2 inhibitors: Part 2. Antidiabetic effects in type 2 diabetic mice. J Pharmacol Sci. 2016; 131(3): 198-208.
187. Tahara A, Takasu T, Yokono M, Imamura M,Kurosaki E. Characterization and comparison of sodium-glucose cotransporter 2 inhibitors in pharmacokinetics, pharmacodynamics, and pharmacologic effects. J Pharmacol Sci. 2016; 130(3): 159-69.
188. Feng M,Dipetrillo K. Non-invasive Blood Pressure Measurement in Mice, in Cardiovascular Genomics: Methods and Protocols. 2009, Humana Press: Totowa, NJ. p. 45-55.
189. Daugherty A, Rateri D, Hong L,Balakrishnan A. Measuring blood pressure in mice using volume pressure recording, a tail-cuff method. J Vis Exp. 2009(27): 1291.
190. Andres-Blasco I, Herrero-Cervera A, Vinue A, Martinez-Hervas S, Piqueras L, Sanz MJ*, et al.* Hepatic lipase deficiency produces glucose intolerance, inflammation and hepatic steatosis. J Endocrinol. 2015; 227(3): 179-91.
191. Daugherty A, Manning MW,Cassis LA. Antagonism of AT2 receptors augments angiotensin II-induced abdominal aortic aneurysms and atherosclerosis. Br J Pharmacol. 2001; 134(4): 865-70.
192. Rateri DL, Davis FM, Balakrishnan A, Howatt DA, Moorleghen JJ, O'connor WN*, et al.* Angiotensin II induces region-specific medial disruption during evolution of ascending aortic aneurysms. Am J Pathol. 2014; 184(9): 2586-95.
193. Sun J, Sukhova GK, Yang M, Wolters PJ, Macfarlane LA, Libby P*, et al.* Mast cells modulate the pathogenesis of elastase-induced abdominal aortic aneurysms in mice. J Clin Invest. 2007; 117(11): 3359-68.
194. El-Daly M, Pulakazhi Venu VK, Saifeddine M, Mihara K, Kang S, Fedak PWM*, et al.* Hyperglycaemic impairment of PAR2-mediated vasodilation: Prevention by inhibition of aortic endothelial sodium-glucose-co-Transporter-2 and minimizing oxidative stress. Vascul Pharmacol. 2018; 109: 56-71.
195. Bradford MM. A rapid and sensitive method for the quantitation of microgram quantities of protein utilizing the principle of protein-dye binding. Anal Biochem. 1976; 72: 248-54.
196. Pedro T, Martinez-Hervas S, Tormo C, García-García AB, Saez-Tormo G, Ascaso JF*, et al.* Oxidative stress and antioxidant enzyme values in lymphomonocytes after an oral unsaturated fat load test in familial hypercholesterolemic subjects. Transl Res. 2013; 161(1): 50-6.
197. Vitseva OI, Tanriverdi K, Tchkonia TT, Kirkland JL, Mcdonnell ME, Apovian CM*, et al.* Inducible Toll-like receptor and NF-kappaB regulatory pathway expression in human adipose tissue. Obesity (Silver Spring). 2008; 16(5): 932-7.
198. Rice DR, White AG, Leevy WM,Smith BD. Fluorescence Imaging of Interscapular Brown Adipose Tissue in Living Mice. J Mater Chem B. 2015; 3(9): 1979-89.

199. Martorell S, Hueso L, Gonzalez-Navarro H, Collado A, Sanz MJ,Piqueras L. Vitamin D Receptor Activation Reduces Angiotensin-II-Induced Dissecting Abdominal Aortic Aneurysm in Apolipoprotein E-Knockout Mice. Arterioscler Thromb Vasc Biol. 2016; 36(8): 1587-97.
200. Escudero P, Navarro A, Ferrando C, Furio E, Gonzalez-Navarro H, Juez M*, et al.* Combined treatment with bexarotene and rosuvastatin reduces angiotensin-II-induced abdominal aortic aneurysm in apoE(-/-) mice and angiogenesis. Br J Pharmacol. 2015; 172(12): 2946-60.
201. Siefert SA,Sarkar R. Matrix metalloproteinases in vascular physiology and disease. Vascular. 2012; 20(4): 210-6.
202. Saito T, Hasegawa Y, Ishigaki Y, Yamada T, Gao J, Imai J*, et al.* Importance of endothelial NF-kappaB signalling in vascular remodelling and aortic aneurysm formation. Cardiovasc Res. 2013; 97(1): 106-14.
203. Huang M, Zeng S, Zou Y, Shi M, Qiu Q, Xiao Y*, et al.* The suppression of bromodomain and extra-terminal domain inhibits vascular inflammation by blocking NF-kappaB and MAPK activation. Br J Pharmacol. 2017; 174(1): 101-15.
204. Chen J, Williams S, Ho S, Loraine H, Hagan D, Whaley JM,Feder JN. Quantitative PCR tissue expression profiling of the human SGLT2 gene and related family members. Diabetes Ther. 2010; 1(2): 57-92.
205. Diaz-Rodriguez E, Agra RM, Fernandez AL, Adrio B, Garcia-Caballero T, Gonzalez-Juanatey JR,Eiras S. Effects of dapagliflozin on human epicardial adipose tissue: modulation of insulin resistance, inflammatory chemokine production, and differentiation ability. Cardiovasc Res. 2018; 114(2): 336-46.
206. Mancini SJ, Boyd D, Katwan OJ, Strembitska A, Almabrouk TA,Kennedy S. Canagliflozin inhibits interleukin-1beta-stimulated cytokine and chemokine secretion in vascular endothelial cells by AMP-activated protein kinase-dependent and -independent mechanisms. Sci Rep. 2018; 8(1): 5276.
207. Ramella M, Boccafoschi F, Bellofatto K, Follenzi A, Fusaro L, Boldorini R*, et al.* Endothelial MMP-9 drives the inflammatory response in abdominal aortic aneurysm (AAA). Am J Transl Res. 2017; 9(12): 5485-95.
208. Szekanecz Z, Shah MR, Pearce WH,Koch AE. Human atherosclerotic abdominal aortic aneurysms produce interleukin (IL)-6 and interferon-gamma but not IL-2 and IL-4: the possible role for IL-6 and interferon-gamma in vascular inflammation. Agents Actions. 1994; 42(3-4): 159-62.
209. Furio E, Garcia-Fuster MJ, Redon J, Marques P, Ortega R, Sanz MJ,Piqueras L. CX3CR1/CX3CL1 Axis Mediates Platelet-Leukocyte Adhesion to Arterial Endothelium in Younger Patients with a History of Idiopathic Deep Vein Thrombosis. Thromb Haemost. 2018; 118(3): 562-71.
210. Wang C, Zhang C, Zhou F, Gao L, Wang Y, Wang C,Zhang Y. Angiotensin II induces monocyte chemoattractant protein1 expression by increasing reactive oxygen speciesmediated activation of the nuclear factorkappaB signaling pathway in osteoblasts. Mol Med Rep. 2018; 17(1): 1166-72.
211. Mikolajczyk TP, Nosalski R, Szczepaniak P, Budzyn K, Osmenda G, Skiba D*, et al.* Role of chemokine RANTES in the regulation of perivascular inflammation, T-cell accumulation, and vascular dysfunction in hypertension. Faseb j. 2016; 30(5): 1987-99.
212. Silva IVG, De Figueiredo RC,Rios DRA. Effect of Different Classes of Antihypertensive Drugs on Endothelial Function and Inflammation. Int J Mol Sci. 2019; 20(14): 3458.
213. Hueso L, Ortega R, Selles F, Wu-Xiong NY, Ortega J, Civera M*, et al.* Upregulation of angiostatic chemokines IP-10/CXCL10 and I-TAC/CXCL11 in human obesity and their implication for adipose tissue angiogenesis. Int J Obes (Lond). 2018; 42(8): 1406-17.

214. Fuster JJ, Ouchi N, Gokce N,Walsh K. Obesity-Induced Changes in Adipose Tissue Microenvironment and Their Impact on Cardiovascular Disease. Circ Res. 2016; 118(11): 1786-807.
215. Cignarelli A,Genchi VA. Insulin and Insulin Receptors in Adipose Tissue Development. Int J Mol Sci. 2019; 20(3): 759.
216. Carlsen H, Haugen F, Zadelaar S, Kleemann R, Kooistra T, Drevon CA,Blomhoff R. Diet-induced obesity increases NF-kappaB signaling in reporter mice. Genes Nutr. 2009; 4(3): 215-22.
217. Shoelson SE, Lee J,Goldfine AB. Inflammation and insulin resistance. J Clin Invest. 2006; 116(7): 1793-801.
218. Ferrannini E, Muscelli E, Frascerra S, Baldi S, Mari A, Heise T*, et al.* Metabolic response to sodium-glucose cotransporter 2 inhibition in type 2 diabetic patients. J Clin Invest. 2014; 124(2): 499-508.
219. Connelly KA, Zhang Y, Visram A, Advani A, Batchu SN, Desjardins JF*, et al.* Empagliflozin Improves Diastolic Function in a Nondiabetic Rodent Model of Heart Failure With Preserved Ejection Fraction. JACC Basic Transl Sci. 2019; 4(1): 27-37.
220. Lim VG, Bell RM, Arjun S, Kolatsi-Joannou M, Long DA,Yellon DM. SGLT2 Inhibitor, Canagliflozin, Attenuates Myocardial Infarction in the Diabetic and Nondiabetic Heart. JACC Basic Transl Sci. 2019; 4(1): 15-26.
221. Middleton RK, Lloyd GM, Bown MJ, Cooper NJ, London NJ,Sayers RD. The pro-inflammatory and chemotactic cytokine microenvironment of the abdominal aortic aneurysm wall: a protein array study. J Vasc Surg. 2007; 45(3): 574-80.
222. Golledge AL, Walker P, Norman PE,Golledge J. A systematic review of studies examining inflammation associated cytokines in human abdominal aortic aneurysm samples. Dis Markers. 2009; 26(4): 181-8.
223. Izhak L, Wildbaum G, Jung S, Stein A, Shaked Y,Karin N. Dissecting the autocrine and paracrine roles of the CCR2-CCL2 axis in tumor survival and angiogenesis. PLoS One. 2012; 7(1): e28305.
224. Suffee N, Hlawaty H, Meddahi-Pelle A, Maillard L, Louedec L, Haddad O*, et al.* RANTES/CCL5-induced pro-angiogenic effects depend on CCR1, CCR5 and glycosaminoglycans. Angiogenesis. 2012; 15(4): 727-44.
225. Leng W,Ouyang X. The SGLT-2 Inhibitor Dapagliflozin Has a Therapeutic Effect on Atherosclerosis in Diabetic ApoE(-/-) Mice. Mediators Inflamm. 2016; 2016: 6305735.
226. Nakajima K, Mita T, Osonoi Y, Azuma K, Takasu T, Fujitani Y,Watada H. Effect of Repetitive Glucose Spike and Hypoglycaemia on Atherosclerosis and Death Rate in Apo E-Deficient Mice. Int J Endocrinol. 2015; 2015: 406394.
227. Xu L, Nagata N, Nagashimada M, Zhuge F, Ni Y, Chen G*, et al.* SGLT2 Inhibition by Empagliflozin Promotes Fat Utilization and Browning and Attenuates Inflammation and Insulin Resistance by Polarizing M2 Macrophages in Diet-induced Obese Mice. EBioMedicine. 2017; 20: 137-49.
228. Xu L, Nagata N, Chen G, Nagashimada M, Zhuge F, Ni Y*, et al.* Empagliflozin reverses obesity and insulin resistance through fat browning and alternative macrophage activation in mice fed a high-fat diet. BMJ Open Diabetes Res Care. 2019; 7(1): e000783.
229. Cherney DZ, Perkins BA, Soleymanlou N, Har R, Fagan N, Johansen OE*, et al.* The effect of empagliflozin on arterial stiffness and heart rate variability in subjects with uncomplicated type 1 diabetes mellitus. Cardiovasc Diabetol. 2014; 13: 28.
230. Solini A, Giannini L, Seghieri M, Vitolo E, Taddei S, Ghiadoni L,Bruno RM. Dapagliflozin acutely improves endothelial dysfunction, reduces aortic stiffness and renal resistive index in type 2 diabetic patients: a pilot study. Cardiovasc Diabetol. 2017; 16(1): 138.

231. Shigiyama F,Kumashiro N. Effectiveness of dapagliflozin on vascular endothelial function and glycemic control in patients with early-stage type 2 diabetes mellitus: DEFENCE study. Cardiovasc Diabetol. 2017; 16(1): 84.
232. Sugiyama S, Jinnouchi H, Kurinami N, Hieshima K, Yoshida A, Jinnouchi K*, et al.* The SGLT2 Inhibitor Dapagliflozin Significantly Improves the Peripheral Microvascular Endothelial Function in Patients with Uncontrolled Type 2 Diabetes Mellitus. Intern Med. 2018; 57(15): 2147-56.
233. Oelze M, Kröller-Schön S, Welschof P, Jansen T, Hausding M, Mikhed Y*, et al.* The sodium-glucose co-transporter 2 inhibitor empagliflozin improves diabetes-induced vascular dysfunction in the streptozotocin diabetes rat model by interfering with oxidative stress and glucotoxicity. PLoS One. 2014; 9(11): e112394.
234. Madaan T, Husain I, Akhtar M,Najmi AK. Exploring novel pharmacotherapeutic applications and repurposing potential of sodium glucose CoTransporter 2 inhibitors. Clin Exp Pharmacol Physiol. 2018; 45: 897-907.
235. Majewski C,Bakris GL. Blood pressure reduction: an added benefit of sodium-glucose cotransporter 2 inhibitors in patients with type 2 diabetes. Diabetes Care. 2015; 38(3): 429-30.
236. Steven S, Oelze M, Hanf A, Kröller-Schön S, Kashani F, Roohani S*, et al.* The SGLT2 inhibitor empagliflozin improves the primary diabetic complications in ZDF rats. Redox Biol. 2017; 13: 370-85.
237. Zhou H, Wang S, Zhu P, Hu S, Chen Y,Ren J. Empagliflozin rescues diabetic myocardial microvascular injury via AMPK-mediated inhibition of mitochondrial fission. Redox Biol. 2018; 15: 335-46.
238. Tikkanen I, Narko K, Zeller C, Green A, Salsali A, Broedl UC,Woerle HJ. Empagliflozin reduces blood pressure in patients with type 2 diabetes and hypertension. Diabetes Care. 2015; 38(3): 420-8.
239. Habibi J, Aroor AR, Sowers JR, Jia G, Hayden MR, Garro M*, et al.* Sodium glucose transporter 2 (SGLT2) inhibition with empagliflozin improves cardiac diastolic function in a female rodent model of diabetes. Cardiovasc Diabetol. 2017; 16(1): 9.
240. Aroor AR, Das NA, Carpenter AJ, Habibi J, Jia G, Ramirez-Perez FI*, et al.* Glycemic control by the SGLT2 inhibitor empagliflozin decreases aortic stiffness, renal resistivity index and kidney injury. Cardiovasc Diabetol. 2018; 17(1): 108.
241. Li L, Konishi Y, Morikawa T, Zhang Y, Kitabayashi C, Kobara H*, et al.* Effect of a SGLT2 inhibitor on the systemic and intrarenal renin-angiotensin system in subtotally nephrectomized rats. J Pharmacol Sci. 2018; 137(2): 220-23.
242. Vijaynagar B, Bown MJ, Sayers RD,Choke E. Potential role for anti-angiogenic therapy in abdominal aortic aneurysms. Eur J Clin Invest. 2013; 43(7): 758-65.
243. Kaji K, Nishimura N, Seki K, Sato S, Saikawa S, Nakanishi K*, et al.* Sodium glucose cotransporter 2 inhibitor canagliflozin attenuates liver cancer cell growth and angiogenic activity by inhibiting glucose uptake. Int J Cancer. 2018; 142(8): 1712-22.
244. Nishibe T, Dardik A, Kondo Y, Kudo F, Muto A, Nishi M*, et al.* Expression and localization of vascular endothelial growth factor in normal abdominal aorta and abdominal aortic aneurysm. Int Angiol. 2010; 29(3): 260-5.
245. Longo GM, Xiong W, Greiner TC, Zhao Y, Fiotti N,Baxter BT. Matrix metalloproteinases 2 and 9 work in concert to produce aortic aneurysms. J Clin Invest. 2002; 110(5): 625-32.
246. Wang X,Khalil RA. Matrix Metalloproteinases, Vascular Remodeling, and Vascular Disease. Adv Pharmacol. 2018; 81: 241-330.
247. Sawada H, Hao H, Naito Y, Oboshi M, Hirotani S, Mitsuno M*, et al.* Aortic iron overload with oxidative stress and inflammation in human and murine

abdominal aortic aneurysm. Arterioscler Thromb Vasc Biol. 2015; 35(6): 1507-14.
248. Yao D, Wang S, Wang M,Lu W. Renoprotection of dapagliflozin in human renal proximal tubular cells via the inhibition of the high mobility group box 1-receptor for advanced glycation end products-nuclear factor-κB signaling pathway. Mol Med Rep. 2018; 18(4): 3625-30.
249. Escudero P, Martinez De Marañón A, Collado A, Gonzalez-Navarro H, Hermenegildo C, Peiró C*, et al.* Combined sub-optimal doses of rosuvastatin and bexarotene impair angiotensin II-induced arterial mononuclear cell adhesion through inhibition of Nox5 signaling pathways and increased RXR/PPARα and RXR/PPARγ interactions. Antioxid Redox Signal. 2015; 22(11): 901-20.
250. Chilton R, Tikkanen I, Cannon CP, Crowe S, Woerle HJ, Broedl UC,Johansen OE. Effects of empagliflozin on blood pressure and markers of arterial stiffness and vascular resistance in patients with type 2 diabetes. Diabetes Obes Metab. 2015; 17(12): 1180-93.
251. Neeland IJ, Mcguire DK, Chilton R, Crowe S, Lund SS, Woerle HJ*, et al.* Empagliflozin reduces body weight and indices of adipose distribution in patients with type 2 diabetes mellitus. Diab Vasc Dis Res. 2016; 13(2): 119-26.
252. Cheeseman C. Solute carrier family 2, member 9 and uric acid homeostasis. Curr Opin Nephrol Hypertens. 2009; 18(5): 428-32.
253. Nishimura R, Tanaka Y, Koiwai K, Inoue K, Hach T, Salsali A*, et al.* Effect of empagliflozin monotherapy on postprandial glucose and 24-hour glucose variability in Japanese patients with type 2 diabetes mellitus: a randomized, double-blind, placebo-controlled, 4-week study. Cardiovasc Diabetol. 2015; 14: 11.
254. Mudaliar S, Alloju S,Henry RR. Can a Shift in Fuel Energetics Explain the Beneficial Cardiorenal Outcomes in the EMPA-REG OUTCOME Study? A Unifying Hypothesis. Diabetes Care. 2016; 39(7): 1115-22.
255. Ye J. Emerging role of adipose tissue hypoxia in obesity and insulin resistance. Int J Obes (Lond). 2009; 33(1): 54-66.
256. Goossens GH, Bizzarri A, Venteclef N, Essers Y, Cleutjens JP, Konings E*, et al.* Increased adipose tissue oxygen tension in obese compared with lean men is accompanied by insulin resistance, impaired adipose tissue capillarization, and inflammation. Circulation. 2011; 124(1): 67-76.
257. Booth A, Magnuson A,Foster M. Detrimental and protective fat: body fat distribution and its relation to metabolic disease. Horm Mol Biol Clin Investig. 2014; 17(1): 13-27.
258. Mathieu P, Boulanger MC,Despres JP. Ectopic visceral fat: a clinical and molecular perspective on the cardiometabolic risk. Rev Endocr Metab Disord. 2014; 15(4): 289-98.
259. Liu Y, Chen Y, Zhang J, Liu Y, Zhang Y,Su Z. Retinoic acid receptor-related orphan receptor alpha stimulates adipose tissue inflammation by modulating endoplasmic reticulum stress. J Biol Chem. 2017; 292(34): 13959-69.
260. Lau P, Fitzsimmons RL, Pearen MA, Watt MJ,Muscat GE. Homozygous staggerer (sg/sg) mice display improved insulin sensitivity and enhanced glucose uptake in skeletal muscle. Diabetologia. 2011; 54(5): 1169-80.
261. Auclair M, Roblot N, Capel E, Fève B,Antoine B. Pharmacological modulation of RORα controls fat browning, adaptive thermogenesis, and body weight in mice. Am J Physiol Endocrinol Metab. 2021; 320(2): E219-e33.
262. Monnier C, Auclair M, Le Cam G, Garcia MP,Antoine B. The nuclear retinoid-related orphan receptor RORα controls circadian thermogenic programming in white fat depots. Physiol Rep. 2018; 6(8): e13678.

263. Kanda H, Tateya S, Tamori Y, Kotani K, Hiasa K, Kitazawa R*, et al.* MCP-1 contributes to macrophage infiltration into adipose tissue, insulin resistance, and hepatic steatosis in obesity. J Clin Invest. 2006; 116(6): 1494-505.
264. Weisberg SP, Hunter D, Huber R, Lemieux J, Slaymaker S, Vaddi K*, et al.* CCR2 modulates inflammatory and metabolic effects of high-fat feeding. J Clin Invest. 2006; 116(1): 115-24.
265. Huber J, Kiefer FW, Zeyda M, Ludvik B, Silberhumer GR, Prager G*, et al.* CC chemokine and CC chemokine receptor profiles in visceral and subcutaneous adipose tissue are altered in human obesity. J Clin Endocrinol Metab. 2008; 93(8): 3215-21.
266. Zernecke A, Shagdarsuren E,Weber C. Chemokines in atherosclerosis: an update. Arterioscler Thromb Vasc Biol. 2008; 28(11): 1897-908.
267. Kumar N, Kojetin DJ, Solt LA, Kumar KG, Nuhant P, Duckett DR*, et al.* Identification of SR3335 (ML-176): a synthetic RORα selective inverse agonist. ACS Chem Biol. 2011; 6(3): 218-22.
268. Wang R, Campbell S, Amir M, Mosure SA,Bassette MA. Genetic and pharmacological inhibition of the nuclear receptor RORα regulates T(H)17 driven inflammatory disorders. Nat Commun. 2021; 12(1): 76.
269. Solt LA, Banerjee S, Campbell S, Kamenecka TM,Burris TP. ROR inverse agonist suppresses insulitis and prevents hyperglycemia in a mouse model of type 1 diabetes. Endocrinology. 2015; 156(3): 869-81.
270. Barbarroja N, López-Pedrera R, Mayas MD, García-Fuentes E, Garrido-Sánchez L, Macías-González M*, et al.* The obese healthy paradox: is inflammation the answer? Biochem J. 2010; 430(1): 141-9.
271. Kadiri S, Auclair M, Capeau J,Antoine B. Depot-Specific Response of Adipose Tissue to Diet-Induced Inflammation: The Retinoid-Related Orphan Receptor alpha (RORalpha) Involved? Obesity (Silver Spring). 2017; 25(11): 1948-55.
272. Arkan MC, Hevener AL, Greten FR, Maeda S, Li ZW, Long JM*, et al.* IKK-beta links inflammation to obesity-induced insulin resistance. Nat Med. 2005; 11(2): 191-8.
273. Tourniaire F, Romier-Crouzet B, Lee JH, Marcotorchino J, Gouranton E, Salles J*, et al.* Chemokine Expression in Inflamed Adipose Tissue Is Mainly Mediated by NF-κB. PLoS One. 2013; 8(6): e66515.
274. Jiang HY, Wek SA, Mcgrath BC, Scheuner D, Kaufman RJ, Cavener DR,Wek RC. Phosphorylation of the alpha subunit of eukaryotic initiation factor 2 is required for activation of NF-kappaB in response to diverse cellular stresses. Mol Cell Biol. 2003; 23(16): 5651-63.